UNIVERSITÀ DEGLI STUDI DI TRIESTE

XXIX CICLO DEL DOTTORATO DI RICERCA IN NANOTECNOLOGIA

Development of nanostructured substrates for quantification of anticancer drugs in biofluids with Surface Enhanced Raman Scattering (SERS)

Settore scientifico-disciplinare: CHIM/07

DOTTORANDA
Silvia Dalla Marta

COORDINATORE
Prof. Lucia Pasquato

SUPERVISORE DI TESI
Prof. Valter Sergo

ANNO ACCADEMICO 2015/2016

DallaMarta Valter Sergo Lucia Pasquato

“Tell me and I forget,

teach me and I may remember,

involve me and I learn.”

Benjamin Franklin

Abstract

To date, therapeutic drug monitoring (TDM), that is the quantification of anticancer drugs in biofluids of oncological patients, is expensive and time consuming. Such a quantitative determination is crucial for a successful chemotherapic treatment due to the high interpatient variability of the anticancer drugs levels in biofluids. A frequent TDM turns out to be necessary to limit as far as possible the heavy side-effects of the treatment. Thus, the development of a new Point Of Care (POC) tool for a faster and less expensive TDM is highly desirable. Surface Enhanced Raman Scattering (SERS) is a surface-sensitive technique able to detect low concentrations of specific analytes in liquid environments. The high sensitivity given by metal nanostructured materials, the specificity given by Raman spectroscopy, the rapidity of the measurements and the possibility to develop inexpensive solid SERS substrates point to SERS as an appropriate platform for TDM. Moreover, solid SERS substrates together with the availability of portable instruments make this technique a possible new POC tool to quantify the drugs were a quick response is needed.

The aim of this doctoral project is the development and the optimization of cost-efficient, repeatable and sensitive solid SERS substrates for quantitative analysis of antitumoral drugs in biofluids such as human serum.

In the first part of this doctoral thesis, a general introduction about Raman spectroscopy, SERS and SERS as quantitative technique will be reported.

In the second chapter, the development and the optimization of repeatable solid SERS substrates constituted by metal nanoparticles deposited on filter paper with a simple dipping method, it will be presented. Specifically, four kinds of substrates developed with dip-coating method will be presented, differing depending on the type of nanoparticles used: i) citrate capped gold nanoparticles (c-Au NPs); ii) citrate capped silver nanoparticles (c-Ag NPs); iii) citrate capped silver Nanostars (NSs) and iv) hydroxylamine reduced silver nanoparticles (h-Ag).

As the first step, I performed a systematic study on c-Au and c-Ag paper made substrates using two different non resonant analytes as probe molecules (i.e. Adenine and 4-Mercaptobenzoic acid). The aim was to optimize the parameters involved in the development procedure (i.e. the kind of filter paper, the NPs concentration and the presence of an aggregating agent) exploring how they affect the repeatability of the substrates. Optimized paper-based SERS substrates aiming at building a platform for quantitative analysis will be presented in terms of inter- and intra- sample repeatability, sensitivity and long term stability. Then, solid substrates based on different nanoparticles, namely h-Ag and NSs, will be presented and discussed from a repeatability point of view. The SERS signal variation, hence the repeatability, will be quantified calculating the relative standard deviation (RSD%). Finally, the SERS substrates giving the best performance in terms of sample repeatability were found to be the optimized c-Au and c-Ag. These substrates feature an intra- and inter- sample repeatability suitable for quantitative analysis, with RSD values <20% for the intra- and <10% for the inter- sample repeatability. h-Ag substrates show good intra- sample repeatability values (with a RSD < 20%) but a quite large inter- sample variability (28% RSD). Ag NSs, instead, feature RSD values (30%) too large to allow a quantitative analysis with such kind of substrates.

In the third part of the work, I will present some applications of the substrates developed in the first part. In particular, preliminary results will be reported, which are related to Methotrexate (MTX) and Imatinib (IMT) rapid quantification, in model solutions mimicking biofluids as well as in real biofluids such as human serum. Optimized c-Au and h-Ag paper-made substrates were used for the analysis of MTX and IMT, respectively. The direct quantification of MTX and IMT spiked in human serum will be presented by means of combined SERS with paper-made solid substrates and a multivariate Partial Least Squares Regression (PLSR) model. The model performance will be judged on the basis of the Root Mean Square Error of Prediction (RMSEP), which quantifies the quantification accuracy and precision.

The multivariate calibration model for the drugs in human serum will be built in a concentration range of 0.1 ~ 150 μM for MTX and 0.5 ~ 10 μM for IMT. The chemometric models for the anticancer drugs quantification in human serum yield a RMSEP of 31.57 μM for MTX and 1.13 μM for IMT, respectively. Finally, the lower limit of detection (LOD) and the lower limit of quantification (LOQ) with the paper-made substrates developed in this thesis, were found to be, respectively, 17.4 and 38.3 μM for MTX and 2.29 and 6.0 μM for IMT.

Esposizione riassuntiva

Finora, il monitoraggio terapeutico di farmaci (Therapeutic Drug Monitoring, TDM), ovvero la quantificazione di farmaci antitumorali presenti nei fluidi corporei di pazienti in chemioterapia, richiede tempo ed è costosa. A causa della elevata variabilità interpersonale dei livelli di farmaco nei fluidi corporei, tale determinazione quantitativa è cruciale per il successo del trattamento chemioterapico. Inoltre, è necessario un monitoraggio frequente al fine di limitare il più possibile gli ingenti effetti collaterali del trattamento stesso. Pertanto, lo sviluppo di un nuovo dispositivo Point Of Care (POC) per monitorare il livello di farmaci in maniera più rapida e meno costosa si rivela di grande utilità. La spettroscopia Raman amplificata da superfici (SERS, dall'inglese Surface Enhanced Raman Spectroscopy) è una tecnica di superficie in grado di rilevare basse concentrazioni di specifiche molecole in soluzione. L'elevata sensibilità dovuta ai materiali metallici nanostrutturati, la specificità della spettroscopia Raman, la rapidità delle misure e la possibilità di sviluppare substrati solidi SERS a basso costo, rendono la SERS una tecnica appropriata per il TDM. Inoltre, i substrati solidi SERS, assieme alla disponibilità di strumentazioni portatili, rendono tale tecnica un possibile nuovo strumento POC per quantificare il livello di farmaci dove e quando è necessaria una risposta immediata.

Lo scopo di questo progetto di dottorato è lo sviluppo e l'ottimizzazione di substrati solidi SERS economici, ripetibili e sensibili per l'analisi quantitativa di farmaci antitumorali in fluidi corporei come il siero sanguigno.

Nella prima parte di questa tesi si riporta un'introduzione generale sulla spettroscopia Raman, sulla SERS e sulla SERS come tecnica quantitativa.

Nel secondo capitolo, si presenta lo sviluppo e l'ottimizzazione di substrati solidi SERS ripetibili costituiti da nanoparticelle metalliche adsorbite su carta da filtro attraverso una semplice tecnica di immersione. Nella fattispecie, verranno presentati quattro tipologie di substrati, differenti a seconda del tipo di nanoparticelle utilizzate, ottenuti con la tecnica a immersione: i) nanoparticelle d'oro ricoperte da citrato (c-Au NPs); ii) nanoparticelle

d'argento ricoperte da citrato (c-Ag NPs); iii) nanostelle d'argento ricoperte da citrato (Ag NSs) e iv) nanoparticelle d'argento ridotte da idrossilammina (h-Ag NPs).

in una prima fase, viene eseguito uno studio sistematico sui substrati di carta di c-Au e c-Ag utilizzando due differenti analiti non risonanti come molecole sonda (i.e. Adenina e acido 4-mercaptobenzoico). Lo scopo di tale studio è quello di ottimizzare i parametri coinvolti nella procedura di sviluppo dei substrati (i.e. il tipo di carta da filtro, la concentrazione di nanoparticelle e la presenza di un agente aggregante) esaminando come essi influenzano la ripetibilità dei campioni. Verranno dunque presentati substrati di carta ottimizzati a fini di analisi quantitative in termini di ripetibilità inter- e intra- campione, di sensibilità e di stabilità nel tempo. Successivamente, verranno presentati e discussi i substrati solidi ottenuti con differenti nanoparticelle, ovvero h-Ag NPs e Ag NSs, da un punto di vista di ripetibilità. La variazione del segnale SERS, quindi la ripetibilità, viene quantificata attraverso il calcolo della deviazione standard relativa (RSD %). I substrati SERS ottimizzati c-Au e c-Ag sono risultati essere i più ripetibili. Tali substrati presentano una ripetibilità intra- e inter- campione adatta ad analisi quantitative, con valori di RSD <20% per la ripetibilità intra- e <10% per la inter- campione. I substrati h-Ag mostrano una buona ripetibilità intra- campione (con una RSD <20%) ma una variabilità inter- campione piuttosto elevata (RSD <28%). I substrati di Ag NSs, invece, presentano valori di ripetibilità (RSD 30%) troppo elevati per permettere un'analisi quantitativa affidabile.

Nella terza parte del lavoro, verranno presentate alcune applicazioni dei substrati sviluppati nella prima parte. In particolare, verranno riportati risultati preliminari di quantificazione rapida di due farmaci antitumorali, il Metotrexato (MTX) e l'Imatinib (IMT), presenti sia in soluzioni modello simulanti fluidi corporei, sia in fluidi corporei reali come il siero sanguigno. Per le analisi di MTX e IMT vengono usati rispettivamente i substrati ottimizzati c-Au e h-Ag. L'analisi quantitativa diretta dei due farmaci aggiunti al siero sanguigno viene effettuata attraverso la combinazione della tecnica SERS con substrati di carta e di un modello multivariato, la regressione parziale dei minimi quadrati (Partial Least Squares Regression, PLSR). La prestazione del modello PLSR viene giudicata sulla base dell'errore di predizione (scarto quadratico medio della previsione o Root Mean Square Error of Prediction, RMSEP), il quale quantifica l'accuratezza e la precisione dell'analisi.

Il modello di calibrazione multivariata per i farmaci in siero vengono costruiti in una finestra di concentrazione di 0.1 ~ 150 µM per il MTX e di 0.5 ~ 10 µM per l'IMT. I modelli di chemiometria costruiti per la quantificazione dei farmaci in siero sanguigno mostrano un RMSEP rispettivamente di 31.57 µM per il MTX e di 1.13 µM per l'IMT. Infine, con i substrati di carta sviluppati in questa tesi, il limite minore di rilevamento (lower Limit of Detection, LOD) e il limite minore di quantificazione (lower Limit of Quantification, LOQ) dei farmaci in esame sono risultati essere, rispettivamente, di 17.4 e di 38.3 µM per il MTX e di 2.29 and 6.0 µM per l'IMT.

Table of content

List of acronyms

4-MBA:	4-Mercaptobenzoic Acid
Ag:	Silver
AGP:	α-1-Acid Glycoprotein
AN:	Area Normalization
Au:	Gold
BC:	Baseline Correction
BSA:	Bovine Serum Albumin
c-Ag:	Citrate capped-Silver
c-Au:	Citrate capped-Gold
CCD:	Charge Coupled Device
CML:	Chronic Myelogenous Leukemia
Cu:	Copper
EF:	Enhancement factor
EM:	Electromagnetic
FE-SEM:	Field Emission-Scanning Electron Microscopy
GIST:	Gastrointestinal Stromal Tumor
h-Ag:	Hydroxylamine reduced-Silver
HPLC:	High Performance Liquid Chromatography
HS:	Human Serum
HSA:	Human serum Albumin
IMT:	Imatinib Mesylate
IR:	Infrared
LC-MS:	Liquid Chromatography – Mass Spectroscopy
LOD:	Low Limit of Detection
LOQ:	Low Limit of Quantification
LSP:	Local Surface Plasmon

MTX:	Methotrexate
N.A.:	Numerical Aperture
NIR:	Near Infrared
NPs:	Nanoparticles
NSs:	Nanostars
NTA:	Nanoparticle Tracking Analysis
PBS:	Phosphate Buffered Saline
PLSR:	Partial Least-Squares Regression
POC:	Point Of Care
RDCV:	Repeat Double Cross Validation
RMSEP:	Root Mean Square Error of Prediction
RSD:	Relative Standard Deviation
RT:	Room Temperature
SC:	Sodium Citrate
SD:	Standard Deviation
SERS:	Surface Enhanced Raman Scattering
SP:	Surface Plasmon
SPB:	Surface Plasmon Band
SPR:	Surface Plasmon Resonance
TDM:	Therapeutic drug monitoring
TEM:	Transmission Electron Microscopy

Chapter 1

Introduction

During my Ph.D. project, solid SERS (Surface Enhancement Raman Scattering) substrates were developed as sensors for chemical quantitative analysis, to be used in particular for Therapeutic Drug Monitoring (TDM)[1]. The aim was to obtain an inexpensive and reliable point of care (POC) tool, capable to rapidly detect and quantify anticancer drugs present in biofluids of patients undergoing chemotherapy.

Cancer is the third death-leading cause in developed countries after heart disease and stroke[2]. Antitumor drugs employed in chemotherapy treatment are in general highly cytotoxic and they often exert their therapeutic effect in a very narrow therapeutic window of concentrations, close to systemic toxicity.

Increased toxicity is associated with high plasma levels of drugs, whereas a low plasma concentration might lead to therapeutic inefficiency. The exposure to antitumoral drugs, and the subsequent impact on therapeutic benefit, can be affected by factors such as large pharmacokinetic variability and inter-individual variability in absorption, distribution and metabolism[3,4]. Food-drug as well as drug-drug interaction might be a source of variability as well. Moreover, the oral targeted drugs are extremely expensive, thus a precise dosage within the therapeutic window might also represent an economic benefit for the public health system[5,6].

Since the demand of personalized targeted therapy is continuously increasing, TDM, or, more specifically, the quantification of anticancer drugs in biofluids, is probably the way to reliably control the plasmatic concentrations of those drugs[1,7]. Current attempts to measure targeted anticancer agent in biofluids employ techniques such as liquid chromatography-tandem mass spectroscopy (LC-MS)[8,9], high performance liquid chromatography coupled to ultraviolet rays (HPLC-UV)[10]. Such kind of techniques are highly sensitive and specific, but with the disadvantage of the need for relatively large and expensive instrumentation, operated by experts with the use of time-consuming protocols. Thus, the development of a new POC tool for a faster and less expensive TDM is highly desirable.

With this regard, nanotechnological devices and their clinical applications in medicine have increasingly gained value. Surface Enhanced Raman Spectroscopy (SERS) has lately drawn growing attention as a tool to measure low concentrations of compounds in body fluids[11]. In particular, this technique could provide an analytical platform for the TDM[7]. SERS, in fact, is a surface-sensitive technique able to detect analytes at low concentrations in liquid environments. Moreover, this is a specific technique since each molecule provides a different fingerprint in the spectral pattern. Finally, in contrast with routine HPLC-MS analysis, SERS requires smaller amount of sample (microliters) for the analyte detection and the analytical response is immediate (few seconds). Therefore, the combination of i) the efficiency and the rapidity of SERS measurements ii) the availability of inexpensive solid nanostructured samples and iii) the availability of portable Raman instruments could be extremely attractive to set up a new POC for TDM.

With this purpose, solid SERS substrates consisting of gold (Au) and silver (Ag) nanoparticles (NPs) loaded on filter paper with the dip-coating method[12] were developed and optimized as quantitative SERS sensors. The choice fell on this type of substrate because of:

- i) the cost-efficiency of the technique (it does not require any instrumentation);
- ii) the easiness of the procedure (it is a simple dipping method whereby the NPs adsorb on the solid support through a self-assembling process);
- iii) the synthesis technique allows to control the tuning of the metal, the size, the shape and the capping of the NPs[13–16];
- iv) the scalability of the process;
- v) the advantages from the use of paper as solid support: paper is cheap, it is porous, flexible, hydrophilic (i.e. allowing the adsorption of the components of the biofluids) and it has a three-dimensional structure (i.e. ensuring a intra- and inter- layer plasmon coupling, enhancing even more the SERS signal[14], hence increasing the substrate sensitivity and efficiency).

Nevertheless, for quantitative analysis applications, the low repeatability is one of the main issue hindering a widespread use of solid SERS substrates developed with a bottom-up self-assembling approach, such as the NPs-paper based substrates. Despite the promising results obtaining so far on paper based solid SERS substrates[13,15–18], there is a lack of information about the repeatability of these substrates in view of quantitative applications (i.e., the substrates homogeneity and the inter-sample repeatability[14,19–23]).

Thus, at first my project aimed at an optimization of these paper substrates in terms of enhancement, but, even more important, in terms of repeatability (defined as the variation in repeated measurements made on the same subject under identical conditions[24]), using two non-resonant analytes as probe molecules. In fact, in spite of its crucial importance, the issue of repeatability is often neglected in SERS literature, and rigorous protocols to assess this property are still missing. Only after such an evaluation, a substrate could be used for real quantitative application. As a second aim of this study, we intended to assess if and how a repeatable SERS substrate could be used to determine an analyte in complex matrices, such as biofluids. The high variability, which is intrinsic to biofluids matrices, makes quantitative SERS measurements challenging. In order to overcome the variability issue, in this study a multivariate calibration model was used to predict the concentration of the drugs. Indeed, multivariate regression, in comparison with the easier univariate calibration, incorporates much of the available spectral information, leading to a more accurate prediction of the concentration of a specific analyte[7].

Chapter 2

The SERS technique

2.1 Raman theory and principles.

Raman spectroscopy is one of the most important techniques used to provide information on chemical structure, to identify substances from characteristic spectral patterns and to determine semi-quantitatively and quantitatively the amount of an analyte in a sample.

In Raman spectroscopy the incident radiation is scattered through the generation of a so called “virtual state”, followed by a rapid transition of the molecule to a vibrational state at lower, higher or same as the initial one. The molecule is irradiated by a UV, UV-visible or Near-Infrared (NIR) monochromatic radiation, whose energy is much higher than the difference between the fundamental and the excited vibrational states (ΔE). This radiation produces a distortion of the electronic cloud distribution, yielding an induced dipole moment of the molecule. The molecule is therefore promoted to a virtual excited state, whose energy depends on the incident radiation energy; subsequently, the molecule rapidly decays to the final state, releasing the scattered radiation. Two types of scattering can be identified: the *Rayleigh* scattering and the Raman scattering, which in turn can be divided into *Stokes* and *anti-Stokes* scattering. The scattered radiation is therefore constituted by slightly different frequencies, depending on the mechanisms and the energetic levels involved; in particular, the scattered photons are:

- photons with the same energy of the incident photons, generated by the Rayleigh scattering;
- photons with less energy of the incident photons, generated by the Stokes scattering;

- photons with major energy of the incident photons, generated by the anti-Stokes scattering.

In figure 2.1 a schematization of the energetic levels involved in the Raman process is reported, showing the Rayleigh, the Stokes and the anti-stokes scattering process.

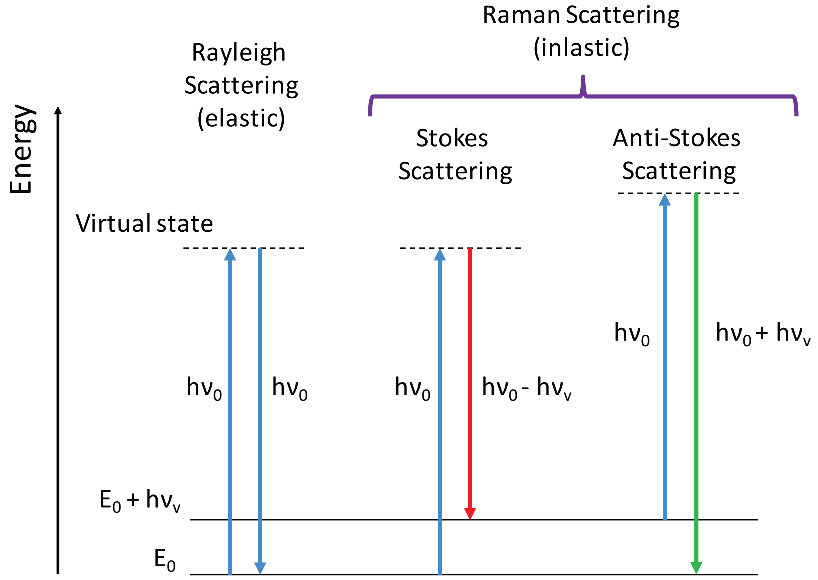

Figure 2.1. Diagram of the Rayleigh and Raman scattering process. Both the incident energy (upward arrows) and the scattered energy (downward arrows) have much larger energies than the energy of a vibration.

In the Stokes scattering, the molecule initially is in its ground state and, after being excited to the virtual state, decays to the first excited vibrational state. The energy of the scattered photon is the following:

$$E = h\upsilon_0 - h\upsilon_v \qquad (2.1$$

where $h\upsilon_0$ corresponds to the energy of the incident photon and $h\upsilon_v$ corresponds to the energy difference between the initial state (the ground state) and the final state (the first excited vibrational state). The Stokes signal is therefore recorded at lower frequencies.

At room temperature not all the molecules are in their ground states. A very small fraction of these ($e^{\Delta E/kT}$) are present in an excited vibrational state, due to the thermal energy. If the molecule is present in an excited state, after the interaction with the incident radiation it might decay to the ground state. In this process, called, as mentioned, anti-Stokes scattering, the molecule transfers part of its energy to the scattered photon, which is being scattered with a higher energy:

$$E = h\upsilon_0 + h\upsilon_v \qquad (2.2$$

The signal generated from the anti-Stokes scattering process is therefor recorded at higher frequencies with respect to the Rayleigh signal (i.e. with negative Raman shifts). The signal intensity of the Raman scattering (Stokes or anti-Stokes) is much weaker compared to the Rayleigh signal, since only one photon in every 10^6-10^8 can be diffused in inelastically[25]. Moreover, since the majority of the molecules at room temperature populates the ground state, the Stokes scattering is a more probable process than the anti-Stokes. Consequently, its signal is more intense than the one generated by the anti-Stokes process.

Entering into the details of the Raman mechanism, from a classical point of view, when a molecule is exposed to a radiation, the electric field with a frequency υ_0 induces a polarization of the electron distribution. Thus, a dipole moment P is induced in the molecule according to the following relation:

$$P = \alpha E = \alpha E^0 \cos 2\pi\upsilon_0 t \qquad (2.3$$

where α is the polarizability, E is the electric field vector, E^0 is the electric field intensity and υ_0 is the frequency of the electromagnetic radiation. Since both P and E are time dependent, the induced dipole moment oscillates in time, leading to emission of radiation. As both μ and E in the equation 2.3) are vector quantities, the polarizability is a tensor and its form depends on the coordinate system chosen and the molecular symmetry:

$$\alpha = \begin{pmatrix} \alpha_{xx} & \alpha_{xy} & \alpha_{xz} \\ \alpha_{yx} & \alpha_{yy} & \alpha_{yz} \\ \alpha_{zx} & \alpha_{zy} & \alpha_{zz} \end{pmatrix} \qquad (2.4$$

The polarizability, if it is supposed to be symmetric, can be expanded in the following Taylor series:

$$\alpha = \alpha^0 + \left(\frac{\partial \alpha}{\partial q}\right)_0 q + \frac{1}{2}\left(\frac{\partial^2 \alpha}{\partial q^2}\right)_0 q^2 + \ldots \tag{2.5}$$

where α^0 is the polarizability value at the equilibrium and q is the deviation from the equilibrium. Then, for a diatomic molecule which vibrates at frequency υ_v, and assuming a simple harmonic motion, its internuclear distance can be written as follow:

$$q(t) = q_0 \cos 2\pi \upsilon_v t \tag{2.6}$$

where q_0 is the amplitude of vibration. Finally, the induced dipole moment assumes the following expression:

$$\alpha = \alpha^0 + \left(\frac{\partial \alpha}{\partial q}\right)_0 q + \frac{1}{2}\left(\frac{\partial^2 \alpha}{\partial q^2}\right)_0 q^2 = \tag{2.7}$$

$$= \alpha_0 E^0 \cos 2\pi \upsilon_0 t + \left(\frac{\partial \alpha}{\partial q}\right)_0 q_0 2\pi \upsilon_0 t \, E^0 \cos 2\pi \upsilon_v t = \tag{2.8}$$

$$= \alpha_0 E^0 \cos 2\pi \upsilon_0 t + \alpha' q_0 E^0 \cos 2\pi(\upsilon_0 + \upsilon_v)t + \alpha' q_0 E^0 \cos 2\pi(\upsilon_0 - \upsilon_v)t \tag{2.9}$$

Where υ_v is the natural frequency of the molecule, υ_0 is the frequency of the electromagnetic radiation, q is the deviation from the equilibrium and α' is the first derivate of the polarizability, which is responsible of the vibrational bands on the Raman spectra[26].

The induced dipole moment is therefore constituted by three components, which oscillate in time: one with the light frequency υ_0, one with a lower frequency ($\upsilon_0 - \upsilon_v$) and one with a larger frequency ($\upsilon_0 + \upsilon_v$). Thus, the molecule scatters three different radiations: the Rayleigh, the Stokes and the anti-Stokes, respectively[27].

As general selection rule for Raman spectroscopy, the scattering is generated by a variation on the polarizability of a molecule:

$$\left(\frac{\partial \alpha}{\partial q}\right)_0 \neq 0 \tag{2.10}$$

Were q is the deviation from the equilibrium. If a vibration does not greatly change the polarizability of the molecule, then the polarizability derivative will be near zero, and the intensity of the Raman band will be weak.

Each molecule produces a different spectral pattern, like a “fingerprint”, in its Raman spectra. Moreover, with this technique it is possible to analyze liquid samples and the intensity of the signal is proportional to the concentration of molecule present in solution. With Raman spectroscopy is therefore possible to extract both qualitative and quantitative information, making such kind of technique a powerful tool for chemical analysis.

2.2 Surface Enhancement Raman Scattering

The main limit of Raman spectroscopy is its relatively low sensitivity. For the analysis of solutions it is necessary to achieve high concentrations, up to millimolar, in order to detect a signal. However, through the use of metallic nanostructural materials (i.e. gold or silver nanoparticles), it is possible to increase the Raman signal of several orders of magnitude, hence improving the sensitivity of the technique.

SERS spectroscopy is a surface-sensitive technique that enhances the Raman scattering intensity of the molecules adsorbed on nanostructures that can support surface plasmons, leading to an electromagnetic field enhancement of the Raman signal[27]. SERS was discovered in 1974 by Fleischman et al. which reported the strong Raman scattering from pyridine adsorbed on a silver roughened electrode[28]. The enhancement is due to the excitation of the so called *surface plasmons*, which characterizes this peculiar materials[29]. The Raman signal of a molecule adsorbed, or close to these nanostructured plasmonic materials, referring to the value of the “free” molecule, can be increased up to a factor 10^{10}, while the typical value is of the order of 10^{3}-10^{7}, depending on the molecule, the kind and the shape of the nanostructured surface/material and the laser[30,31].

In contrast with Raman spectroscopy, in which only the molecule and the incident radiation are involved, in SERS the components involved are three: the molecule, the metal nanostructure and the electron radiation. This difference introduces a much greater degree of complexity to SERS experiments and spectra interpretation. The presence of the nanostructure leads, besides a signal amplification, a variation on the number frequencies, and relative intensity of the bands observed in a spectrum. Hereafter the most important aspects of SERS spectroscopy are considered, in contrast with Raman spectroscopy, for the interpretation of observed SERS spectra[27]:

1. The molecule interacts with a metal nanostructure through different kinds of adsorption processes: *physisorption*, if the interaction is principally due to weak Van der Waals forces, or *chemisorption*, if a chemical bond is formed between the analyte and the atoms constituting the metal nanostructure.
2. The interaction between the laser light and the nanostructures can create a hugely enhanced *local electric field*, which is the principal mechanism in the SERS effect, at the location of the adsorbed molecules.
3. The interaction of the incident radiation and the adsorbed molecules can lead to sample photodegradation (i.e. photodissociation, photoreactions or photodesorption), which is recognized in the spectrum by the observation of the so called "cathedral peaks" of SERS, arising from carbon products of the degradation (i.e. amorphous and graphitic carbon).
4. The interaction radiation-nanostructures depends on the value of the complex dielectric function at the excitation frequency. This will contribute to determine the observed enhancement at that frequency. Moreover, the enhancement is influenced by the shape and the dimension of the nanostructures as well.
5. The relative intensity of the SERS bands into the spectral pattern is determined by the so called "surface selection rules". Surface selection rules cover the symmetry properties of the dipole transitions and the modification of the intensities depending on the proximity of the functional groups to the nanostructured surface.
6. The plasmonic frequencies of the enhancing nanostructures generally employed are resonant with the visible light and the near-IR region of the electromagnetic spectrum. For that reason, the SERS spectra are commonly obtained by excitation with visible or near-IR light.

2.3 Electromagnetic and chemical mechanism

It is currently accepted that the mechanisms involved in the SERS process are the electromagnetic one and, to a minor extent, the chemical one.

From an electromagnetic viewpoint, metals can be considered as a plasma composed of free electrons and positive ion cores. The oscillations of the conduction electrons in a metal nanostructure are called *surface plasmons* (figure 2.2).

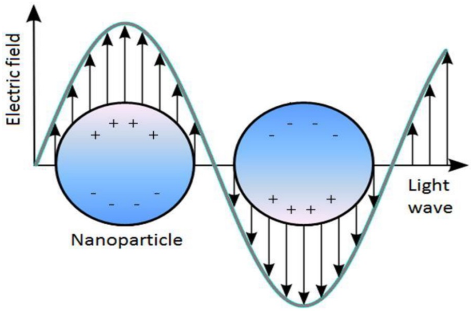

Figure 2.2. Schematization of surface plasmons induced by the incident electromagnetic radiation[32].

The interaction of an incident radiation smaller than the wavelength of the light with the metal nanostructure induces the excitation of the surface plasmons. The polarization of the electrons by the electromagnetic radiation results in a strong induced electric field at the surface of the nanostructure. This induced field is given by:

$$E_{induced} = \left(\frac{\varepsilon(\omega) - \varepsilon_m}{\varepsilon(\omega) + 2\varepsilon_m}\right) E_{incident} \qquad (2.11$$

Where $\varepsilon(\omega)$ is the complex dielectric function of the metal structure and ε_m is the relative permittivity of the surrounding medium. The factor reported within the brackets is the so called *g-factor* and represent the average field enhancement over the particle surface. For a spherical nanoparticle, the SERS effect occurs when exciting electromagnetic radiation is in resonance with the dipolar plasmon of the nanoparticle, according to:

$$\varepsilon(\omega_0) = -2\varepsilon_m \qquad (2.12$$

This resonance condition, which depends on the electron density, is achieved in the UV-visible part of the electromagnetic spectrum for Au, Ag and Cu.

The enhanced Raman scattered light (E_r), resulting from the increased electromagnetic field on the nanostructure, is given by the following equation:

$$E_r = \alpha g E_0 \qquad (2.13$$

Where α is the polarizability, g is the g-factor and E_0 is the incident light.

Furthermore, the Raman-scattered light is also enhanced by a similar process but to a different magnitude (g'). Effectively, the average SERS intensity (I_{SERS}) will be proportional to square of the product of both the gains, that is $I_{SERS} \sim | g \cdot g' |^2$. For low-frequency Raman modes, the gains g and g' can be considered to be almost equal. This feature results in the SERS intensity to be proportional to the fourth power of the gain in the electromagnetic field caused by the nanostructure. Hence, even modest enhancement of the electromagnetic field results in gigantic enhancement of SERS cross section[33].

The SERS enhancement does not require necessarily the direct contact between the molecule and the nanomaterial. Nevertheless, the enhancement effects are highly localized and decay rapidly as the separation between the analyte and the metal particles increases, making SERS a surface-sensitive technique. For a spherical nanoparticle with a radius r, for instance, the dipole field decreases proportionally to $[r/(r+d)]^{12}$. The enhancement is therefore maximum for a molecule adsorbed on the nanostructure and extends its effect up to ~ 10 nm of distance from the surface[29].

In order to obtain information about the molecule-substrate interaction, and the spatial orientation of the molecule adsorbed, besides the electromagnetic mechanism, it is necessary to consider the chemical mechanism as well.

The chemical mechanism is another independent mechanism that enhances the Raman-scattering cross section of the analyte adsorbed on the metal surface. The electronic cloud of the adsorbed molecule can be more or less distorted by the interaction with the metal surface depending on the strength end the kind of bond involved on the adsorption. This interaction imposes a change in the electronic cloud of small molecules, which is more dramatic in the case of chemisorption. The electronic cloud becomes that of a new surface structure, with different point group symmetry, hence with new electronic states which are resonant with respect to the excitation radiation employed, and yielding a new vibrational spectrum. The interaction involved in the adsorption process distorts indeed the molecule polarizability, hence the Raman intensity and the pattern of a SERS spectrum, which may differ from the Raman spectrum of the same free molecule[27].

2.4 Nanoparticles as SERS substrates

The interpretation of the electromagnetic mechanism is based on the idea of "nano-resonators", metallic nanoparticles with different shapes, such as spheres, nanowires, nanostars or other hybrid structures (e.g. metal nanoparticles coated with a silica shell)[34–39].

As already mentioned in the previous section, Au, Ag or Cu nanomaterials achieve the resonant condition, according to the equation 2.12, in the UV-visible part of the electromagnetic spectrum. Thus, when such kinds of materials interact with electromagnetic radiation, the plasmons coherently oscillate in response to the electronic component of the field. Then, if the radiation is resonant with the surface plasmons, a band in the UV-visible spectrum appear, called surface plasmon band (SPB), or extinction band. Surface plasmons give rise to the SERS effect and vary depending on the metal, the shape and the dimensions of the nanoparticle[40,41]. In order to achieve the enhancement of the Raman signal, it is necessary that the SPB of the nanomaterial will be "tuned" with the excitation wavelength. This "tuning" can be modulated by varying the metal, the shape and the dimension of the nanostructure.

In complex metal nanostructures (i.e. aggregated formed by metal NPs) the plasmon modes of the NPs interact electromagnetically, resulting in hybridized plasmonic states. This coupling gives rise to the so-called "bright" and "dark modes". Bright modes are generated by the frequencies of SP, which fall in the visible range of the electromagnetic spectrum, while dark modes usually do not show up in optical absorption experiments.

Dark modes are of essential importance as well for the generation of highest local fields and for the spectroscopic performance of a plasmonic nanostructure.[42,43] As will be discussed in the chapter 2, for instance, Ag NPs feature a SERS enhancement when irradiated in the visible region (i.e. 530 nm) due to the excitation of the bright modes. Nevertheless, in the NIR region (i.e. 785 nm) it is possible to excite their dark modes. The effect is a larger enhancement of the Raman signal leading to a higher band intensity in the SERS spectrum. The correlation between excitation wavelength and SERS bands intensity will be discussed in detail in section 2.3.

Owing to the rapid development of the nanotechnology field, NPs have become object of intense research duo to their optical, electronical and catalytic properties. Metal nanoparticles are employed in several nanotechnology fields thanks to their functionality and optical properties. Nanosensors[44], drug delivery[45], catalysis[46] and diagnostics[47] are just few of their applications in nanotechnology. In this PhD thesis we focused on optical properties of NPs, which are utilized to enhance the Raman signal, taking advantage of the surface plasmons which cause the SERS effect.

SERS substrates can be tentatively classified into three main classes[48–50]:

- Colloidal dispersions.
- Solid metallic nanostructures obtained with top-down processes.
- Solid metallic nanostructures obtained with bottom-up/self-assembly processes.

Colloidal dispersions of metallic nanoparticles are the most popular SERS substrates due to their ease of use, their high enhancement factors and the relative inexpensive synthesis.

Non stabilized NPs tend to attract each other due to the Van der Waal forces and, without repulsive forces able to counteract, they aggregate, eventually leading to precipitation of macro-aggregates. To avoid these effects and to keep the NPs dispersion stable, it is necessary to stabilize the NPs constituting the colloid through either *steric* or *electrostatic stabilization*.

With the steric stabilization, the colloidal aggregation is prevented by adsorbing bulky molecules such as polymers (i.e. polyvinyl alcohol (PVA)), surfactants (cetyltrimethylammonium bromide (CTAB))[41] or ligands (thiols)[51] on the NPs surface, providing a thick protective layer.

The electrostatic stabilization consists in the formation of an electric double layer at the NPs surface. The attractive Van der Waals forces between the bare nanoparticles are counterbalanced by Coulombian forces generated by negatively charged ions adsorbed on the NPs surfaces. In the figure 2.3 a cartoon representing the metal colloid double layer and the Coulombian potential is reported. This is the case, for example, of the citrate stabilized colloids: NPs are surrounded by an electrical double layer formed by positively charged metal and anions which are attracted to them. The result is a Coulombian force avoiding the colloids aggregation[52].

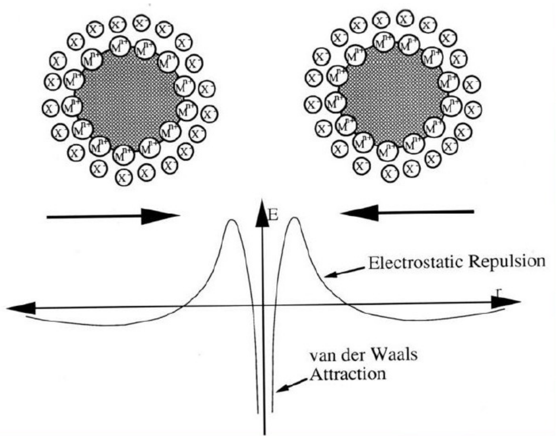

Figure 2.3. Schematic representation of electrostatic stabilization of metal colloids and electrostatic potential[52].

Nevertheless, it is possible to break the Coulombian potential barrier by increasing the ionic strength of the solution or by replacing the ions which surrounds the NPs with a neutral adsorbate. In this way the potential barrier will be break and the colloids will aggregate. This is a crucial point for the NPs used as SERS substrates.

It is been demonstrated that the SERS substrates which feature the larger enhancement are not the single nanoparticles, but their aggregates[27,29]. In particular, the higher enhancement is being observed at the *gaps* of few nanometers between two or more nanoparticles, called *hot spots*. These localized spots can produce SERS enhancement factors of 10^{12} [31]. Thus, with the SERS technique, an aggregation process of the NPs is necessary to produce the enhancement of the Raman signal. As already mentioned, the aggregation will take place by the replacement of the stabilizing ions, such as citrate, with the analyte under SERS detection, or by an increase in ionic strength due to the ions present in the analyte solution. Moreover, since the analyte must adsorb onto the metal surface, it is important that the stabilizer is easily exchangeable with an analyte. Therefore, for SERS applications, electrostatically stabilized colloids are the best choice, rather than the steric stabilization. The choice of the metal colloids depends basically on the kind of analyte, which have to be detected. Not all the functional groups, in fact, feature the same affinity for all the metals.

Concerning the non-colloidal SERS substrates, metal nanostructures can be divided in two classes depending on their preparation: top-down and bottom-up methods. Top down synthetic methods involve direct fabrication of small features on a large area (i.e. electrochemical roughening, lithographic techniques, metal sputtering, etc.). The bottom-up techniques consist in a self-assembly preparation process of the metallic nanostructures forming colloidal aggregations[48] (i.e. dip coating method[50] or glass slides functionalization[53]).

Metallic roughened electrodes, through which the SERS phenomenon have been discovered[54], are active plasmon substrates developed with oxidation-reduction cycles. The main advantage of this kind of substrates is the simplicity of their preparation and use. Nevertheless, depending on roughening procedure used, electrodes can have highly variable surface roughness which results in non-uniform enhancement of the signal[50]. Moreover, the use of metallic roughened electrodes is declined also because of the relatively low enhancement factors typically achievable[55].

One of the main challenge in SERS is the fabrication of SERS substrates featuring an hot spot architecture able to reach the best enhancement of the scattered light[17–19]. For these purposes, there are a lot of top-down techniques and methods to prepare highly ordered solid metallic nanostructure. Lithography-based nanofabrication methods, such as electron beam lithography and reactive ion etching, are well known techniques to prepare highly uniform and reproducible SERS substrates, offering control over the size, the shape and the spacing of the nanostructures. Nevertheless, such kind of techniques are hampered by the slowness of the fabrication process and the high cost[53].

As a non-lithographic method, a technique pioneered by Van Duyne's group, involves the assembly of polystyrene nanospheres into a regular array, using this as a mask to create a periodic nanostructure (metal island films). Metal island film substrates are easy to fabricate, and the SPR wavelength can be tuned by varying the film's thickness and confluence. However, the enhancement factors achieved with these films are generally smaller than those observed with other SERS substrates[55]. Another top-down technique involves the evaporation and sputtering of metal for depositing SERS-active metal on substrates. Other classes of more simple top-down fabrication techniques are, for instance, the in situ synthesis (i.e. the silver mirror reaction[59] or galvanic replacement[50]) and the inkjet printing method. Those two methods have the advantage of being easy to implement and cost-efficient. However, with the in-situ synthesis it is not easy to tune the shape of the nanostructures and a potential industrial process is not easily scalable. The inkjet printing method required a printer and the obstruction of the cartridge by NPs is quite common, producing non uniform and homogeneous SERS samples.

The dip-coating method, on the other hand, is a self-assembly approach to produce solid SERS substrates. It does not require any instrumentation, it could be scalable and allows the tuning of the metal, the shape and the aggregation of the NPs[15]. This technique consists of simply dipping a solid support (i.e. filter paper) onto a colloidal solution for few days and then removing the supernatant. The use of common filter paper as support, besides of being extremely inexpensive, in principle allows a separation of different components present in a complex matrix, similar to chromatographic technique, or the mixing of other reagents with the analyte solution, as in the paper-analytical-devices (PADs)[60–62]. Moreover, the three dimensional structure of cellulose fibers on which the NPs are adsorbed, allows an increasing on the inter-particle coupling, hence the enhancement of the SERS signal[14].

For these reasons, during my Ph.D. project, colloidal solutions of metal nanoparticles were synthetized and then deposited on common filter paper through the dip-coating method in order to optimize non-colloidal SERS substrates for quantitative analysis. In such a way it was possible to develop a cost-efficient, reproducible, scalable and easy-to-produce solid SERS substrates for quantitative analysis.

Within the work presented in this thesis, four kind of metal NPs electrostatically stabilized were synthesized:

- Au NPs obtained with Turkevich method[63] (c-Au NPs).
- Ag NPs obtained with Lee-Meisel method[64] (c-Ag NPs).
- Ag NPs obtained with Leopold Lendl method[65] (h-Ag NPs).
- Ag Nanostars obtained with a two-step process developed by *A. Garcia-Leis et al*[35] (Ag NSs).

The choice of these colloids, and hence their application, depends basically on the type of analyte that have to be detected. Not all the functional groups, in fact, feature the same affinity for all the metals. Moreover, for the adsorption process, the stabilizer present in the surface of the materials (i.e. sodium citrate) must be taken in consideration as well.

The synthesis of metal NPs are based on physico-chemical techniques, depending from which is possible to control NPs shape, their dimension and composition. The most used chemical methods in solutions, such as those employed in this work, allow a better shape and dimension modulation by varying the experimental conditions such as temperature, stirring, rapidity of reagents addition and the concentration of reagents. The details of each synthesis methods will be discussed into the detail in the next chapter.

2.5 Molecules adsorption model

The adsorption process, schematized in figure 2.4, takes place due to attractive intermolecular forces between the adsorbate and the atoms which constituent the surface (the adsorbent). Therefore, the adsorpt (the substance to be adsorbed) diffuses from the bulk of the liquid or gas phase to the adsorbent[66]. Then the molecules adsorb on the surface through two kinds of interactions: physisorption or chemisorption, depending on the adsorption energy.

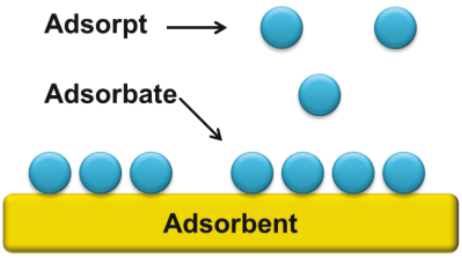

Figure 2.4. Cartoon depicting the main players in the adsorption process.

The amount of adsorbate is determined by several parameters, such as the nature of the adsorbate and the adsorbent, the surface area and the activation energy of the adsorbent, the temperature and the adsorpt concentration. Adsorption process is usually studied through graphs known as *adsorption isotherms*. These graphs represent the amount of adsorbate on the adsorbent as a function if its pressure or concentration at constant temperature and it is described by the function $\Gamma = f(p)$, experimentally determined. Depending on the physical and chemical conditions, several adsorption isotherms are experimentally observed. In figure 2.5 are reported eight common examples.

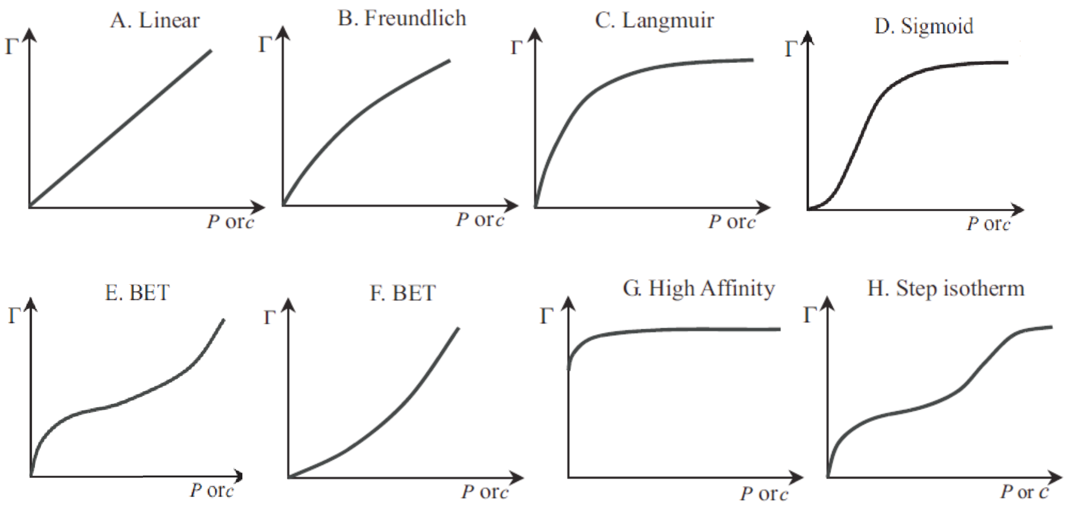

Figure 2.5. Eight types of adsorption isotherms commonly observed. In the case of adsorption from the gas phase, the abscissa is the partial pressure (*P*). In the case of liquid phase, the abscissa is the concentration (*c*)[66].

1. The type A is the linear model, which can be used to describe the initial part of many adsorption isotherms. It is described by the Henry equation:

   $$\Gamma = K_H P \quad (2.14$$

   Where Γ is the surface coverage, K_H is the Henry's constant, and P is the partial pressure.
2. Type B describes a heterogeneous systems consisting of high affinity and simultaneously low affinity regions, which feature the Freundlich adsorption isotherm. This model is described by the following equation:

   $$\Gamma = K_F P^q \quad (2.15$$

   Where K_F and q ($q < 1$) are empirical constants for each adsorbent-adsorbate pair.
3. The case C is the Langmuir model and it is described by the Langmuir adsorption isothermal equation:

   $$\theta = \frac{K_L P}{1+K_L P}\,; \qquad \theta = \frac{\Gamma}{\Gamma_{mon}} \quad (2.16$$

   Where θ is the relative coverage, K_L is the Langmuir constant and Γ_{mon} is the maximum amount of adsorbate which, in the Langmuir model, corresponds to a monolayer. The systems featuring a Langmuir adsorption are characterized by saturation at high concentrations. This is the case of molecules adsorbed on metal nanoparticles where. At low concentration, the molecules approach the bi-dimensional surface adsorbing without reaching the Γ_{mon}. Then, increasing gradually the concentration of the solution, the amount of molecules adsorbed increases until the surface filling and the isothermal curve reaches the plateau. In this case the binding energy does not depends of the presence of other bounded molecules[67].

4. The case D indicates cooperative effects. The molecule interacts better with the surface when another molecule is yet adsorbed due to lateral interactions between the adsorbate and the adsorpt.
5. The type E is the BET (Brunauer, Emmet and Teller) adsorption isotherm. It is quite similar to the previously discovered Langmuir model but extended to a multilayer adsorption. According to this model, the adsorpt interacts first with the adsorbent and then with the adsorbate. In other words, the molecules first form a Langmuir monolayer and then, increasing the concentration or the pressure, the free molecules interact with the ones yet adsorbed, forming a second layer and so on. This kind of isotherm is characterized by two constants: K_{ad}, describing the interaction between the molecule and the surface, and K_2 ($<<$ K_{ad}), describing the intermolecular interaction. If the affinity of a molecule for the substrate is weaker than its affinity for a yet adsorbed molecule (when $K_2 >>$ K_{ad}), the type F is expected[68]. In figure 2.6 the schematic drawing of the Langmuir and the BET isothermal processes are reported.
6. The type G is a high-affinity adsorption isotherm and occurs when the molecules binds very strongly the surface.
7. Finally, type E is a step isotherm. It is a variation of the BET model but the number of layers that can be formed is limited. This curve is typical, for instance, of porous materials. At low pressure a Langmuir monolayer is adsorbed, then a second layer is formed which fills the pores and therefore inhibits the formation of a subsequent layer[66].

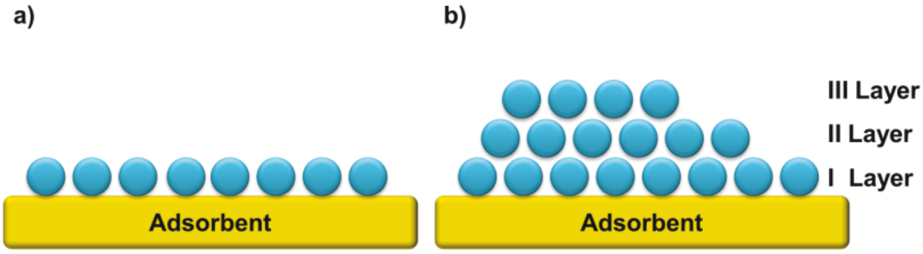

Figure 2.6. Schematic drawing of a) the Langmuir adsorption model (at the saturation point) and b) the multilayer BET adsorption model.

Since the adsorption, as described above, occurs only through an interaction between the adsorbate and the adsorbent, the molecules must have functional groups with some degree of affinity for the metal structure in order to be adsorbed, and hence detected with the SERS technique[69].

For an analyte adsorbed on a SERS substrate, the variation of the SERS signal with the concentration can be fitted with an isotherm adsorption model. In the simplest case of an interaction between a metal nanoparticle and a molecule that does not interact with others, the adsorption process, hence the signal-concentration response is a Langmuir model. The Langmuir isotherm (as I will report in the next two chapters and as reported in several works of analytes quantification through SERS technique[18,22,59,70–72]) is one of the most common models for a SERS system. This is because the molecules, for being detected, must be adsorbed or be in a close proximity to the metal surface, and so just the first layer of the NPs can be "felt" by the metallic nanostructure. This model can be applied when the system deals with a chemisorption equilibrium phenomenon in which the surface is characterized by a fixed number of binding sites. This model features a first linear part in which the molecule concentration increase linearly with the signal, then the signal becomes flat when the surface saturation is reached. Thus, within the linear range of this pattern, is it possible to determine the amount of a specific analyte in solution, therefore, to use the SERS technique as a quantitative tool. Moreover, the trend of the isotherm can provide information about the SERS substrate morphology, the analyte-substrate interaction and the analyte-analyte interaction, as will be discussed in the next chapter of this thesis.

2.6 SERS as a tool for quantitative analysis: potential, issues and limitations.

For specific concentration intervals (i.e. when adsorption sites are still available), the intensity of a band in a SERS spectrum correlates with the concentration of the analyte. The SERS technique can be therefore used as a quantitative technique. In a univariate SERS calibration curve, the intensity of the SERS signal is plotted against the analyte concentration, establishing an empirical correlation between these two quantities. The nature of this correlation, hence the shape of the signal-concentration graph, depends on the nature of the adsorption process, as explained in the paragraph 2.5. Moreover, the molecular fingerprint provided by Raman spectroscopy, allows the identification of one or more bands belonging to a specific molecule even if the analyte is present in a complex mixture. This makes possible the use of SERS as quantitative tool for a specific analyte even if it is present in complex mixtures (i.e. anticancer drugs in human serum).

In figure 2.7, graphics showing the number of the publications founded in Scopus vs years are reported using as search key words “SERS” and “SERS AND quantitative”. It is interesting to see that the publications about the use of SERS as a quantitative technique are approximatively the 8% of the total documents present about SERS.

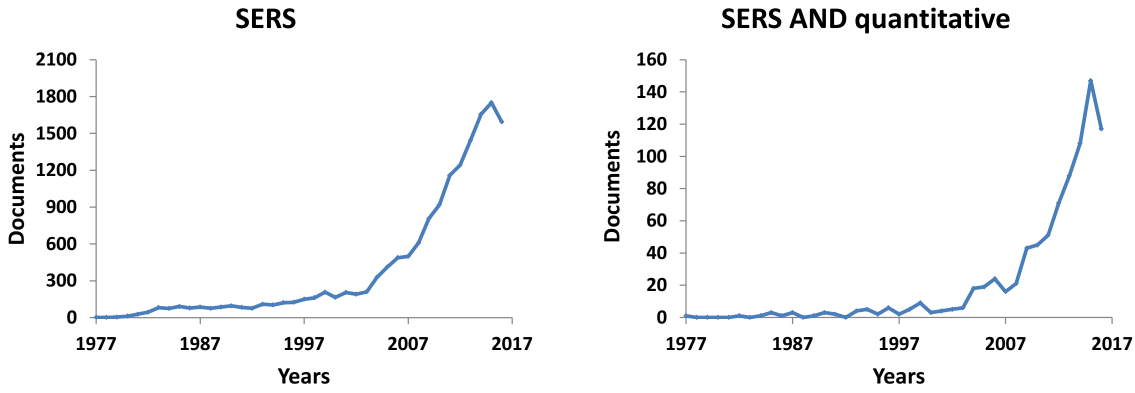

Figure 2.7. Graphics calculated from Scopus showing the number of documents for year using the key words “SERS” (on the left) and “SERS AND quantitative” (on the right).

Despite all the advantages and potentialities of the SERS technique, it is therefore important to underline the limitations of the use of SERS for quantitative purposes, which have so far hindered the use of such kind of technique for routine measurements.

First of all, the analyte must be adsorbed or be in a very closed proximity of the metal nanostructure, otherwise SERS will not occur. Not all the molecules feature affinity for all the substrates, therefore it is necessary to find the “right” substrate for each molecule. Secondly, there is a substantial difference between a colloidal and a non-colloidal SERS substrate. In general, the overall surface available for adsorption *per volume units* is larger in the case of colloidal substrates, resulting in a more intense

SERS spectrum. In a fixed system (i.e. non-colloidal substrates) the molecules have not physically access to the whole surface of the nanostructure: in the case of NPs adsorbed on paper, for instance, a surface moiety is employed with the adsorption on to the cellulose fibers. Moreover, the liquid medium allows Brownian motions of the NPs aggregates in the focal volume probed by the exciting laser: this phenomenon contributes to average the signal over several hot-spots entering and leaving the focal volume during the measuring time, lowering the inter-spectra variability. In a previous work, we investigated the variability of the SERS measurements using different colloidal substrates[11]; in particular, we found a variability of 1 - 6 % depending on the experimental parameters (i.e. kind of metal, wavelength of the laser and capping agent). Those values, for instance, are quite lower in respect to those reported for Au and Ag NPs non-colloidal substrates[13,73]. However, it is important to underline the problems regarding the repeatability (the ability of an operator to consistently repeat the same experiment under the same conditions) and the reproducibility (the variation in measurements made on a subject under changing conditions)[24] of the synthesis batches of colloidal dispersions. To achieve a low variability in the SERS measurements, in fact, the shape and dimensions dispersion should be narrow. This highly depends on the experimental conditions such as temperature, humidity, stirring rate, etc[74], which lead to a low inter-batch reproducibility and repeatability[52].

Besides the batch repeatability problems, for non-colloidal substrates all the advantages of the colloidal dispersions (i.e. higher surface available for the adsorption and Brownian motions) are lost. For instance, if we consider the non-colloidal substrates developed through bottom-up approaches (i.e. NPs loaded to filter paper by dip coating method), the repeatability problem affects i) the colloidal synthesis, ii) the substrates production, which is highly influenced by the operator, and finally iii) the samples measurements. Generally, in literature there is a lack of information about the repeatability of paper-made SERS substrates in view of quantitative applications. In most of the cases the repeatability is not discussed at all[14,19–23] or only the intra- or the inter- sample repeatability is reported[13,15,73,75,76]. Moreover, for paper-made substrates, there are still no works about how the interplay of the experimental parameters (i.e. the kind of the NPs, the concentration of the colloidal solutions, the wavelength of the laser and the porosity of the paper), leads to different results in terms of repeatability of the measurements.

With regard to this aspect, in the next chapter I will present the core of this thesis: a systematic study based on repeatability (intra- sample, hence on the homogeneity and inter- sample) analysis on Ag and Au NPs loaded on filter paper. The aim is optimize such kind of non-colloidal substrates for quantitative analysis in a repeatability point of view, hence the development of substrates which lead to the lowest signal variation with the dip-coating method.

Chapter 3

Development and characterization of solid SERS substrates for quantitative analysis

3.1 Introduction

In this chapter the preparation, the optimization and the characterization of paper-made solid SERS substrates loaded with different kind of NPs will be presented, from a repeatability point of view. In fact, the aim of this work is to obtain reliable, repeatable, cost-efficient, easy to produce and scalable solid SERS substrates as a platform for quantitative analysis.

As discussed in the chapter 2, not all molecules present the same affinity for all kind of metals. As consequence, it is necessary to develop different kind of NPs, tuning the shape, the metal type and the capping agent depending on the analyte, which have to be detected with the SERS technique.

For this purpose, four kinds of substrates characterized by different NPs loaded on filter paper (with the so called dip-coating method[14,20,77]) will be presented: i) sodium citrate-capped Ag (c-Ag) and ii) Au (c-Au) NPs, iii) hydroxylamine reduced Ag NPs (h-Ag) and iv) sodium citrate capped Ag NSs (nanostars).

The dip-coating procedure consists of dipping a piece of common filter paper onto a colloidal solution for few days. During this time, the NPs adsorb onto the cellulose fibers of the paper; then, after the supernatant removal, the substrates are then left in the vials and dried for a few hours in air at room temperature. Then, the substrates are ready to be used. This method was chosen for being a simple and cost-efficient technique: it allows scalable substrates preparation without the necessity of specific laboratory equipment. In fact, the substrates obtained with this method do not require any complex fabrication methodology as physical vapor deposition, electron beam lithography, focused ion beam (FIB), electrochemical deposition or roughening[53,78]. Moreover, in contrast with the in situ synthesis[23,59], it allows a better control of the tuning of the metal, in size and shape, and the capping of the NPs[13–16].

Common filter paper was chosen as solid support because, besides its low-cost, it ensures many more intrinsic advantages and analytical applications for a SERS substrate compared to a bi-dimensional flexible (i.e. PDMS[79]) and non-flexible surfaces (i.e. glass and silicon wafer[14]). Thanks to its porosity and flexibility, it can be used as a swab[20] or in a paper analytical device (PAD[60,80,81]), providing a detection of a target analyte present in a complex mixture[82]. Moreover, the three-dimensional structure of the paper ensures an intra- and inter- layer (formed by the net of the cellulose fibers) plasmon coupling[14], enhancing even more the SERS signal, hence increasing the substrate sensitivity and efficiency.

Nevertheless, the main issue regarding the use of solid SERS substrates developed with a bottom-up self-assembling approach (such as NPs loaded on paper) is the low repeatability. Despite the promising results obtained so far on paper-based solid SERS substrates[13,15–18,83], there is a lack of information about how experimental conditions affect their repeatability in view of quantitative applications. The interplay of the type of the NPs, the concentration of the colloidal dispersions used for the dip-coating step, the wavelength of the laser and the porosity of the paper leads to different results in terms of both overall intensity and repeatability of the measurements.

In order to overcome this issue, I firstly performed a systematic study focused on repeatability (intra- sample, hence on the homogeneity, and inter- sample) analysis on c-Ag and c-Au NPs loaded on filter paper. The task of evaluating the repeatability of a solid SERS substrate is, in itself, nontrivial. Different types, or levels, of repeatability are involved, depending on what set of measurements have to be considered (intra- or inter- substrate).

The aim of this study is to explore how a series of parameters (e.g. concentration of colloidal solution, different porosity of filter paper and the presence of an aggregating agent) affect the analytical performance of the substrates.

Within the experiments, the following parameters were varied in different combinations: i) the porosity of the filter paper, ii) the concentration of metal colloids, iii) the presence of an aggregating agent and iv) the wavelength of the laser source. In particular, a filter paper with pore size of 2 µm and 20 – 25 µm was used in order to investigate which porosity provides the better substrate in terms of overall intensity and both intra- and inter- sample repeatability. For the same reason, we used "as prepared" NPs, as well as concentrated ones. Moreover, we analyzed SERS substrates prepared with or without the presence of sodium citrate as aggregating agent. For electrostatically stabilized NPs, the role of the aggregating agent, which can be an organic or inorganic (such as sodium citrate, HCl, KNO_3, etc.), is to break the potential barrier formed by the stabilizer (see section 2.4). The increasing of the ionic strength induces the aggregation of the NPs, the formation of the "hot spots" and finally their precipitation and adsorption on to the solid support. Mehn and coworkers, for instance, report a study in which Au NSs are induced to adsorb on to the filter paper using sodium citrate as aggregating agent[15], while Hasi et al. employ chloride ions to prepare Ag NPs paper-based SERS substrates[13].

All the substrates developed in the systematic study were analyzed with two off-resonant probe molecules, 4-Mercaptobenzoic acid (4-MBA) and Adenine. The reason for this choice is outlined below, in the section 3.2.3. The substrates were analyzed in terms of i) inter- sample repeatability, ii) intra- sample repeatability, iii) sensitivity, iv) long-term stability and v) overall SERS performance from a quantification point of view.

Another important issue regarding the state of the art of solid SERS substrates (in particular paper based), is the lack of standard protocols supported by adequate statistics. So far, in some cases authors use the relative standard deviation (RSD, also known as coefficient of variation or CV) of the intensity or the area of a SERS band, reporting only the RSD values, without a graphical comparison or a statistical discussion[59,71,75,76,83,84]. Moreover, in most of the cases the repeatability analysis of the samples is not complete, since only the intra- or the inter- sample one is reported[13,15,73,75,76]. Finally, in most of the cases the repeatability is not discussed at all[14,19–23].

Another controversial point is how the spectra were collected for a statistical analysis and discussion. The spectra collected over a solid substrate, in particular the low number of the spectra, could affect the reliability of the repeatability results. So far, spectra are almost always acquired on few (5 – 20) random spots on the substrate, leading to an inaccurate intra- sample repeatability characterization[13,59,71,73,75,76,84–86]. Wang and coworkers, for instance, report an intra- sample repeatability calculated from the RSD obtained on 8 spectra[86]. Villa et al. report an inter- sample repeatability calculated from 5 spectra on 3 different samples[76]. In other works the number of the acquired spectra from which the RSD were calculated is not reported at all[59,71]. Finally, for what concern SERS paper-made substrates commercially available, Ocean Optics company produces Au NPs immobilized on filter paper as SERS sensors. However, the provided data show an intra- and inter- sample repeatability calculated from 5 spectra on 6 different samples. Despite the low values of RSD reported (13% for the intra- and 8% for the inter- saple repeatability), the characterization performed could be unreliable for quantitative analysis[87].

For this reason, in this work the RSD for each sample was calculated from the acquisition of a map (an equally-spaced fixed grid of spectra) consisting of 64 spectra. By doing so, it is possible to scan an adequate region of the sample to reliably evaluate the homogeneity (intra- sample repeatability) of the samples.

To improve the statistical information regarding the graphical representation of both intra- and inter- sample repeatability, the results will be presented and analyzed with Tukey's plots. This kind of box plot allows to visually estimate the distribution of a numerical data set. It is a graphical representation of a variation of a statistical data population, in the specific case the distribution of the mean integrated areas for each spectrum acquired in a map.

The spectra distribution will be discussed in terms of -intra and -inter sample repeatability for each experimental condition. In this way, the development procedure of the dip-coating method was optimized, yielding a paper-made substrates loaded with c-Au and c-Ag NPs for quantitative analysis.

Then, other two kinds of paper-made SERS substrates will be presented, characterized and discussed as well in terms of intra- and inter- sample repeatability: h-Ag and Ag NSs loaded filter paper.

The study regarding the Ag NSs loaded filter paper and colloidal repeatability was performed at IEM-CSIC (Instituto de Estructura de la Materia, Consejo Superior de Investigación Cientifica) in Madrid, with the collaboration of the group of Dr. Santiago Sanchez Cortés.

h-Ag and Ag NSs were developed with the optimized procedure of dip-coating method obtained from the systematic study. The only exceptions are the use of “as prepared” colloidal dispersions and, in the case of h-Ag substrates, the use of KNO_3 as aggregating agent (the reason of this choice will be explained in the next section). However, applying the same procedure to different NPs does not necessarily result in a better repeatability. In this sense, another systematic study should be performed on each kind of new substrate. For the sake of time, I assumed that the optimal conditions found for c-Ag and c-Au substrates might be applied as well for the preparation of h-Ag and Ag NSs.

3.2 Experimental section

3.2.1 Materials and reagents

All chemicals, solvents and the filter paper with 20 μm of pore size (qualitative filter paper, grade 4 Whatman) were purchased from Sigma-Aldrich and used as received. Filter paper with 2 μm of pore size (qualitative filter paper, 410) where purchase from VWR international (Milan, Italy). Phosphate buffered saline solution (PBS) (pH 7.4) was prepared by dissolving one PBS tablet (Sigma-Aldrich) in Milli-Q water (200 mL). All glassware used for NPs preparation was carefully cleaned with aqua regia and thoroughly rinsed with Milli-Q water. For all cleaning procedures and preparation of solutions, Milli-Q water was used.

3.2.2 Paper-made SERS substrates preparation

c-Au NPs were synthesized according to a protocol described by Turkevich et al.[63]. Briefly, 10.6 mg of $NaAuCl_4$ were dissolved in 25 mL of Milli-Q water and heated to boiling. Of the solution, 750 μL of 1% sodium citrate were then rapidly added under vigorous magnetic stirring. The solution was kept boiling under stirring for 20 min.

c-Ag NPs were synthesized according to a protocol described by Lee-Meisel et al.[64]. Briefly, 45 mg of $AgNO_3$ were dissolved in 250 mL of Milli-Q water and heated to boiling. Five milliliters of a 1% sodium citrate tribasic solution were then added dropwise to the $AgNO_3$ solution under vigorous magnetic stirring. The solution was kept boiling under stirring for 1 hour. Both Au and Ag colloidal solutions obtained were stored in dark at RT and were stable for at least 8 months.

h-Ag NPs were prepared by the Leopold-Lendl method[65]. Briefly, 0.017 g of $AgNO_3$ were dissolved in 90 mL Milli-Q water, to which a solution consisting of 0.021 g of hydroxylamine hydrochloride and 18 mg of NaOH dissolved in 9.5 mL of Milli-Q water was rapidly added under stirring. After few seconds, silver colloids were obtained which were stable for at least 1 week (stored in dark at RT)[88].

Ag NSs were prepared according to a protocol described by Garcia-Leis et al.[35] The NPs were obtained by chemical reduction of Ag^+ in two steps and using as reducing agent neutral hydroxylamine in a first stage and sodium citrate in a second step. Briefly, 500 μL of neutral hydroxylamine $6.02 \cdot 10^{-2}$ M was mixed with 500 μL of NaOH (0.05 M). Afterward, 9 mL of $AgNO_3$ $1.1 \cdot 10^{-3}$ M was added dropwise to the first solution under stirring. The suspension became brown. After 5 min, 100 μL of 1% sodium citrate tribasic solution was added rapidly to the mixture. The final suspension, showing a dark gray color, was shaken for 15 min before its storage in dark at RT.

The c-Ag and c-Au colloidal solutions obtained were concentrated using a minispin Eppendorf centrifuge for 30 minutes at 6000 rpm (2415 g) and 10000 rpm (6708 g) for c-Au and c-Ag NPs respectively. Thus, the supernatant solutions above the NPs pellets were removed in order to reach a solution concentrated 10 times in volume.

For the systematic study, 8 different types of solid SERS substrates were prepared for both c-Au NPs and c-Ag NPs; in particular: i) with not concentrated (i.e. as prepared) NPs and with a filter paper with 2 μm of pore size, ii) with 10 times in volume concentrated NPs and with a filter paper with 2 μm of pore size, iii) with not concentrated NPs and with a filter paper with 20 μm of pore size, iv) with 10 times in volume NPs with a filter paper with 20 μm of pore size. All these types of substrates were also prepared in the presence of 20 mM sodium citrate as aggregating agent. The choice of sodium citrate as aggregating agent is due to two different reasons: i) citrate ions are already adsorbed onto the NPs surfaces from the synthesis reaction, ii) citrate adsorbs onto the NPs surfaces through relatively weak bonds, allowing the exchange with the target molecule, hence its SERS detection.

For the substrates prepared with the aggregating agent, a piece of 1 cm^2 of paper with 2 or 20 µm of porosity was placed on the bottom of a cylindrical glass vial (total capacity of 10 mL) containing 3 mL of c-Au or c-Ag colloidal solution (concentrated or not); then the sodium citrate was added up to a final concentration of 20 mM. The presence of the citrate leads to a color change of the colloidal solution from red to grey for Au NPs and from grey to dark grey for Ag NPs, indicating NPs aggregation. The vials containing the colloid and the filter paper were then stocked in dark at RT for one week ("incubation"); during the incubation, the NPs deposited on paper on the vial bottom. After incubation, the colorless, transparent supernatant solution, devoid of nanoparticles, was removed with a plastic syringe, taking extra care not to touch or move the paper substrate. For the substrates developed without the aggregating agent, protocol above explained was applied without the adding of the sodium citrate to the colloidal solution. The substrates were then left in the vials and dried for a few hours in air at RT and then stocked in Milli-Q water until used. If they are dried, the NPs do not detach from the support, indicating the stability of the substrates in liquid environments.

Ag NSs and h-Ag solid SERS substrates were prepared with the same protocol, using as prepared NPs (not concentrated), filter paper with 2 µm of pore size and 20 mM of aggregating agent (sodium citrate for Ag NSs and KNO_3 for h-Ag substrates). With the using of KNO_3 salt, the h-Ag substrates result being citrate-free: there are no background problems generated by the still adsorbed citrate onto the NPs surfaces. Those NPs, in fact, do not show background signals (see figure 3.19-c), as in the case of c-Au NPs (see figure 3.12), whose spectral peaks could interfere with the analyte SERS signals. As second aspect, the analyte has no exchange problems with the sodium citrate in the adsorption process. The analyte, in fact, can adsorb directly to the metal surface without having to remove the capping agent (e.g. sodium citrate) previously adsorbed on the NPs. This aspect is particularly important in the case of molecules featuring less affinity for the metal nanostructure in respect to the pre-adsorbed citrate. Moreover, for those NPs, the chloride ions act as stabilizing agents. The negatively charged surface can be exploited in the adsorption process of positively charged molecules due to the ionic-pair interaction. Moreover, since the chloride ions are smaller than the citrate, is it possible to detect the analyte with SERS, without any exchange process[89].

3.2.3 Analytes preparation for SERS measurements

4-MBA and Adenine were chosen as probe molecules for three reasons. i) The molecules are bound to the metal surfaces through different functional groups (through the thiol for 4-MBA[90] and through the purine nitrogens for Adenine[91,92]). This allows a characterization and a sensitivity study of the substrates for both kinds of chemical interactions. ii) Both analytes are non-resonant (the UV-vis spectra of Adenine and 4-MBA in the UV-vis spectra feature an adsorption band, respectively, at 263 nm[93] and 302 nm[94]). This allows a SERS characterization of the substrates that does not depend on the nature on the analyte but only on the characteristic of the plasmonic structure, hence this characterization is indicative of the substrates repeatability and sensitivity. iii) Both analytes feature a SERS spectra with an isolated, narrow and intense band (740 cm^{-1} for Adenine and 1583 cm^{-1} for 4-MBA) generated by one vibrational normal mode (the ring breathing). This allows the analysis of the band areas without any interference with other bands or convolutions of those, ensuring a better reliability of the results.

Mother solutions 1 mM of 4-MBA and Adenine were prepared dissolving the analytes in MeOH and 1N NaOH, respectively.

For the measurements of repeatability and shelf life of the substrates, the mother solutions were diluted to a final analyte concentration of 10 μM in PBS in order to reach a constant pH of 7.4. The low 10 μM concentration were chose to test the repeatability performance of the substrates were they are used for quantitative analysis. Nevertheless, this concentration could not be any lower to ensure the SERS detection of both analytes with all kind of different substrates and with all the laser sources.

For the calibration curves, further dilutions in PBS of the 10 μM solution were obtained. For all experiments, each substrate (as prepared, 1 cm^2) was cut in 4 pieces of 5 mm x 5 mm, that were incubated for 5 minutes (to test the substrates performance for rapid analysis) in the analyte solution. After the incubation, the samples were gently rinsed with Milli-Q water, in order to remove the molecules not directly adsorbed onto the NPs surface, and then were dried for 15 minutes at RT in air before SERS analysis.

3.2.4 Instrumentation, SERS spectra and images acquisition

Since the concentration, the shape and the diameter distributions are critical factors in the development of repeatable and reproducible substrates, the colloidal dispersions were characterized with different techniques able to quantify all those parameters: UV-visible spectroscopy, TEM (Transmission Electron Microscopy) and NTA (Nanoparticle Tracking Analysis). Then, the SERS substrates were characterized with SEM (Scanning Electron Microscopy) and SERS.

The c-Ag, c-Au and h-Ag colloids were characterized by UV–visible absorption spectroscopy after each preparation using a Lambda 20bio UV–visible spectrometer (Perkin-Elmer, Monza, Italy). The extinction spectra of Ag NSs were recorded on a Shimadzu 3600 spectrometer equipped with a photo-multiplier tube for light detection in the UV−visible range, and an InGaAs detector for the NIR was employed to obtain the plasmon absorption spectra. All spectra were recorded after dilution with Milli-Q water, keeping a constant 1:10 v/v ratio between colloidal dispersion and water. Plastic cuvettes were used to acquire the h-Ag, c-Ag and c-Au spectra and quartz cuvettes for the Ag NSs spectra.

The concentration of the c-Ag and c-Au colloidal dispersions was determined, in collaboration with Prof. Amelia Gamini of the University of Trieste, through the NTA technique (Nanosight LM10, Malvern Instruments, UK), equipped with a 633 nm laser (Malvern).

TEM images of Ag NSs were taken using a JEOL JEM-1011 at Centro Nacional de Biotecnología (CNB), CSIC, Madrid and a Philips EM 208 for c-Ag and c-Au NPs at university of Trieste.

SEM images of Ag NSs paper made substrates were obtained at CNB, CSIC, Madrid using a Hitachi SU-6600, 1 kV voltage acceleration, coupled to an energy dispersive X-ray (EDX) detector.

SEM images of c-Au and c-Ag substrates were obtained at Politecnico of Torino using an in-lens detector of a Zeiss SUPRA 40 (Zeiss SMT, Oberkochen, Germany) field emission electron microscope (FESEM). 5 kV voltage acceleration was used for paper and for Ag-pSi substrates and 10 kV was used for Ag-PDMS substrates.

SERS spectra of c-Ag, c-Au and h-Ag were obtained by means of a Renishaw inVia

Raman microscope (Renishaw plc, Wotton-under-Edge, UK) equipped with a microscope Leica DMLM with a 10× objective (N.A. 0.25). Three laser sources were used to excite the samples: a 785 nm diode laser (Toptica, with a 450 mW output power), a 633 nm HeNe laser (Melles-Griot, 35 mW), and a 514 nm Ar-ion laser (Modulaser, 50 mW). The spectrograph was equipped with a 1200 lines/mm (for 785 nm excitation) or with a 1800 lines/mm (for 514 nm excitation) grating, and a charge-coupled device (CCD) detector. The frequency calibration for all gratings was done using the emission lines of a Ne lamp. Before each measurement, calibration was checked using as reference the 520 cm^{-1} vibrational band of a silicon wafer.

SERS spectra of Ag NSs were collected on a Renishaw Raman InVia spectrometer equipped with an electrically cooled CCD camera. Samples were excited by using the 532 nm laser line provided by a frequency-doubled Nd:YAG laser and a power of 2.5 mW at the sample. A 20× objective (N.A. 0.4) was used for the spectra collection.

To avoid thermal and photodegradation, filters were used to reduce the laser power at the sample. In particular, 0.5% of the laser output power was used for the maps acquired with 785 nm and 532 nm excitation wavelength and 100% of the laser output power was used with 514 nm. Moreover, the laser power density at the sample was decreased for both lasers upon increasing the diameter of the laser spot using the “defocusing” option (at a value of 100%) of the InVia Raman microscope. With an objective of 10× and a defocusing of 100%, the diameter of the laser spot is founded to be 20 μm for both 785 and 514 nm. Such diameters were calculated with the method proposed by Cai and coworkers[95].

To facilitate handling, before each measurement each paper substrate was attached to a standard glass microscope slide. The slide was then immobilized onto the microscope stage.

For the repeatability studies, from each substrate a set of 64 SERS spectra was acquired from a square grid of 8 x 8 spectra, yielding a small map (400 μm × 400 μm area with a 50 μm step). All these maps were recorded using the “static” acquisition mode of the WiRE software, centered on the SERS band of interest. For the analytes under investigation, we chose the most intense bands of the spectra, at 740 cm^{-1} for Adenine and at 1583 cm^{-1} for 4-MBA, corresponding to the ring breathing mode of the molecules[90,92]. In all maps, spectra were recorded using a single scan (5 s of exposure time for each spectrum).

SERS spectra for the calibration curves were recorded using the “extended” acquisition mode of WiRE Software, over a wavenumber range from 600 to 1500 cm^{-1} for Adenine and from 800 to 1700 cm^{-1} for 4-MBA; all spectra were recorded using one accumulation (10 s exposure time) at 7 random locations on the sample.

3.2.5 Data pre-processing, analysis and plotting

All data were collected using the WiRE 3.2 software (Renishaw). Data pre-processing and analysis was performed within the R software[96] environment for statistical computing and graphics building. Special attention was paid to spectral data pre-processing [e.g., offset-Baseline Correction (BC) and Area Normalization (AN)]. The pre-processing workflow consisted of five steps: (i) removal of cosmic rays; (ii) BC; (iii) smoothing interpolation (using a LOESS Local Polynomial Regression Fitting, with a step of 0.5) to increase the signal to noise ratio; (iv) AN; and (v) calculation of median, standard deviation (SD) and relative standard deviation (RSD%).

In particular, data import and export, pre-processing, and visualization (i.e. SERS spectra, Tukey’s plots and calibration curves) were performed with the *hyperSpec* package[97] for R. For BC, a first-order polynomial baseline was automatically fit to the spectral range and subtracted from each spectrum of the dataset using the modpolyfit function from the package *baseline*[98]. *ChemCal* package[99] was used to plot the calibration curves.

In order to obtain a reliable comparison of the area bands obtained with different laser sources, all the spectra were normalized. In particular, the area values of the analytes bands under investigation were normalized with the value of the maximum intensity of the Si band (520 cm^{-1}) recorded with the same laser. Then, data were normalized for the power percentage used for the spectra acquisitions. We chose to normalize the data with the Si band value instead of with the laser power on the sample, in order to consider all the optical path and components, from the laser source to the CCD. By doing so, data obtained with different lasers could be compared, since they were normalized with respect to the spectrograph efficiency (otherwise dependent on the excitation laser used).

3.3 Results and discussion

3.3.1 Systematic study on c-Ag and c-Au paper-made substrates

3.3.1.1 NPs and substrates characterization

After each synthesis, the colloidal solutions were characterized with the UV-visible spectroscopy. The SPB of a metal colloid gives information about the dispersion and average dimension of the NPs, whose variability affects the Raman enhancement. A low repeatability of the colloidal synthesis could therefore lead to a low repeatability of the analyte SERS signal. Consequently, the synthesis repeatability is the first step toward the development of a repeatable solid SERS substrate.

In figure 3.1 UV-visible extinction spectra of three different synthesis batches of both c-Au and c-Ag NPs are reported. c-Au NPs feature a SPB at 540 ± 2 nm, while the Ag NPs at 410 ± 2 nm. All these values are consistent with the values previously reported in literature[74,88,100]. The SPBs featured by the extinction spectra of the different colloidal batches indicate a good repeatability in the shape and dimension of both c-Ag and c-Au NPs.

The colloids were also characterized by TEM. TEM micrographs (see the insets in figure 3.1) show that the Au NPs have a spherical shape with a diameter of 50 nm, while the Ag NPs show a broader shape distribution with respect to the Au NPs, with diameters ranging between 50 and 100 nm.

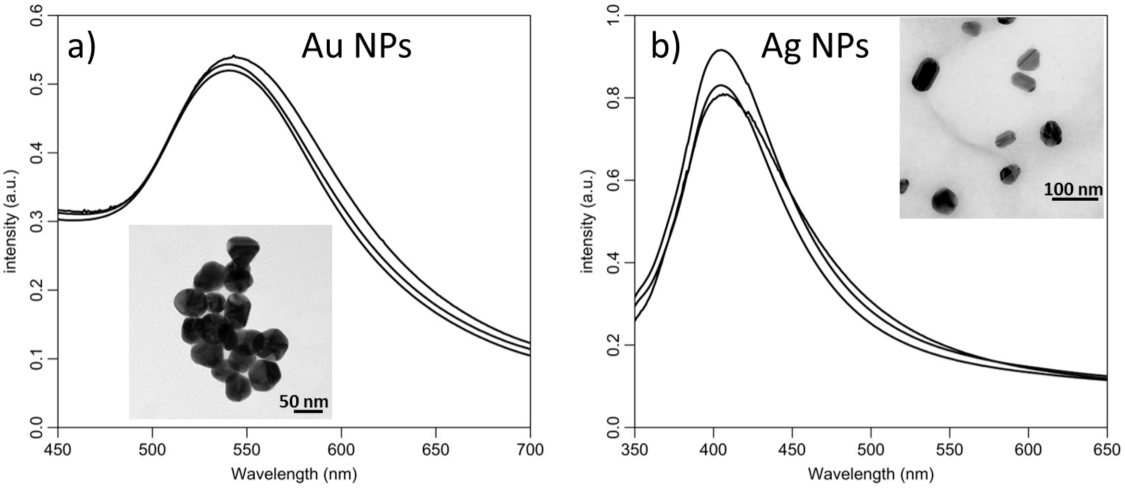

Figure 3.1. UV-visible adsorption spectra over 3 synthesis batches and TEM images (insets) of a) c-Au NPs (TEM images acquired with 100 K of magnification) and b) c-Ag NPs (TEM images acquired with 80 K of magnification).

c-Ag and c-Au SERS solid substrates were characterized with Field Emission Scanning Electron Microscopy (FE-SEM). A FE-SEM comparison of c-Ag and c-Au substrates images at 100 K of magnification is reported in figure 3.2. From the images is it possible to distinguish the different distribution of shape and dimension of the different kind of NPs immobilized on the paper support. While c-Au NPs feature a spherical shape with 50 nm of diameter, the c-Ag NPs are present as spherical NPs, nanowires and nanorods; moreover, such kind of NPs present a larger dimension, in agreement with the data presented in literature[101]. From the TEM and SEM images, it is possible to observe that the shape and dimension of the NPs is conserved during the adsorption process of the NPs onto the cellulose fibers of the paper.

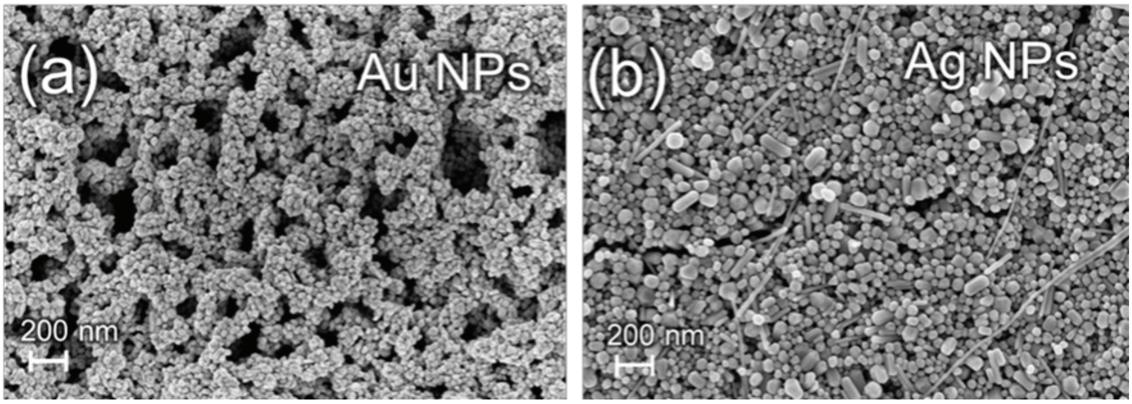

Figure 3.2 FE-SEM images with the same magnification (100 k) of a) c-Au NPs, as prepared in of 20 mM sodium citrate and b) c-Ag NPs, 10x concentrated in presence of 20 mM sodium citrate.

In figure 3.3 and 3.4 the FE-SEM images of respectively c-Ag and c-Au are reported, since the substrates were prepared in different conditions. For both c-Au and c-Ag substrates, it is possible to observe the effect of both concentrations of the colloidal dispersion and presence of an aggregating agent on the overall final NPs density on the paper surface. The amount of NPs adsorbed onto the cellulose fibers increases with both concentration (as already observed by Ngo et al.[14]) and presence of sodium citrate, consistently with the results of Mehn et al.[15]. Moreover, from the images reported in figure 3.3 and 3.4, it is evident that these two elements act synergistically on the NPs deposition process. Despite what claimed by Hasi et al.[13], the present work demonstrates the possibility of loading Ag NPs citrated-reduced on filter paper with the dip-coating method: the uniform and high density adsorption of the NPs is not hampered by the electrostatic repulsion between the negatively charged citrate caped NPs and the carboxyl groups of the cellulose.

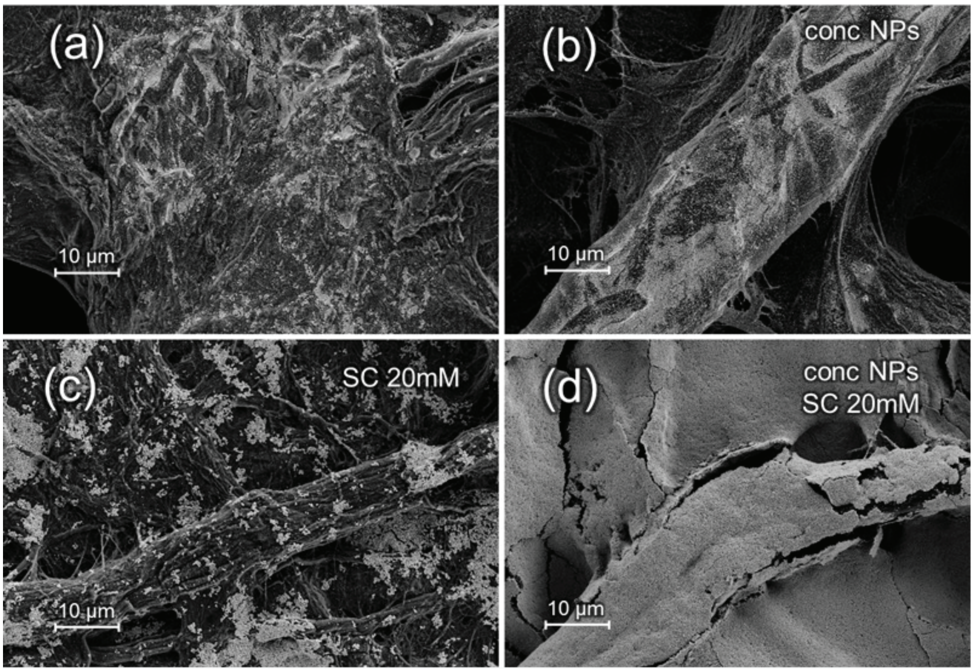

Figure 3.3 FE-SEM images with the same magnification (5 k) of c-Ag NPs, as prepared (a, c) or 10x concentrated (b, d), loaded on filter paper in absence (a, b) or presence (c, d) of 20 mM sodium citrate (SC).

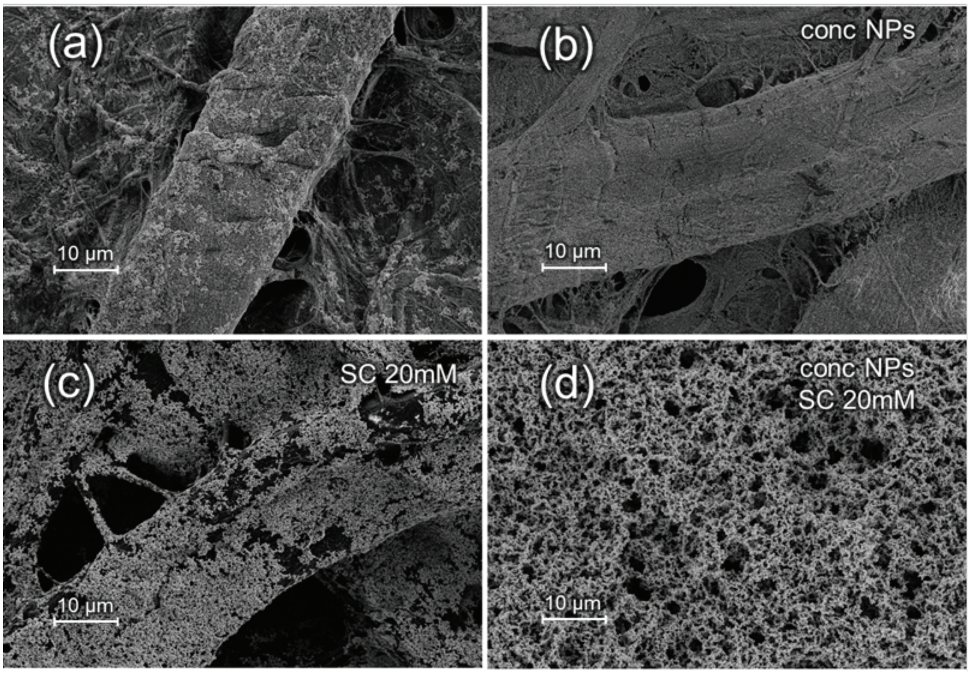

Figure 3.4 FE-SEM images with the same magnification (5 k) of c-Au NPs, as prepared (a, c) or 10x concentrated (b, d), loaded on filter paper in absence (a, b) or presence (c, d) of 20 mM sodium citrate (SC).

3.3.1.2 Effect of paper porosity, aggregating agent and NPs concentration on substrates repeatability

The c-Ag and c-Au substrates obtained in different conditions of colloid concentration, paper porosity and presence of sodium citrate were investigated in terms of intra- and inter- samples repeatability.

Raman mapping of four replicas of each type of c-Ag and c-Au substrates were performed after samples incubation in 4-MBA and Adenine PBS solutions. For all c-Ag substrates, SERS maps were collected with the 514 nm and 785 nm excitation wavelengths; for c-Au substrates, since neither 4-MBA nor Adenine spectral signature could be detected at 514 nm, all the data were collected with 785 nm laser.

In figure 3.5 we report, as examples, the map-averaged SERS spectra of Adenine and 4-MBA obtained from “as prepared” Au and Ag colloids deposited on a filter paper with an average porosity of 2 µm, in presence of sodium citrate as aggregating agent.

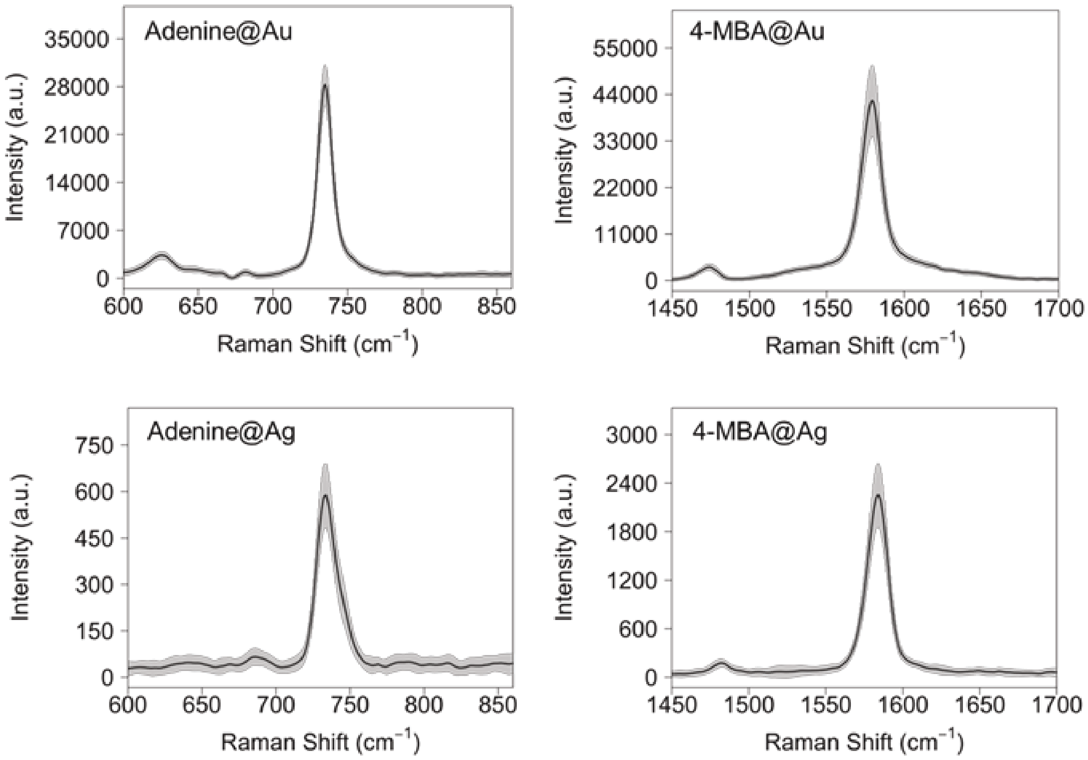

Figure 3.5. Mean SERS spectra of adenine and 4-MBA acquired on c-Au and c-Ag substrates, calculated from maps consisting of 64 spectra acquired at 785 nm for the c-Au substrates and at 514 nm for the c-Ag substrates. Shaded areas represent +/-1 intensity standard deviation (SD).

The results in terms of intra- and inter- sample intensity repeatability for each kind of substrate, excitation wavelength and probe molecule were compared in the Tukey's box plot reported in figure 3.6. We quantified both intra- and inter- sample repeatability and represented it graphically in this figure 3.6, using RSD%. The RSD% was calculated with equation 3.1, dividing the standard deviation (SD) with the average signal (M) obtained from the maps:

$$\mathrm{RSD}(\%) = \frac{\mathrm{SD}}{\mathrm{M}} \cdot 100 \qquad (3.1$$

In particular, for the intra- sample repeatability values, SD and M were the standard deviation and the mean integrated area calculated from the 64 spectra acquired for each map. For the inter- sample repeatability, the RSD values were evaluated among the 4 replicas sharing the same experimental conditions; in this case SD and M were calculated with the mean values of the 4 distributions.

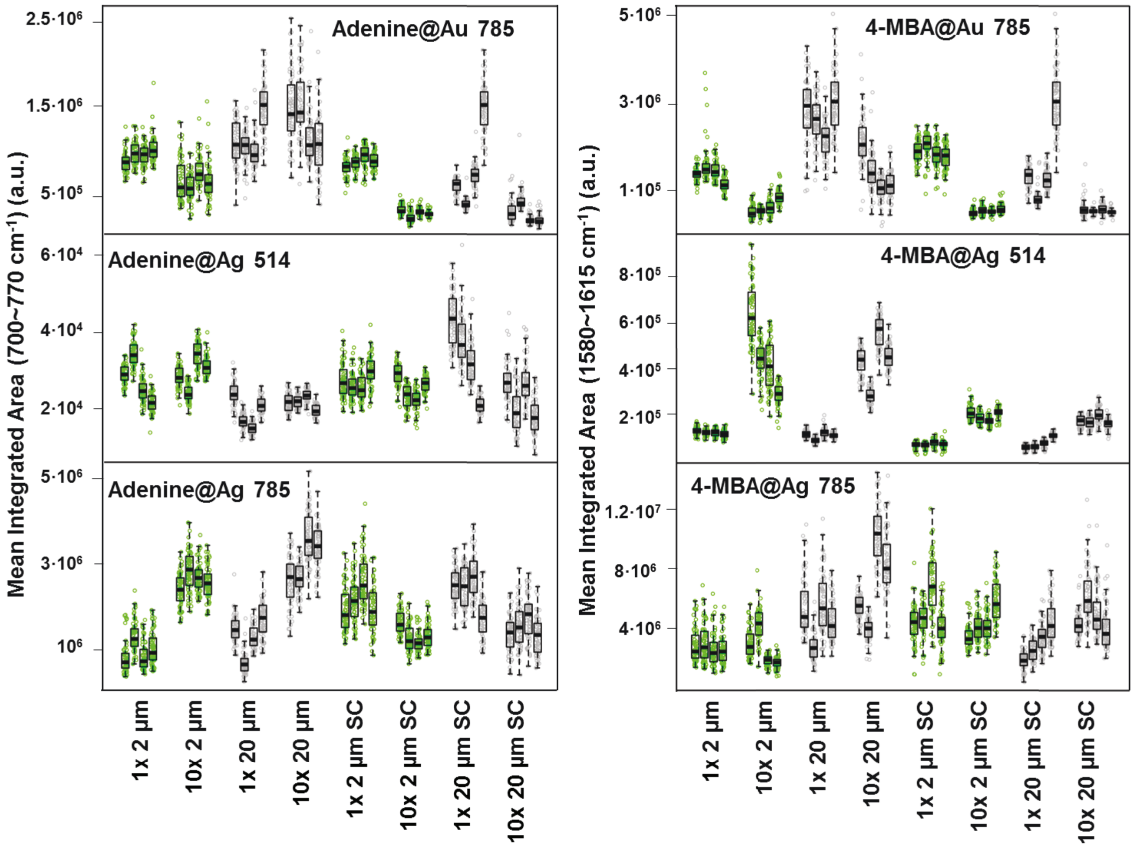

Figure 3.6. Comparison of the distributions of SERS intensities integrated over the area of the Adenine and 4-MBA band. Each column (box) represents the complete distribution of integrated intensities, calculated over a SERS maps for different substrates, grouped according to analyte, metal and excitation wavelength, with 4 replicas for each group. For the distributions, the intra- and inter- sample Relative Standard Deviation (RSD%) values are reported in Tables 3.1-3.3. Different colors correspond to different paper porosity (green for 2 µm, grey for 20 um). Along the median value, the first and the third quartiles of the data distributions are indicated, as bottom and top of the boxes. 1x and 10x correspond to non-concentrate and concentrate colloidal dispersion, respectively; 2 µm and 20 µm to the porosity of the paper and SC is referred to Sodium Citrate.

In figure 3.7 the "aggregated" distributions (the data for all conditions but one are grouped together in a single dataset) for both analytes in terms of intra- [(A), (B) and (C)] and inter- [(D), (E) and (F)] RSD % are reported. The plotted distributions include all spectra acquired for both analytes, in order to evaluate the difference caused only by the experimental conditions (sodium citrate, NPs concentration and paper porosity), one at a time. In this way it is possible to analyze only the experimental parameters regarding the substrates, irrespectively of the molecule used as probe analyte. The graphics are grouped according to the presence or the absence of sodium citrate [(A), (D)], the NPs concentration [(B), (E)] and the porosity of the paper [(C), (F)]. Furthermore, the distributions are plotted in different colors according to the combination excitation wavelength–NPs: green for c-Ag NPs at 514 nm, blue for c-Ag at 785 nm and red are for c-Au at 785 nm. All the intra- and inter- RSD% values for each molecule are reported in tables 3.1-3.3.

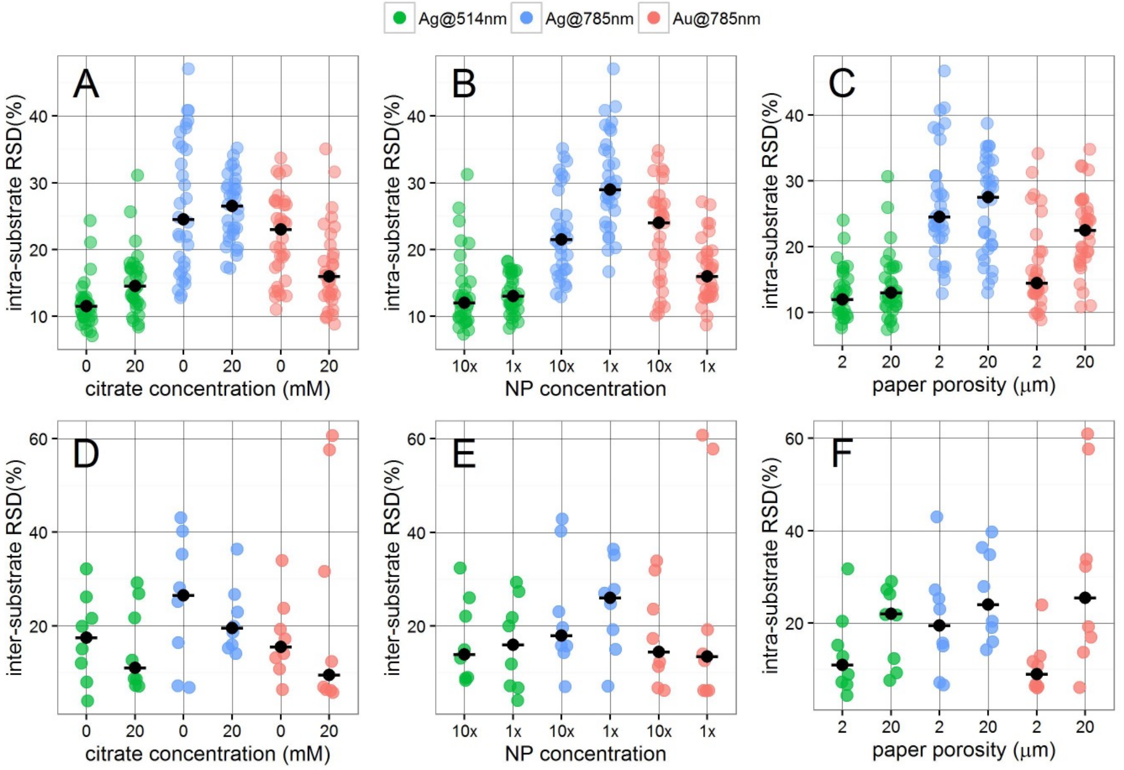

Figure 3.7. Comparison of the distributions of RSD % and median calculated from the aggregated intensities integrated over the area of the Adenine and 4-MBA band. On top are reported the intra- sample RSD %; at the bottom are plotted the inter- sample RSD % calculated over 4 replicas for each group. Each column represents the complete distribution of RSD %, calculated over a SERS maps for different substrates and grouped according to the presence of the aggregating agent, the NPs concentration and the porosity of the paper. For the distributions, the intra- and inter- sample Relative Standard Deviation (RSD%) values are reported in Tables 3.1-3.3. Different colors correspond to different combination NPs-excitation wavelength (in green: c-Ag-514nm, in blue: c-Ag-785 nm, in red: c-Au-785 nm).

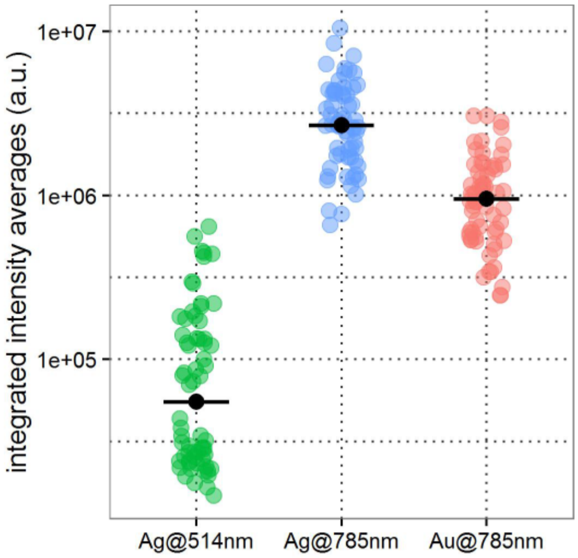

Figure 3.8 Comparison of the aggregated distributions and median calculated from mean integrated area over the Adenine and 4-MBA band for each collected map. Different colors correspond to different combination NPs-excitation wavelength (in green: c-Ag-514nm, in blue: c-Ag-785 nm, in red: c-Au-785 nm).

c-Au substrates	**785 nm**		**RDS % intra sample (RSD % inter-sample)**	
	Porosity	**NPs Concentration**	**No Citrate**	**Citrate**
4-MBA	**2µm**	**1x**	10.8, 27.3, 14.1, 14.3 (13.4)	12, 13.7, 16.2, 15.6 (6.2)
		10x	27.9, 14.3, 26.9, 19.4 (23.7)	14.7, 16.0, 10.4, 17.9 (7.3)
	20 µm	**1x**	27.5, 19.8, 20.4, 23.7 (14.4)	17.9, 22.7, 18.2, 23.7 (60.6)
		10x	27.5, 32.0, 25.3, 26.6 (34.1)	32.0, 11.3, 21.1, 11.5 (6.4)
Adenine	**2µm**	**1x**	13.4, 12.6, 12.5, 14.8 (6.1)	12.5, 9.3, 12.8, 9.8 (6.0)
		10x	34.3, 24.5, 19.4, 31.5 (10.7)	14.9, 21.6, 11.7, 9.8 (11.7)
	20 µm	**1x**	21.8, 17.0, 18.4, 18.5 (19.3)	13.8, 13.4, 17.3, 18.5 (57.6)
		10x	26.6, 24.2, 24.0, 31.5 (17.0)	35.3, 25.6, 18.9, 24.5 (32.3)

Table 3.1. Intra- and inter- sample repeatability values (RSD) of the 4-MBA band area between 1550 ~ 1615 cm^{-1}, and of the Adenine band area, between 700 ~ 770 cm^{-1}, calculated from SERS maps for all kind of c-Au substrates. The spectra have been acquired at 785 nm. The inter- sample repeatability was obtained from the integrated intensity averages calculated for each map of the same kind of substrate.

c-Ag substrates	**514 nm**		**RDS % intra sample (RSD % inter-sample)**	
	Porosity	**NPs Concentration**	**No Citrate**	**Citrate**
4-MBA	**2um**	**1x**	11.0, 9.8, 12.1, 12.4 (4.4)	16.7, 15.9, 15.7, 18.3, (6.6)
		10x	21.0, 17.4, 24.0, 15.4 (31.6)	13.9, 11.6, 9.6, 9.4 (9.1)
	20 um	**1x**	12.4, 11.6, 14.1, 9.5 (12.1)	17.8, 16.9, 16.8, 9.5 (26.8)
		10x	12.8, 12.1, 12.8, 11.3 (25.6)	12.8, 13.3, 15.5, 12.5 (9.4)
Adenine	**2um**	**1x**	8.4, 9.7, 12.6, 11.8 (20.0)	16.7, 13.7, 12.8, 13.4 (7.4)
		10x	9.7, 9.1, 9.8, 8.5 (14.7)	10.4, 13.0, 12.2, 8.4 (12.5)
	20 um	**1x**	12.9, 12.3, 10.4, 10.7 (21.8)	15.5, 17.2, 17.0, 10.7 (29.0)
		10x	11.4, 8.2, 7.2, 8.8 (7.6)	19.0, 31.1, 21.4, 26.4 (21.7)

Table 3.2. Intra- and inter- sample repeatability values (relative standard deviation) of the 4-MBA band area between 1550 ~ 1615 cm^{-1}, and of the Adenine band area, between 700 ~ 770 cm^{-1}, calculated from SERS maps for all kind of c-Ag substrates. The spectra have been acquired at 514 nm. The inter- sample repeatability was obtained from the integrated intensity averages calculated for each map of the same kind of substrate.

c-Ag substrates	**785 nm**		**RDS % intra sample (RSD % inter-sample)**	
	Porosity	**NPs Concentration**	**No Citrate**	**Citrate**
4-MBA	**2um**	**1x**	38.1, 41.3, 41.2, 36.0 (6.9)	29.1, 23.3, 27.9, 31.3 (26.9)
		10x	31.3, 24.8, 17.5, 21.1 (42.6)	21.5, 20.7, 22.9, 23.3 (23.4)
	20 um	**1x**	34.5, 32.7, 35.3, 30.1 (28.4)	33.4, 29.5, 28.1, 30.1 (35.6)
		10x	15.0, 18.2, 19.3 15.0 (40.0)	20.0, 29.0, 31.1, 35.3 (20.2)
Adenine	**2um**	**1x**	47.3, 27.8, 38.8, 37.8 (24.7)	26.4, 24.1, 22.5, 28.0 (15.2)
		10x	15.8, 16.9, 12.6, 14.9 (7.4)	16.5, 25.0, 19.3, 22.1 (15.6)
	20 um	**1x**	21.9, 39.0, 21.7, 27.2 (35.2)	17.1, 19.6, 19.6, 27.2 (18.6)
		10x	22.4, 13.3, 16.3, 14.4 (16.3)	33.1, 32.4, 30.0, 34.1 (14.1)

Table 3.3. Intra- and inter- sample repeatability values (relative standard deviation) of the 4-MBA band area between 1550 ~ 1615 cm^{-1}, and of the Adenine band area, between 700 ~ 770 cm^{-1}, calculated from SERS maps for all kind of c-Ag substrates. The spectra have been acquired at 785 nm. The inter- sample repeatability was obtained from the integrated intensity averages calculated for each map of the same kind of substrate.

From the Tukey's plots reported in figure 3.6, the distributions values of RDS% in figure 3.7 and the related values reported on the tables 3.1-3.3, it is possible to draw some conclusions.

In general, the dependence of the inter- sample repeatability is less evident than that of intra- sample (see fig. 3.7). For the intra- sample repeatability, in fact, the change of the parameters (e.g. using not concentrated and concentrated colloidal dispersions) produces a larger variation in the RSD % compared to the one obtained for the inter-sample repeatability. This means that the experimental parameters affect more the homogeneity of the substrates than their intra- sample repeatability, which depends more from their preparation, hence from the operator handling.

Concerning the correlation with the excitation source, it is possible to observe a general effect of the wavelength of the laser on the SERS intensity and RSD on the c-Ag substrates. For the sake of clarity, in figure 3.8 are reported the intensity data (integrated over the areas of the molecules) grouped by excitation wavelength. In this graph, all the distributions calculated for the spectra acquired with the same excitation wavelength and metal type are plotted together. From the figure 3.8 it is evident that c-Ag substrate-785 nm is the combination yielding the most intense spectra (two orders of magnitude larger with respect to the excitation at 514 nm).

This could be explained taking in consideration the EM mechanism and in particular the LSP (Localized Surface Plasmons) of two closely spaced nanoparticles (hot spot). As explain in Chapter 2 (section 2.4), when two NPs interact to each other, their plasmon modes interact electromagnetically as well, resulting in hybridized plasmonic states. Those states are commonly referred as "bright modes", since they can be directly excited and observed with the incident light, and "dark modes"[43].

Since Ag NPs feature a SPR in the visible region (figure 3.1), it is possible to excite their "bright modes" with a 514 nm laser, responsible of the Raman enhancement at this wavelength. Nevertheless, exciting the NPs with a NIR wavelength (785 nm) is it likely that the dark modes are excited as well. Apparently, this leads a larger enhancement of the Raman signal, hence an higher band intensity[42,102].

Despite the weaker intensity, the c-Ag substrate with 514 nm laser yields more repeatable results. In fact, data dispersion reported in figure 3.8 increases by approximately 50% upon near-infrared excitation, especially in the case of intra- sample repeatability. At the moment it is difficult to explain this fact. Possibly, a hypothesis could be tentatively formulated taking in consideration the dark modes. At 785 nm the enhancement is higher compared to the one at 514 nm due to the presence of dark modes. Moving the laser spot at 785 nm from a region rich in hot spots to another poorer one, the difference on the spectra intensity is larger with respect to the same collection at 514 nm. This results in a higher RSD if the substrates are excited at 785 nm.

The data clearly show that the combination yielding the best SERS efficiency in terms of signal intensity is the c-Ag substrate with 785 nm laser. Therefore, this combination could be the best choice for qualitative analysis. For quantitative purposes, we suggest that for c-Ag substrates it is better to use as excitation wavelength the 514 nm laser instead the 785 nm, whereby the intra- sample RSD values increase from 10 ~ 20% to 20 ~ 40%.

On average, the combination c-Ag with 514 nm laser also appears to be less affected by parameters such as NPs concentration, aggregating agent and paper porosity. On the other hand, these parameters seem to affect other metal-laser combinations. In particular, the repeatability of c-Au NPs paper substrate, when excited at 785 nm, improves by using less porous paper and by adding citrate. Using “as prepared” c-Au NPs seems to improve intra-substrate repeatability and to reduce the variability among different replicas.

Substrates developed with a lower porosity filter paper feature better intra- and inter-sample repeatability for both c-Au and c-Ag NPs and for both analytes. These results disagree with the ones observed by Cheng et al.[59] since the authors observed a negligible variation between SERS signals acquired on filter paper with different pore size. This general behavior of the filter paper can be explained with its intrinsic three-dimensional structure. A lower porosity of the paper implies a denser structure of the fibers onto which the NPs can be adsorbed. Thus, within the area illuminated by the laser spot, the surface appears more homogenous and less irregular with respect to the paper with 20 μm of porosity. The consequence is a minor variation of the laser focus, hence a minor variation of the SERS signal from a spectra to another acquired inside the map and from a map to another.

Using a filter paper with 2 μm of pore size as support, both c-Au and c-Ag SERS substrates feature RSD values below 16% with both analytes (see tables 3.1-3.3); such RSD values could allow performing quantitative analysis.

Not always does a parameter affect the repeatability of different types of substrates in same way. For instance, the use of concentrated nanoparticles improves the repeatability of c-Ag NPs substrates, but worsen the repeatability of c-Au NPs. This might be related to the different NPs concentration as found in the "as prepared" metal colloids. c-Au colloids are, in fact, more concentrated than c-Ag colloids, as can be seen in SEM images (fig. 3.3 and 3.4). This is consistent with the NTA experiments performed to measure the colloidal solutions concentrations, from which it can be inferred that Au NPs are one order of magnitude more concentrated compared with the Ag NPs ($5 \cdot 10^9$ NPs/ml for Au and $4 \cdot 10^8$ NPs/ml for Ag).

Ngo et al. observed that, for c-Au paper-made substrates developed with the dip-coating method, the SERS signal increases linearly with the colloidal concentration of Au NPs[14]. In contrast, I observe that the c-Au substrates, obtained with concentrated nanoparticles, feature a lower SERS intensity for both MBA and Adenine and a general larger RSD (see figure 3.7).

This phenomenon could be explained with the 3D structure of the whole substrate and with the relation between paper porosity and the density of the NPs absorbed onto the support. The c-Au substrates made with concentrated colloidal solution presents a denser NPs layer (see FESEM image 3.4). The surface of the paper results almost completely covered by the NPs (see figure 3.4), with the result that the substrate almost loses its three dimensional structure to become a two-dimensional one; as consequence, the laser cannot diffuse below the surface, inside the three dimensional structure of the paper: thus there are less scattered photons which can be collected from hot spots below the surface and the signal becomes less intense. The signal decrease with the c-Au NPs was observed by Villa et al.[76] as well. This behavior indicates that the enhancement coupling between the NPs in the interlayer structure of the support is necessary for a sensitive and efficient substrate.

It is interesting to observe that c-Ag substrates feature a different behavior depending on the analyte. With 4-MBA, in contrast with what observed for Au substrates, the SERS intensity grows increasing the NPs concentration for all the kind of c-Ag substrates, while with Adenine there are no revealing differences on the signal SERS intensity changing the colloidal solution concentration. The lack of correlation between the SERS intensity and the NPs concentration could be explained in terms of analyte-NPs interaction. Adenine is bound less strongly with the metal with respect to 4-MBA and the difference that can be observed changing the parameters is less evident. Moreover, the RSD values vary depending on the other parameters, such as the aggregating agent and the porosity of the paper. On the other hand, the increase of the SERS intensity with the NPs concentration observed with 4-MBA could probably be due to the minor concentration of colloidal solution of the c-Ag NPs obtained from the synthesis with respect to the c-Au NPs.

The citrate effect on the RSD is not as relevant as we expected observing the SEM images reported in figures 3.3 and 3.4. Indeed, those images show a better coverage of the cellulose fibers support when the substrates are prepared in the presence of the aggregating agent. Therefore, we expected a general improvement on the RSD values due to a more homogeneous hot spot distribution, in spite of the fact that, for c-Ag substrates, the intra- and inter- sample repeatability values do not clearly correlate with the presence the aggregating agent. Instead, for the c-Au substrates it is possible to observe a general improvement with the aggregating agent on both intra- and inter-RSD (see table 3.1), which yields a more appropriate substrate for quantitative analysis. This result is in agreement with what observed by Mehn et al.[15]. Moreover, in contrast to what was observed by Ross et al., with c-Au NPs loaded filter paper[83], the signal intensity does not increase dramatically with the use of an aggregating agent. This aspect could be probably explained with the nature of the salt. For this study an organic salt was used, instead an inorganic one as the agent employed by Ross et al. This point to the fact that the nature of the salt used is another parameter to take into account for further studies, since it apparently affects the overall intensity.

Finally, from the Tukey's plots and the values reported on the tables 3.1, 3.2 and 3.3, it is possible to find the best combination of the parameters to develop c-Au and c-Ag substrates in terms of intra- and inter- sample repeatability and SERS intensity. Is it therefore possible to conclude that, independently from the kind of analyte used as probe molecule, the c-Au substrates featuring the best SERS performance for quantitative purposes are developed with i) a filter paper with 2 μm of porosity, ii) in the presence of the aggregating agent and iii) with an "as prepared" (i.e. non concentrated) colloidal dispersion. Such kind of substrates features an intra- sample RSD included between 9% and 16%, and an inter- sample RSD of 6% for the both analytes. For c-Ag NPs, the best substrates were obtained with the same conditions but using a 10x in volume concentrated colloidal solution. Such substrates, with the excitation wavelength at 514 nm, present an intra- sample repeatability between 8% and 14% and an inter- sample repeatability of 9% for 4-MBA and 13% with Adenine.

3.3.1.3 Substrates stability in time

Long term stability experiments were performed on both c-Au and c-Ag substrates in order to study how the intensity of SERS spectra changes in time if the substrates are stocked in air at room temperature. For this shelf-life assessment study, the substrates featuring the best repeatability were chosen (see above), and a 10 μM Adenine solution was chosen as sample.

SERS maps have been acquired in a time interval ranging from day 0, immediately after the removal of the substrates from the water, to day 80.

Tukey's plots of the variation of the SERS signal collected in the Raman maps in time of both c-Au and c-Ag substrates are reported in figure 3.9. All Raman maps were acquired with the same experimental conditions used for the systematic study, reported in the experimental section.

From the Tukey's plots is possible to see a different behavior of the c-Au and c-Ag substrates when they are stocked in air. There are evidences in literature that the signal intensity of the c-Ag substrates with filter paper decreases after 1 to 3 days due to the surface oxidation of the NPs[59,86]. However in agreement with the study of Hasi et al.[85], is it possible to observe that on c-Ag substrates the SERS intensity of the Adenine band seems to decrease after four weeks (figure 3.9-b), while the RSD for the substrates stocked in air increases after one day.

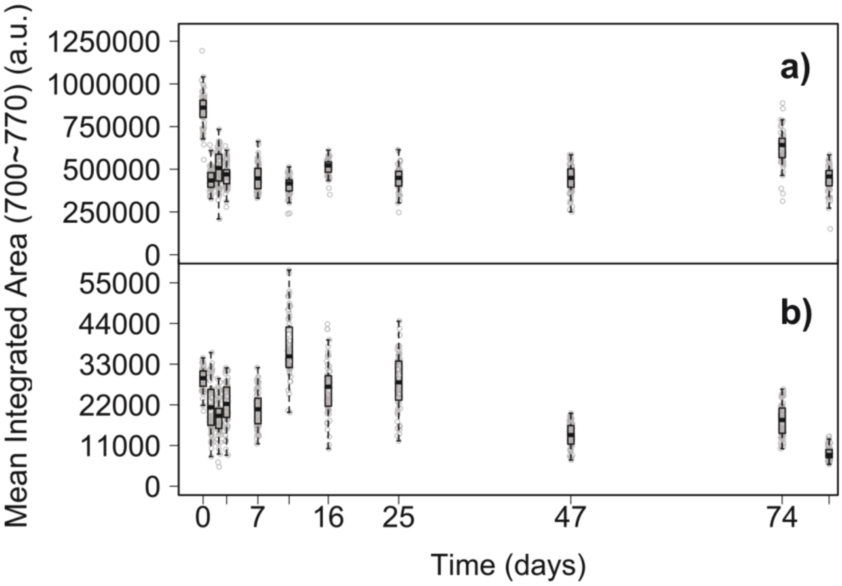

Figure 3.9. Variation in time of SERS integrated band area of the Adenine (700~770 cm-1) on a) c-Au substrates, acquired at 785 nm, and on b) c-Ag substrates, acquired at 514 nm. The measurements were collected from day 0 (fresh substrates) to the day 80. The substrates were stocked in air, at room temperature and in the dark.

The shelf life for c-Au substrates was evaluated for the first time. In this case, differently from what is observed with c-Ag, the signal decreases by 70% after the first day, while the RSD remains constant.

The combined efficiency and uniformity analysis performed among 2 mounts, since the intensity signal decreases quite significantly after the first day for c-Au and after the third week for c-Ag substrates, shows that both substrates should be stock in Milli-Q water to maintain constant their SERS properties. Whereby, an air stocking can affect the efficiency (signal intensity) of c-Au and the repeatability of c-Ag substrates.

3.3.1.4 Enhancement factor calculation

Since its difficult to know the effective SERS active area of the substrates as well as the number of molecules adsorbed on the NPs, a practical enhancement factor (EF) have been determined by the following expression, as reported in literature[21]:

$$\mathrm{EF} = \left(\frac{\mathrm{I_{SERS}}}{\mathrm{I_{Raman}}}\right)\left(\frac{\mathrm{M_{Raman}}}{\mathrm{M_{SERS}}}\right) \qquad (3.2$$

where the intensity I is the average height of a selected band (the 1583 cm^{-1} band of 4-MBA or the 740 cm^{-1} band of Adenine) in normal Raman or SERS spectra, and M is the molarity of the Adenine and 4-MBA solutions. The EF's were calculated for c-Au and c-Ag substrates developed with the optimized conditions (filter paper of 2 μm of porosity, with 20 mM of sodium citrate, with a colloidal solution not concentrated for Au substrates and 10x concentrated for Ag substrates). We thus measured the Raman signal of 10 μM Adenine and 4-MBA on the substrates with c-Ag and c-Au NPs, and the Raman signal of 0.3 M of Adenine and 0.5 M of 4-MBA dried on the substrates without NPs. It was not possible to determine an EF for Ag substrates with the 514 nm laser because of the fluorescence background produced by the scattering of the cellulose with this excitation wavelength, which totally overwhelmed the Raman signal of the analyte on the bare paper support. Therefore, all the spectra for this study were acquired with the laser at 785 nm.

The EF determined this way on c-Au substrates for Adenine and 4-MBA were found to be $4.35 \cdot 10^3$ and $4 \cdot 10^3$, respectively. The EF obtained for c-Ag substrates for both molecules are $2.4 \cdot 10^7$ and $3.2 \cdot 10^7$, respectively. As expected, the practical EFs calculated as previously described for the two analyte are rather similar. Analogous results for non-resonant analytes are reported in literature for spherical Au NPs loaded filter paper[15,83], while for non-spherical Au NPs (i.e. nanorods) the EF reported are quite larger[16,20]. On the other hand, the c-Ag substrates feature an EF two orders of magnitude larger compared with the h-Ag substrates developed by Hasi et al.[13] with hydroxylamine reduction.

3.3.1.5 Adenine and 4-MBA quantification

SERS performance of c-Ag and c-Au substrates in terms of quantitative analysis was assessed by obtaining the calibration curves of Adenine (figure 3.10) and of 4-MBA (figure 3.11).

As in the case of time stability study, the substrates that feature the best SERS performance for quantitative analysis were chosen (i.e. the ones with the lowest RSD).

The adsorption curves were derived plotting the mean integrated area over a SERS band (700 ~ 770 cm^{-1} for Adenine and 1550 ~ 1583 cm^{-1} for 4-MBA) at different concentrations of analyte.

The average SERS spectra of Adenine and 4-MBA on both c-Ag and c-Au substrates are reported in figures 3.10a-b and 3.11a-b. SERS spectra were obtained incubating the substrates in aqueous solutions at different concentration of the analyte, from the lowest detectable concentration up to concentrations where the SERS intensity tend to saturate due to the formation of a monolayer and the depletion of the surface sites available for adsorption. The zero concentration values in the calibration curves were calculated from the background spectra of the substrates without the analyte (reported in figure 3.12).

These two analytes work as model analytes for the application of these substrates to quantitative analysis, and univariate calibration models can be constructed fitting the data with a Langmuir isotherm (as reported in figures 3.10c-d and 3.11c-d). However, the calibration model obtained for 4-MBA on c-Ag substrates (figure 3.11d) seems to work worse: in particular, at high concentrations, the signal intensity slightly decreases, whereas it should remain constant. This could be due to the inter- sample variability, a fluctuation of the laser power or an experimental inaccuracy from the operator. The univariate calibration curve can be constructed as well for specific concentration ranges where the response is linear (insets of figures 3.10c-d and 3.11c-d).

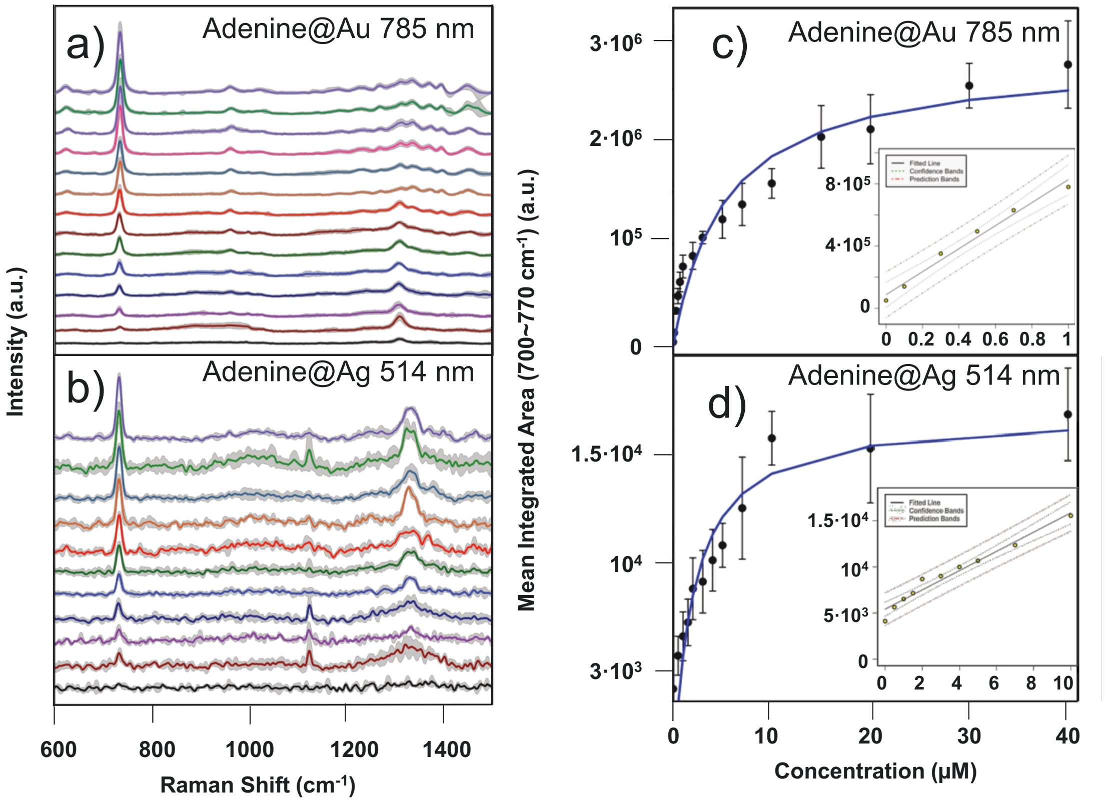

Figure 3.10. Average SERS spectra (+/-1 intensity SD as grey shaded areas) at several concentrations of Adenine on a) c-Au substrates, collected at 785 nm and on b) c-Ag substrates, collected at 514 nm. Adsorption curves of c) Adenine on c-Au and d) on c-Ag, fitted with Langmuir isotherms (error bars represent +/- 1 SD over 7 replicates). In the insets of c) and d) are reported the calibration curves with 95% confidence (uncertainty in the curve estimation) and prediction (uncertainty about the new values on the curve) intervals for concentration ranges with a linear response.

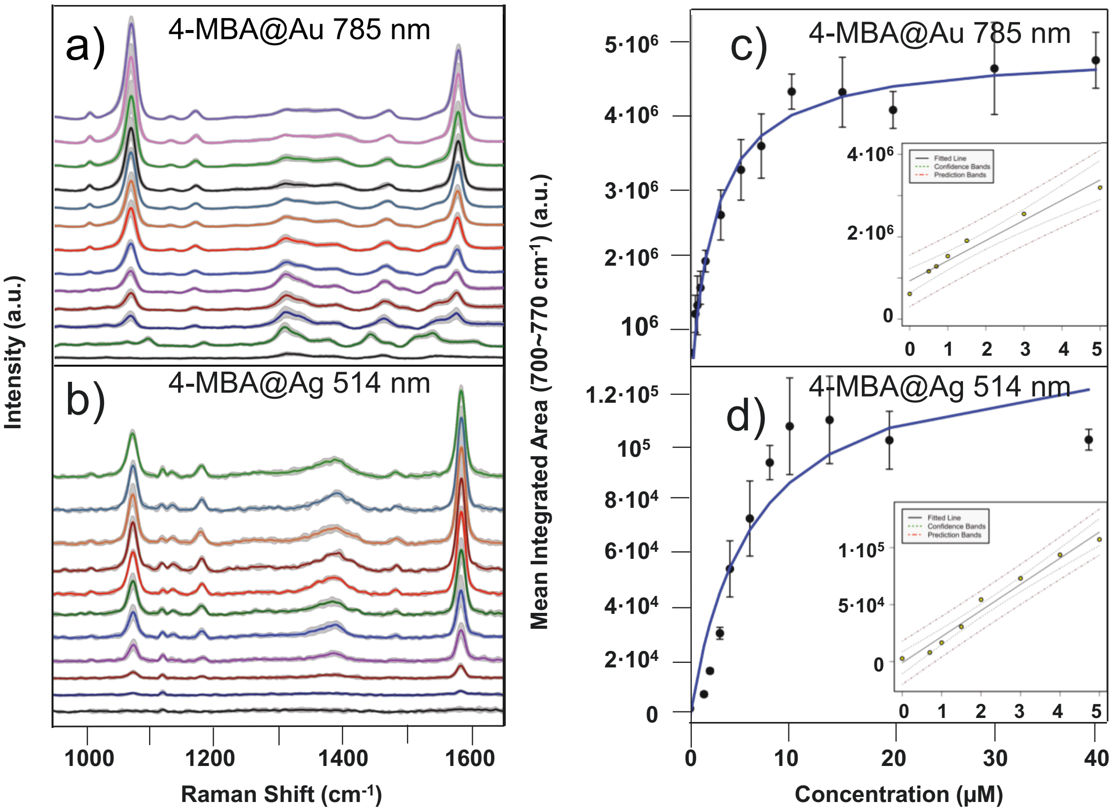

Figure 3.11. Average SERS spectra (+/-1 intensity SD as grey shaded areas) at several concentrations of 4-MBA on a) c-Au substrates, collected at 785 nm and on b) c-Ag substrates, collected at 514 nm. Adsorption curves of c) Adenine on c-Au and d) on c-Ag, fitted with Langmuir isotherms (error bars represent +/- 1 SD over 7 replicates). In the insets of c) and d) are reported the calibration curves with 95% confidence (uncertainty in the curve estimation) and prediction (uncertainty about the new values on the curve) intervals for concentration ranges with a linear response.

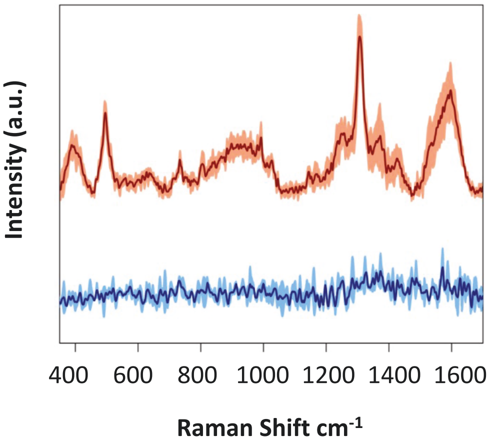

Figure 3.12. Mean and relative standard deviation of the backgrounds of c-Au solid SERS substrate (in red), acquired at 785 nm, and on c-Ag solid SERS substrate (in blue), acquired at 514 nm.

The R^2 values, the LOD (Lower Limit of Detection) and LOQ (Limit of Quantification) are reported in table 3.4 for the two analytes and the two substrates under investigation. Since the LOD values may change with the experimental set up (i.e. soaking time, excitation wavelength and probe analyte) it is difficult to compare the data with the literature. Nevertheless, the LOD values for c-Ag loaded filter paper are similar to the one obtained with picric acid on Ag nanotriangles loaded filter paper (1 µM)[86]. Also the LOD and LOQ values calculated for c-Au are similar to those calculated by Villa et al.; in this case they used c-Au substrates, even if they were obtained with a different method, and employed a similar probe molecule (LOD = 0.18 µM, LOQ = 0.54 µM)[76].

		R^2	LOD (µM)	LOQ (µM)
Au	**Adenine**	0,9753	0,29	0,54
	4-MBA	0,9408	1,95	4,07
Ag	**Adenine**	0,9585	2,65	4,83
	4-MBA	0,9720	1,27	2,27

Table 3.4. R^2, LOD and LOQ values calculated from the linear range of the calibration curves of Adenine and 4-MBA on Ag and Au solid SERS substrates.

It is worth noting that for all analyte-substrate combinations, the linear range of concentration covers about 1 order of magnitude. In particular, for c-Ag substrates it is 1 ~ 10 µM for Adenine and 0.7 ~ 5 µM for 4-MBA. The linear work range on c-Au substrate is 0.1 ~ 1 µM for Adenine (rather shorter in respect to the range obtained under similar conditions by Villa et al.[76]) and 0.5 ~ 5 µM for 4-MBA.

It is interesting that Adenine features the lowest (0.29 µM LOD and 0.54 µM LOQ) and the highest (2.65 µM LOD and 4.83 µM LOQ) values of detection and quantification, respectively on c-Au and c-Ag substrates; moreover, the Langmuir isotherm for c-Au substrates reach the saturation at lower analyte concentration (1 µM) with respect to the c-Ag substrates, for which the Langmuir isotherm reaches the saturation at 10 µM. This behavior of Adenine could reflect the different affinity for the two metals, which is higher for the c-Au than for the c-Ag NPs. 4-MBA on the other hand, feature the opposite trend of LOD, with intermediate values, reflecting a better affinity for c-Ag NPs.

3.3.2 Ag NSs paper-made substrates

3.3.2.1 NSs and paper-made substrates characterization

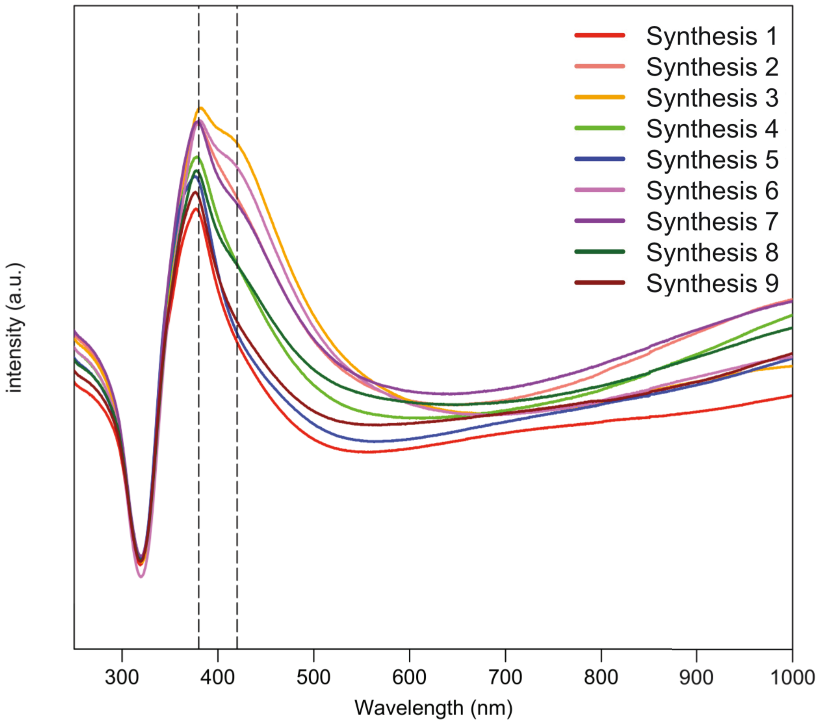

Figure 3.13 UV-visible adsorption spectra of 9 synthesis batches of NSs prepared under the same experimental conditions.

In figure 3.13 the SPR of 9 Ag NSs synthesis performed with the same protocol are reported. The band at 380 nm is present for all NSs batches, but there is a difference at 420 nm, indicating a variability in shape, hence a lower repeatability with respect to Lee-Meisel colloids (fig. 3.1).

From the figure 3.13, it is possible to distinguish 3 groups of adsorption spectra: the first features a huge contribution of the SPR at 380 nm and a little one at 720 nm; the second is characterized by a huge contribution of 380 nm band, a medium contribution at 420 nm, present as a shoulder, and a small SPR in the NIR region; finally, the third group presents as huge contribution of 380 nm band as the first two groups, a higher contribution (in respect with the group 2) at 420 nm, and a SPR in the NIR region.

All those changes in the adsorption spectra indicate that NSs with different morphologies are being synthetized. In order to investigate the different shapes and dimensions of the NSs, both the colloidal solutions and the solid paper-made substrates were characterized with TEM and SEM, respectively.

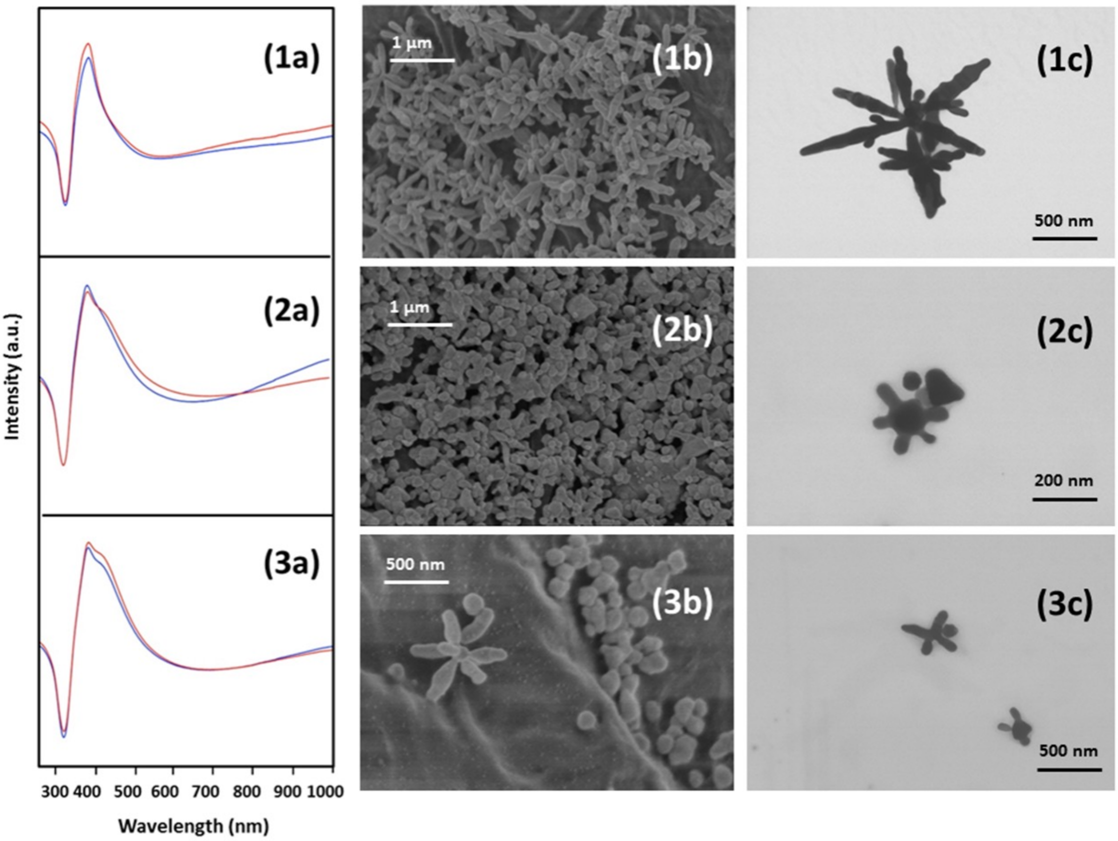

Figure 3.14. On the left: 1-3a) UV-visible adsorption spectra of the 3 groups of Ag NSs synthesis. In the middle: 1-3b) SEM images of Ag NSs paper solid substrates corresponding to the 3 groups of synthesis. On the right: 1-3c) TEM images of Ag NSs corresponding to the 3 groups of synthesis.

From the figure 3.14, it is possible to see the different morphologies of the NSs, which present different adsorption spectra (insets 1-3a on the figure 2.14). Notably, comparing the UV-vis spectra, TEM and SEM images of the insets 1-3 in figure 3.14, the contribution at 420 nm indicates the presence of NSs with shorter spikes and a presence of spherical NPs. Instead, NSs featured by branched and long spikes (inset 3c), do not show this contribution in the extinction spectra, which is characterized by the only 380 nm SPB.

The SEM images (insets 1-3b on the figure 3.14) show the adsorption, as in the case of c-Ag NPs, of the Ag NSs on to the cellulose fibers. Mehn and coworkers report a study on Au NSs immobilized on filter paper as solid SERS substrate[15]. Nevertheless, this is the first time that solid paper-made SERS substrates with Ag NSs are presented.

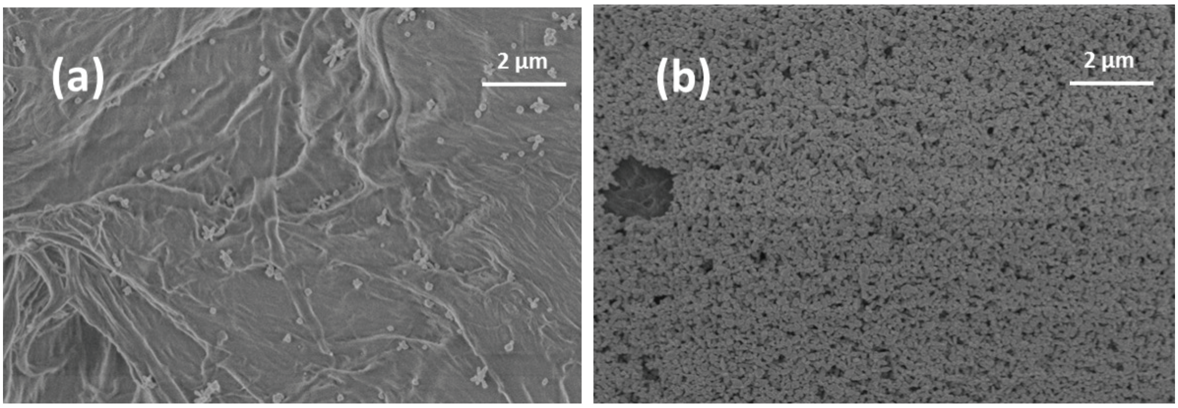

Figure 3.15 Ag NSs loaded filter paper with 2 µm of porosity obtained a) without sodium citrate and b) with 20 mM sodium citrate.

In figure 3.15, SEM images of Ag NSs paper-made substrates developed with and without the presence of the aggregating agent. The presence of the aggregating agent, as in the case of c-Ag NPs, induces the adsorption of the NSs onto the cellulose fibers, leading to an almost complete coverage of the support.

3.3.2.2 NSs paper-made substrates repeatability

The effect of sodium citrate on the Ag NSs substrates repeatability and sensitivity, as in the case of c-Ag NPs substrates, were evaluated. Raman mapping of three replicas of Ag NS substrates obtained in presence of sodium citrate and three replicas of those obtained without the aggregating agent were performed after samples incubation in 4-MBA PBS solutions. All the SERS maps were collected with the 532 nm excitation. In order to evaluate the effect of the sodium citrate on the substrates sensitivity (independently from the variation due to the synthesis) and repeatability, the same batch was used for the preparation of both kinds of substrates. In figure 3.16 the average SERS spectra of 4-MBA acquired on both kind of substrates (prepared without citrate and with citrate) are reported. The reported distribution was obtained over the integrated area of the 4-MBA band. In figure 3.17-a, the distributions of SERS intensities for the substrates prepared with and without citrate are reported and compared. The RSD values regarding the intra sample repeatability are reported in table 3.4.

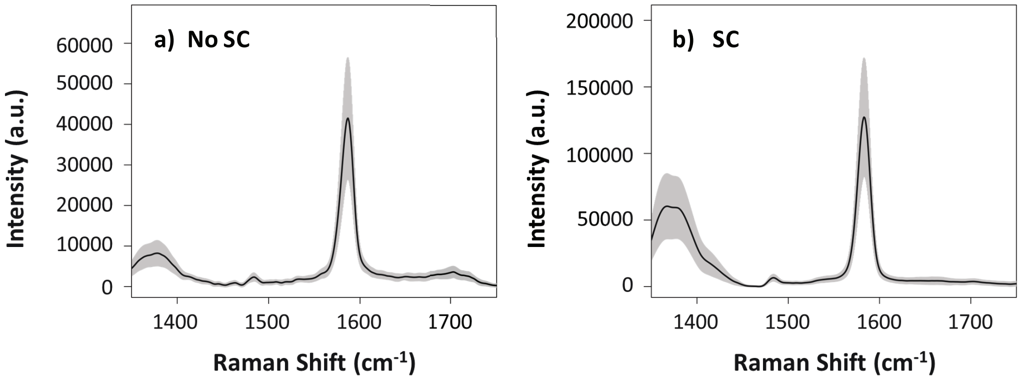

Figure 3.16. Mean SERS spectra of 4-MBA acquired Ag NSs substrates obtained a) without sodium citrate (SC) and b) with SC calculated from maps consisting of 64 spectra acquired at 532 nm. Shaded areas represent +/-1 intensity SD.

It is possible to observe the difference of the intensity between the SERS signal substrates acquired on the two kinds of substrates. The sodium citrate does not have an effect on the intra- and inter- sample repeatability, but on the signal intensity. The RSD values in fact (see table 3.5), are similar in both cases; however, the signal intensity is larger if the substrates were prepared with the aggregating agent.

For this reason, I decided to perform the repeatability experiment with 4-MBA on the substrates obtained in presence of sodium citrate. The repeatability study was performed over 9 samples, grouped according to the synthesis preparation of colloidal NSs. Three replicas of substrates obtained with three different synthesis batches, for a total of nine samples, were analyzed. In figure 3.17-b the comparison of the distributions of SERS intensities for the 9 samples obtained with the 3 different synthesis batches is reported. In table 3.5 all the RSD % values for the intra- sample repeatability of each sample are reported.

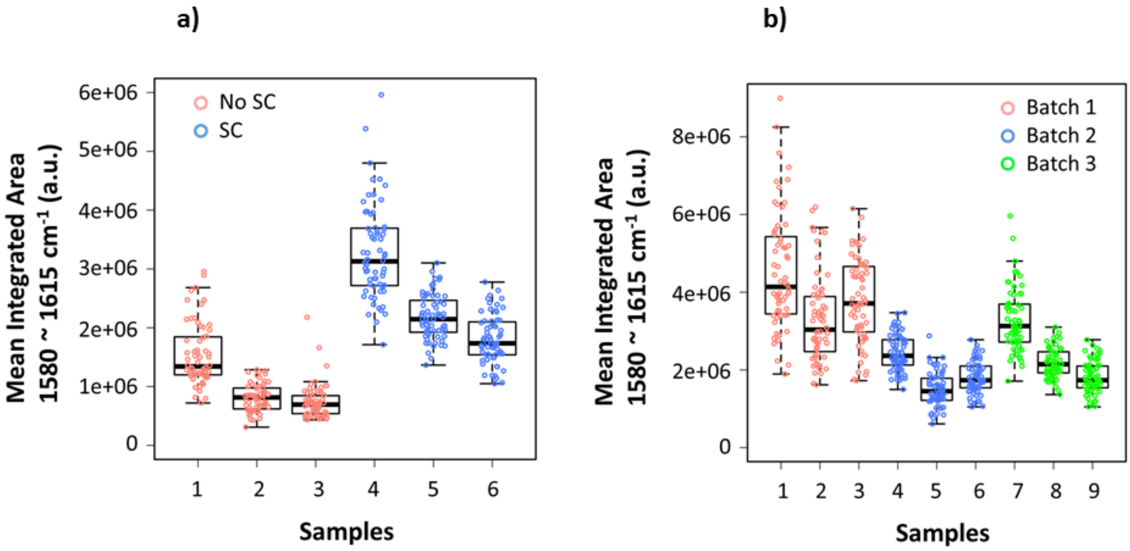

Figure 3.17. Comparison of the distributions of SERS intensities integrated over the area of the 4-MBA band. Each column (box) represents the complete distribution of integrated intensities, calculated over a SERS maps for different substrates. The distributions are grouped according to a) the absence (in red) and the presence (in blue) of SC; and b) the synthesis preparation (in red: synthesis 1; in blue: synthesis 2; in green: synthesis 3).

No SC (RSD%)	SC - batch 1 (RSD%)	SC - batch 2 (RSD%)	SC - batch 3 (RSD%)
34, 29, 28	34, 35, 28	19, 27, 27	23, 17, 23

Table 3.5. Intra- sample repeatability values (RSD) of the 4-MBA band area between 1550 ~ 1615 cm^{-1} calculated from SERS maps with the substrates obtained without citrate and with citrate for the three synthesis batches. The spectra have been acquired at 532 nm. The inter- sample repeatability was obtained from the integrated intensity averages calculated for each map of the same kind of substrate.

From the values reported in table 3.5, the intra- sample repeatability, independently from the presence of the citrate, is larger than those calculated for the c-Ag solid SERS substrates. However, to provide an explanation for the high signal variation shown by NSs paper-based substrates is not trivial. Since we used the same filter paper, the 20 mM citrate as aggregating agent, and we acquired the maps with the 514 nm laser, we can exclude those parameters as the reason of the large RSD values. Perhaps, the low homogeneity featured by the NSs substrates could be due to the intrinsic morphology of the NSs. Such kind of structures, in fact, features a high number of hot spots, especially at their tips[103]. In bulk solutions, the scattered signal is mediated from the Brownian motions of the NPs. When the NSs are fixed onto a support, the scattered signal depends on the NSs layer morphology, hence on the plasmonic response of the NSs. The presence of intrinsic hot spots on the NSs can yield a higher signal variation with respect to a substrate with spherical NPs. Besides the intra- sample repeatability, this behavior can affect the inter- sample repeatability as well. The RSD value for the inter-sample repeatability among the batches for the 3 synthesis was in fact found to be 37%. Nevertheless, it would be interesting to obtain models (such as local field EM simulations) to investigate the hot spots behavior present on the NSs tips, the hot spots generated by the aggregations of the NSs and comparing the results with the spherical c-Ag NPs systems.

Finally, the enhancement factor of the Ag NSs substrates, calculated in according to the equation 3.2, was $3 \cdot 10^8$. This value (obtained with 4-MBA and 785 nm laser) was found to be 1 order of magnitude larger in respect to the EF calculated on c-Ag (see section 3.3.1.4), indicating a good sensitivity of such kind of substrates. Moreover, the EF of Ag NSs results being pretty much higher in respect with the EF featured by Au NSs coated filter paper, which is $3.8 \cdot 10^3$, reported by Mehn et al.[15].

Nevertheless, the intra- and inter- sample repeatability featured by Ag NSs solid SERS substrates, besides the low synthesis repeatability, is clearly too poor to allow a quantitative application for this kind of substrates.

3.3.3 h-Ag NPs paper-made substrates

3.3.3.1 h-NPs characterization and substrates repeatability

In figure 3.18 the UV-visible adsorption spectra of the two different synthesis batch of h-Ag NPs are reported, which were used to prepare the solid SERS substrates. Both colloidal solutions feature a SPB at 405 nm, indicating a good repeatability in the shape and dimension of those kinds of NPs. The values are consistent with the values previously reported in literature[65].

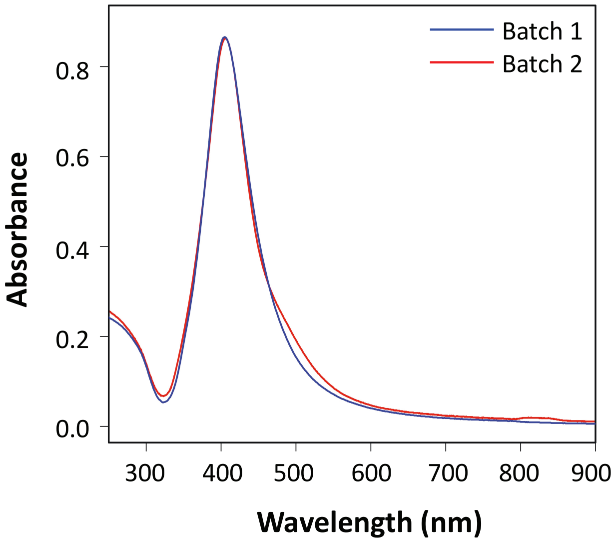

Figure 3.18. UV-visible adsorption spectra of 2 syntheses batches of h-Ag.

The h-Ag solid SERS substrates were prepared with the optimized procedure discussed in the section 3.3.1, with the exception of the use of an inorganic salt (KNO_3) as aggregating agent. The choice of this salt is due to three principal reasons: i) with the use this salt, the h-Ag substrates are citrate-free. The analyte has no exchange problems with the sodium citrate in the adsorption process and there are no background issues generated by the still adsorbed citrate onto the NPs surfaces. ii) For those NPs, the chloride ions act as stabilizing agents. The negatively charged surface can be exploited in the adsorption process of positively charged molecules due to the ionic-pair interaction. iii) Since the chloride ions are smaller than the citrate, is it possible to detect the analyte with SERS, without any exchange process[89].

Also in this case, both intra- and inter- sample repeatability of the SERS substrates were characterized through the acquisition of a Raman map (figure 3.19-a), consisting of 64 spectra, with a 514 nm laser. For this study, Adenine 10 μM was used as probe analyte in a buffer solution at pH of 7.4.

The mean spectrum with +/-1 SD of Adenine (centered on the 740 cm^{-1} band) is reported in figure 3.19-b. The repeatability study of the h-Ag substrates was performed among 6 samples for each synthesis batch, for a total of 12 samples. The results in terms of intra- and inter- sample repeatability were compared in the Tukey's box plot reported in figure 3.19-d and the relative values of intra- and inter- sample repeatability calculated are reported in table 3.6.

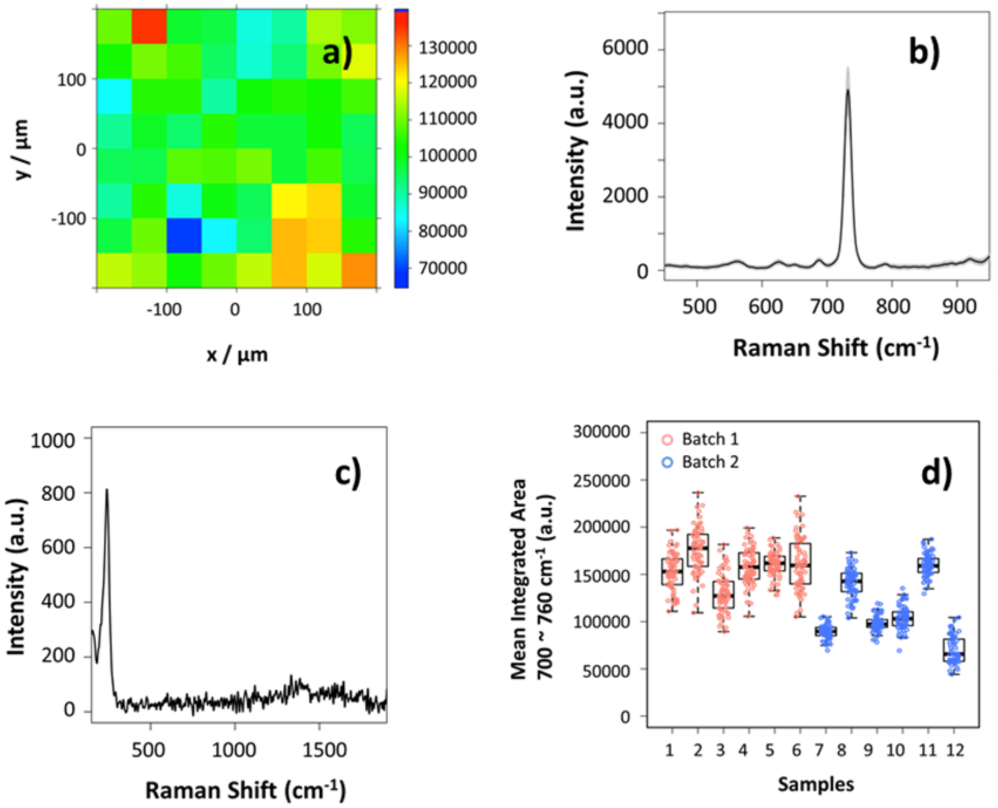

Figure 3.19. a) Raman map acquired at 514 nm on h-Ag substrate with 10 µM Adenine. b) Mean SERS spectra of Adenine calculated from the collected maps. Shaded areas represent +/-1 intensity SD c) Background of the h-Ag substrates acquired at 514 nm in a range of 200 ~ 1800 cm^{-1}. d) Comparison of the distributions of SERS intensities integrated over the area of the Adenine band. Each column (box) represents the complete distribution of integrated intensities, calculated over the maps for different substrates, grouped according to the two synthesis batch. For the distributions, the intra- and inter- sample RSD % values are reported in Table 3.6.

	Synthesis 1	**Synthesis 2**
Intra- sample RSD %	13.1, 13.9, 16.0, 12.3, 8.2, 17.2	8.2, 10.7, 8.5, 11.8, 7.3, 20.7
Inter- sample RSD %	16.3	30
Total inter- sample RSD %	28	

Table 3.6. Intra- and inter- sample repeatability values (RSD) of the Adenine band area between 700 ~ 770 cm^{-1} calculated from SERS maps acquired on the substrates prepared with the two synthesis batches. The inter- sample RSD % was obtained from the integrated intensity areas calculated for each map of the same kind of substrate. The inter- sample RSD % are reported among the 6 replicas for each synthesis batch and among the total (12) number of samples.

The intra- sample RSD % over 12 different independent substrates and two different synthesis batches was found to be between 7% and 21% (with an average value around 12%). Those results are in agreement with the data obtained by Hasi et al. for the h-Ag paper substrates prepared with chloride ions as aggregating agent[13].

Comparable intra- sample RSD values (see table 3.6) are expected since the extinction spectra reported in figure 3.18 are quite similar (indicating that both colloids present similar shape and dimension distributions). Despite the relatively low intra- sample repeatability values for both synthesis batches, the inter- sample RSD for the batch 2 is quite large with respect to the batch 1. In particular, RSD of 16% and 30% were found for the synthesis 1 and 2, respectively; the RSD calculated among all the substrates was found to be 28%. The distributions obtained from the samples 7, 9, 10 and 12 show average intensities that are lower with respect to those obtained from batch 1. Therefore, h-Ag substrates feature a worse inter- sample repeatability compared with the c-Ag substrates.

Also worth mentioning is the absence of background signals in the wavelength region of interest (250 ~ 1800 cm^{-1}) for analytes fingerprints (see figure 3.19-c). The only intense band is at 245 cm^{-1} and can be attributed to the Ag-Cl stretching[104]. In literature, the presence and characteristics of the background signal are often overlooked, although they can significantly impact on the overall performance of the substrates. With respect to this issue, the flat background observed for h-Ag substrates is quite a distinctive advantage.

Finally, the enhancement factor of the h-Ag substrates was $3 \cdot 10^8$ (value obtained with Adenine and 785 nm laser), the same found for the Ag NSs substrates. The EF of h-Ag substrates is 3 orders of magnitude larger in respect to the EF calculated on h-Ag substrates developed by Hasi et al.[13] and one order of magnitude larger than the EF calculated for c-Ag substrates (see section 3.3.1.4). This is in agreement with what observed by Cañamares et al.[89] for silver colloids and it could be probably due to the nature of the capping agent. With h-Ag NPs no exchange process is required for the analyte adsorption process, as in the case of citrate-capped colloids. Chloride ions allow the formation of an ionic pair interaction with the analyte and, since they are smaller than the citrate molecule, it is possible to detect the analyte without a direct adsorption onto the metal surface.

Besides the good intra- and inter- sample repeatability, the paper-made h-Ag substrates feature a good sensitivity, indicating a promising potential for quantitative analysis of anticancer drugs.

3.4 Conclusions

In this chapter paper-made substrates loaded with 4 kind of different NPs were presented: i) c-Au paper-made and ii) c-Ag paper-made substrates; iii) Ag NSs paper-made substrates, and iv) h-Ag paper-made substrates.

The aim of the systematic study performed on the c-Ag and c-Au paper-made substrates, was to find the optimal conditions to develop an inexpensive and repeatable paper-made SERS substrate from metal colloids using the dip-coating method. The results were compared and it was found that the experimental parameters affect the substrates performance in terms of overall efficiency (i.e. enhancement capacity) and repeatability. The wavelength of the laser greatly affects the SERS intensity and the repeatability of the c-Ag substrates: the combination yielding the best SERS efficiency in terms of signal intensity, hence allowing a qualitative analysis, is the c-Ag substrates with 785 nm laser. However, for quantitative purposes, those substrates perform better with the 514 nm laser. Another parameter which notably affects both intra- and inter-sample repeatability of both c-Au and c-Ag substrates is the porosity of the filter paper. Substrates developed with a filter paper with 2 μm of porosity result more homogeneous and repeatable, hence suitable for quantitative analysis. The concentration of the NPs affects the repeatability of the substrates in a different way, depending on the kind of NPs. For c-Ag NPs, the use of concentrated NPs improves the repeatability of the substrates, while for c-Au NPs it is better to use “as prepared” colloidal dispersions. Finally, the effect of the aggregating agent is not as relevant as the other parameters. For c-Ag substrates, the repeatability values do not correlate with the presence of the citrate; however, for c-Au substrates the citrate yields more appropriate substrates for quantitative analysis.

In conclusion, independently from the kind of analyte, the c-Au substrates featuring the best SERS performance for quantitative purposes are developed with i) a filter paper with 2 µm of porosity, ii) in the presence of the aggregating agent and iii) with an "as prepared" (i.e. non concentrated) colloidal dispersion. For c-Ag NPs, the best substrates were obtained with the same conditions but using a 10x in volume concentrated colloidal solution.

With the same protocol which leads to a lower intra- and inter- sample RSD % for c-Ag substrates, Ag NSs and h-Ag paper-made substrates were prepared. The only difference was in the use of not concentrated NPs ("as prepared").

The optimized paper made substrates c-Au, c-Ag and feature an intra- and inter- sample repeatability suitable for quantitative analysis, with RSD values <20% for the intra- and <10% for the inter- sample repeatability. On the other hand, the intra- sample values featured by Ag NSs (around 30%) hindered the use of such kind of substrates for quantitative purposes. h-Ag NPs substrates show quite good intra- sample RSD values (7-20%) and a slightly larger inter- sample RSD (28% among 12 samples and 2 synthesis batch). For what concern the intra- sample repeatability, such kind of substrates performed worst in respect with the c-Ag NPs in terms of inter- sample repeatability.

For all the paper-made substrates the EF upon 785 nm excitation was calculated. The most sensitive substrates were the h-Ag and the Ag NSs (EF $3 \cdot 10^8$); the c-Ag NPs featured an EF of $3 \cdot 10^7$ and, finally, the c-Au substrates were found to be the relatively less sensitive substrates, with an EF of $4 \cdot 10^3$. This is not unexpected, since in literature it is generally well recognized that Ag substrates perform better than Au substrates in terms of EF.

The c-Ag and c-Au substrates were characterized also in terms of quantitative features, having a LOD below 2 and 2.7 µM and a LOQ below 4 and 4.9 µM for the c-Au at 785 nm and c-Ag substrates at 514 nm, respectively. Moreover, such kinds of substrates feature a working range of linearity of about 1 order of magnitude of concentrations with a R^2 between 0.9753 and 0.9408, depending on the analyte – substrate combination.

Finally, for the c-Ag and c-Au substrates the long term stability was characterized. The study also revealed that c-Ag substrates stocked in air at RT retain their enhancing capabilities, although the overall performance in terms of absolute average intensity and

RSD vary unpredictably in time. On the other hand, c-Au substrates display a decrease of the analyte band intensity after the first day, but then remain stable as far as absolute intensity and RSD are concerned. Nevertheless, our experience suggests that it is better to stock the substrates in Milli-Q water to avoid the loss of plasmonic activity and the repeatability performance.

In conclusion, it has been demonstrated that the optimized dip-coating method, which is easy to use, cost-efficient and scalable, with the right conditions could be a reliable method to produce sensitive, efficient and repeatable substrates for quantitative analysis. However, timescales such as drying time or incubation time of the substrates into the analyte solutions may condition their repeatability and enhancement capacity. Leaving the substrates at air for too long periods of times, for instance, can reduce their enhancement capacity. As consequence, if those periods are not the same for each sample, the enhancement capacity of the substrates will be different, leading to an higher inter- sample variability. The handling of the substrates is another critical point for their repeatability. When the substrates are not dried, the nanostructures are not yet completely immobilized onto the cellulose fibers of the paper. Thus, quick movements during the supernatant extraction, for instance, can alter the homogeneity of the NPs layers, leading to a higher intra- and inter- sample variability. In view of a scalable production process, an “industrial automation” (a mechanization) of the dip-coating method could eliminate the timescales variability as well as the operator-dependence, leading to more repeatable substrates.

Chapter 4

Towards Point of Care: anticancer drugs quantification in biofluids with paper – made SERS substrates

4.1 Introduction

In this chapter an attempt to employ the substrates presented and characterized in Chapter 2 for the quantitative determination of a chemotherapeutic drug in human serum samples by means of SERS will be reported. Solid SERS substrates constituted by c-Au and h-Ag NPs substrates were used for rapid (i.e. few minutes) analysis of human serum spiked with different concentrations of anticancer drugs: Imatinib Mesylate (IMT) and Methotrexate (MTX).

As mentioned in the Introduction, TDM is the clinical practice of measuring specific drug concentrations at designated intervals to maintain a constant regime in a patient's bloodstream, thereby optimizing individual dosage regimens[1]. TDM is highly recommended in clinical settings to provide individualized patient treatment, optimizing the efficacy of drugs with a narrow therapeutic window, while minimizing side effects.[105]

The concentrations of MTX and IMT were chosen in a range designed to cover typical therapeutic plasmatic values (from nanomolar to millimolar) in oncological patients. The pertinent calibration was obtained by using multivariate regression techniques such as Partial Least-Squares Regression (PLSR), in collaboration with chemometricians. Stability selection was employed to select the variables optimizing the model stability, rather than its accuracy, and double cross validation was used to evaluate the capability of a PLSR model to accurately predict and extract spectral variations correlated to drug concentrations.

Imatinib Mesylate (4-[(4-methyl-1-piperazinyl)methyl]-N-[4-methyl-3-[[4-(3-pyridinyl)-2-pyrimidinyl]amino]-phenyl] benzamide methanesulfonate; Gleevec, Novartis, Basel, Switzerland) is an oral targeted tyrosine kinase inhibitor approved in the treatment of chronic myelogenous leukemia (CML) and gastrointestinal stromal tumor (GIST)[106]. Methotrexate (2,4-diamine-N,10-methylpteroyl glutamic acid) is a folate antagonist included in anti-neoplastic and anti-rheumatic drugs. It is one of the most widely used anti-cancer agents, with indications and established protocols for several children's and adult's cancers.[107]

The chemical structures of MTX and IMT are reported in figure 4.1a-b. IMT and MTX feature a λ_{max} in the UV-vis spectrum at 281 nm[108] and 372 nm[109], respectively.

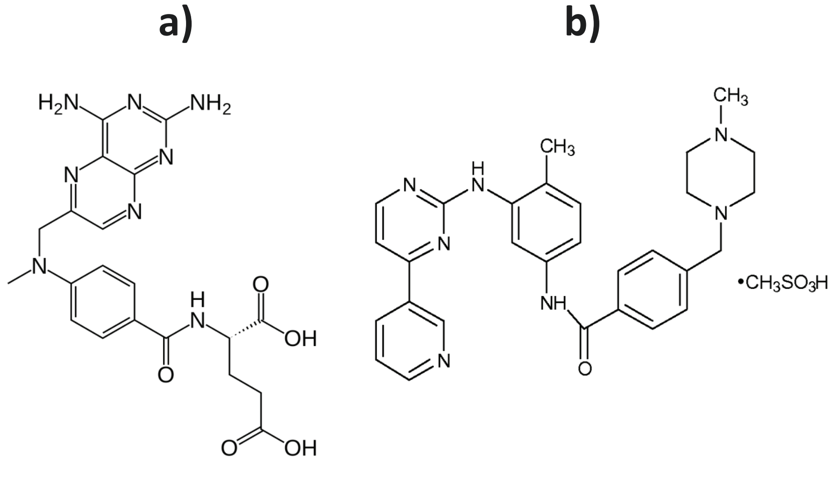

Figure 4.1. Chemical structures of a) Methotrexate (MTX) and b) Imatinib Mesylate (IMT).

For IMT, while no upper concentration limit has been yet firmly established, a lower limit of plasmatic concentration has been proposed in different studies. In CML patients the lower threshold has been established in a concentration range between 1 µM (560 ng/ml) and 3.7 µM (2158 ng/ml)[110–113]. In GIST patients, the lower threshold was proposed to be 1.7 µM (1030 ng/ml)[114].

Serum MTX concentrations can vary over 5 orders of magnitude (10 nM to 1 mM) from one patient to another using a single fixed dose, and in the same patient during treatment.[115] For MTX therapy, it is usually desirable to reach an initial serum concentration between 10 and 100 µM, and then maintaining it for prolonged periods (12 to 36 hours), which must drop to less than 200 nM after 72 hours. The plasma MTX concentration at 48 hours after the start of MTX infusion should be <1 µM, as high-risk toxic, adverse effects are associated with concentrations >10 µM.[116]

Because of its remarkable advantages such as rapidity, simplicity, and relatively low costs, recent data on buffered aqueous solutions of MTX suggested that the combination of SERS spectroscopy with multivariate statistical analysis could be a promising analytical tool for therapeutic drug monitoring[117,118].

Rath et al. report a semi-quantitative assay for the detection of IMT in human plasma at concentration of 1.7 µM (1 µg/ml) and above, with Raman Spectroscopy, drop coating deposition Raman spectroscopy and SERS[119].

However, SERS approaches quantifying either IMT or MTX directly in serum or other complex biofluids, have not been reported yet.

A first important issue is related to the "free drug" available in serum. These anticancer drugs, in fact, are known to bind to circulating proteins in blood. MTX for instance is bound for 50% to albumin and IMT for 95% to albumin and α-1-acid glycoprotein [AGP][7,120–123]. Therefore, only the unbound fraction can be detected with SERS in human serum, if no deproteinization step is performed.

Another important issue regarding the quantification through SERS is data analysis. The building of a calibration curve with univariate regression, as we quantified Adenine and 4-MBA in chapter 3, could be arduous if the analyte is present in a complex matrix (i.e. human serum), which is subject to intra- and inter-individual variability. Univariate calibration, in fact, consists on the variation of the signal intensity of a specific band with the variation of the analyte concentration. However, because of the increased complexity and lower S/N ratio of the SERS spectra obtained in complex matrix, the correlation of any individual band with the analyte concentration was rather low and a univariate regression approach resulted in a poor prediction of the drug concentration. Nevertheless, a multivariate analysis based on PLS regression overcomes this issue, allowing the construction of a prediction model of concentrations based on the entire spectral variability.

4.2 Experimental section

4.2.1. Materials and reagents

All chemicals, human serum for IMT quantification and solvents were of analytical reagent grade; they were purchased from Sigma-Aldrich (Milan, Italy) and used as received. Filter paper with 2 μm pore size (qualitative filter paper, 410) was purchased from VWR International (Milan, Italy). Phosphate buffered saline solution (PBS) (pH 7.4) was prepared by dissolving a PBS tablet (Sigma-Aldrich) in Milli-Q water (200 mL). Human serum for MTX quantification was obtained from healthy volunteers.

All glassware used for silver nanoparticle preparation was carefully cleaned with aqua regia and thoroughly rinsed with Milli-Q water. For all cleaning procedures and preparation of solutions, Milli-Q water was used.

4.2.2 MTX samples preparation for SERS measurements

c-Au paper-made SERS substrates (presented in chapter 3), were employed for all the MTX analysis.

A MTX stock standard solution was prepared by dissolving 5.0 mg of MTX hydrate (>98% HPLC, Sigma-Aldrich) powder in 0.2 mL of 0.1 M sodium hydroxide and diluting to 10 mL in a volumetric flask with PBS solution. The MTX stock standard solution was then diluted to 100 μM in PBS, aliquoted for single use and stored at -20°C.

Further dilutions were performed in 4% Bovine Serum Albumin (BSA) – PBS, a surrogate matrix frequently used to simulate plasma and serum, because its pH (7.4) and ionic strength (150 mM) are similar to those of the two biofluids. BSA was used instead of (Human Serum Albumin) HSA because it was readily available and less expensive. BSA was also added at a concentration of 40 g/L to simulate the protein content of serum. Such dilutions were performed at room temperature before analysis and in a dark room, to avoid MTX photodegradation. A set of eleven calibration standards was prepared in the concentration range of 0.1 ~ 20 µM for MTX. For the validation of the analytical method in a real-life matrix, calibration standards were prepared by spiking drug-free human serum with appropriate amounts of MTX stock solutions, keeping a constant 1:4, v/v ratio between serum and PBS. The final calibration range for MTX in diluted serum was 0.1 ~ 300 µM. Small drops of 5 µL of both MTX solutions and spiked serum samples were deposited on the nanostructured paper substrates and allowed to dry (15 min).

Among blood sample types (whole blood, plasma, and serum), in the present work serum was selected because (i) it retains most of the substances present in blood while not being subject to blood cell interference, (ii) it does not contain anticoagulants which might interfere with the spectroscopic signal due to the drug[11].

4.2.3 IMT samples preparation for SERS measurements

h-Ag paper-made SERS substrates (see chapter 3), were employed for all the IMT analysis.

A 1 mM stock standard solution of IMT (≥ 98% HPLC, Sigma-Aldrich) was prepared in Milli-Q water. For the testing of molecule-substrate system and the analytical method, a set of 11 further dilutions of the stock solution was performed in PBS. The dilutions were prepared for a final concentration range of IMT of 700 nM ~ 30 µM. Further dilutions of mother solution were then performed in 4% Bovine Serum Albumine (BSA) – PBS. In this case, 10 calibration standards were prepared for a final concentration range of IMT of 2.5 ~ 20 µM. The substrates were then dipped for 30 minutes into the solutions, allowed to dry (15 minutes) and then analyzed. For the validation of the analytical method in a real-life matrix, calibration standards were prepared by spiking drug-free human serum with appropriate amounts of IMT stock solutions, keeping a constant 20:1, v/v ratio between serum and PBS. The final calibration range for MTX in serum was 0.5 ~ 10 µM. Small drops of 2.5 µL of both MTX solutions and spiked serum samples were deposited on the nanostructured paper substrates and allowed to dry (15 min). In order to prepare a serum spiked solution as close as possible to a real sample, the human serum was not diluted.

4.2.4 Instrumentation, SERS spectra and images acquisition

All MTX SERS spectra were recorded with Renishaw inVia (Renishaw plc, Wotton-under-Edge, UK) equipped with a microscope Leica DMLM with a 10× objective (N.A. 0.25). Since analyses are performed on c-Au substrates, a 785 nm diode laser (Toptica, with a 450 mW output power) was used as excitation source. The spectrograph was equipped with a 1200 lines/mm grating, and a charge coupled device (CCD) camera. The frequency calibration for all gratings was performed using the emission lines of a Ne lamp.

SERS spectra of PBS IMT and PBS-BSA 4% IMT were recorded with a Renishaw Raman InVia spectrometer, equipped with a microscope Leica DMLM with a 20× objective (N.A. 0.40) and an electrically cooled CCD camera. Samples were excited by using the 532 nm laser line provided by a frequency-doubled Nd:YAG laser, with a power of 2.5 mW delivered to the sample. The spectral resolution was 2 cm^{-1}.

SERS spectra were registered over a wavenumber range of 600 ~ 1800 cm^{-1}, using the "extended" acquisition mode of the InVia Raman microscope. All spectra were recorded using an accumulation of one scan (10 s exposure each) at 6 random locations on the substrate surface.

Instrument settings were optimized to maximize signal and minimize saturation or sample degradation arising from laser excitation. In particular, the laser power density at the sample was decreased down to 0.5% by increasing the diameter of the laser spot using the "defocusing" option (100%) of the InVia Raman microscope.

SERS spectra of spiked IMT human serum were recorded with a portable Raman spectrophotometer (i-Raman plus, BWTEK) equipped with a TE cooled 2048 pixel CCD array and a 785 nm laser. The spectral resolution is 3.5 cm^{-1}, the potential spectral range is from 150 cm^{-1} up to 4000 cm^{-1} and the diameter of the spot is 80 μm. The instrument is equipped with a video microscope (BAC151B Series) for Raman Microscopy analysis. A 20× objective (NA = 0.40) was used for the spectra acquisitions. The spectra were acquired at 3 different locations on the sample, over the entire wavenumber range 150 ~ 4000 cm^{-1}, using an accumulation of two scans (10 s exposure each) and a laser power of 10%. For each sample 3 spectra at different locations on the surface of the substrate were acquired.

Before each measurement, the instrumental calibration was checked using as reference the 520 cm^{-1} vibrational band of a silicon wafer.

To facilitate handling, each 5 mm × 5 mm paper substrate was attached with a double-sided tape to a standard microscope slide (25 mm × 75 mm) immobilized onto the microscope stage.

Data recorded with Renishaw instrumentation were collected by WiRE 3.2 software (Renishaw). Data recorded with i-Raman plus were collected by BWSpec^{TM} software.

4.2.5 Data preprocessing, analysis and plotting

All data analysis and pre-processing was performed within the R software environment for statistical computing and graphics building[96] on the *pls*[124] and *glmnet*[125] packages. Special attention was paid to spectral data pre-processing for the purpose of outlier rejection and improvement in the robustness and accuracy of subsequent calibration models. First, the spectral region between 350 and 1700 cm^{-1} was selected for analysis. Then, the pre-processing workflow consisted of five steps: (i) removal of cosmic rays; (ii) BC; (iii) smoothing interpolation to increase the signal to noise ratio and to reduce the number of data points per spectrum (reduction of the dimensionality of the data); (iv) AN; and (v) outlier detection/removal by Principal Component Analysis (PCA). In particular, data import and export, pre-processing, and visualization were performed with the *hyperSpec* package[97] for R; for BC, a fourth-order polynomial baseline was fit automatically to the whole spectral range and subtracted from each spectrum of the dataset using the modpolyfit function from the package *baseline*[98]; peak picking was performed using detectPeaks from the *MALDIquant*[126] package. Anomalous spectra were automatically discarded by the pcout function from the package *mvoutlier*[127]. After the elimination of the outliers, the procedure was continually repeated until no more outliers were identified, in a self-consistent process.

Univariate calibration (IMT in PBS and PBS – BSA solutions) was obtained plotting the 1300 cm^{-1} peak intensity variation with the drug concentration. The curve was then fitted with a Langmuir function. Finally, the linear range of the curve with confidence and prediction bands was plotted using *chemCal* package[99].

For multivariate calibration Partial Least Squares Regression (PLSR) models were used to establish a relationship between the drugs concentrations and spectral data[128]. Briefly, PLSR is a multivariate statistical method widely used in spectroscopy that aims at building a model bringing in relationship the variations of the spectral data (X matrix, the predictors) to a series of relevant targets (the Y matrix, the dependent variables) according to the linear equation $Y = XB + E$, where B is a matrix of regression coefficients and E is a matrix of residuals. The goal of PLRS is to predict Y from X and to describe their common structure.

Basically, PLSR reduces the data to a small number of latent variables, maximizing the covariance between the spectral data (X) and the property to be modelled (Y, in this case, the drugs concentration). It is followed by a regression step where the decomposition of X is used to predict Y.

The model was then validated with the Repeated Double Cross-Validation (RDCV) strategy[129]. The aim is to optimize through an iterative process the complexity of PLSR models and to independently estimate the model performance for test set objects.

Finally, model performance was judged on the basis of the Root Mean Square Error of Prediction (RMSEP).

4.3 Results and discussion

4.3.1 Methotrexate detection and quantification in surrogate matrixes and serum

Figure 4.2 shows the normal Raman spectrum of the MTX powder, along with the SERS spectra of 10 μM MTX in aqueous solutions and diluted human serum. The molecular structure of MTX is reported as well as inset of figure 4.2.

All SERS spectra were acquired on c-Au paper-made substrates with the 785 nm laser. For this preliminary study, we used diluted human serum instead of undiluted serum. This choice was made to limit the overall amount of biofluid needed, as well as because diluted samples were easier to work with than undiluted ones, which are rather viscous and tend to foam upon mixing. For these reasons, diluted serum is routinely used in analytical and clinical settings[130]. Moreover, we observed that dilution does not significantly influence SERS spectra as acquired using c-Au substrates (see figure 4.3)

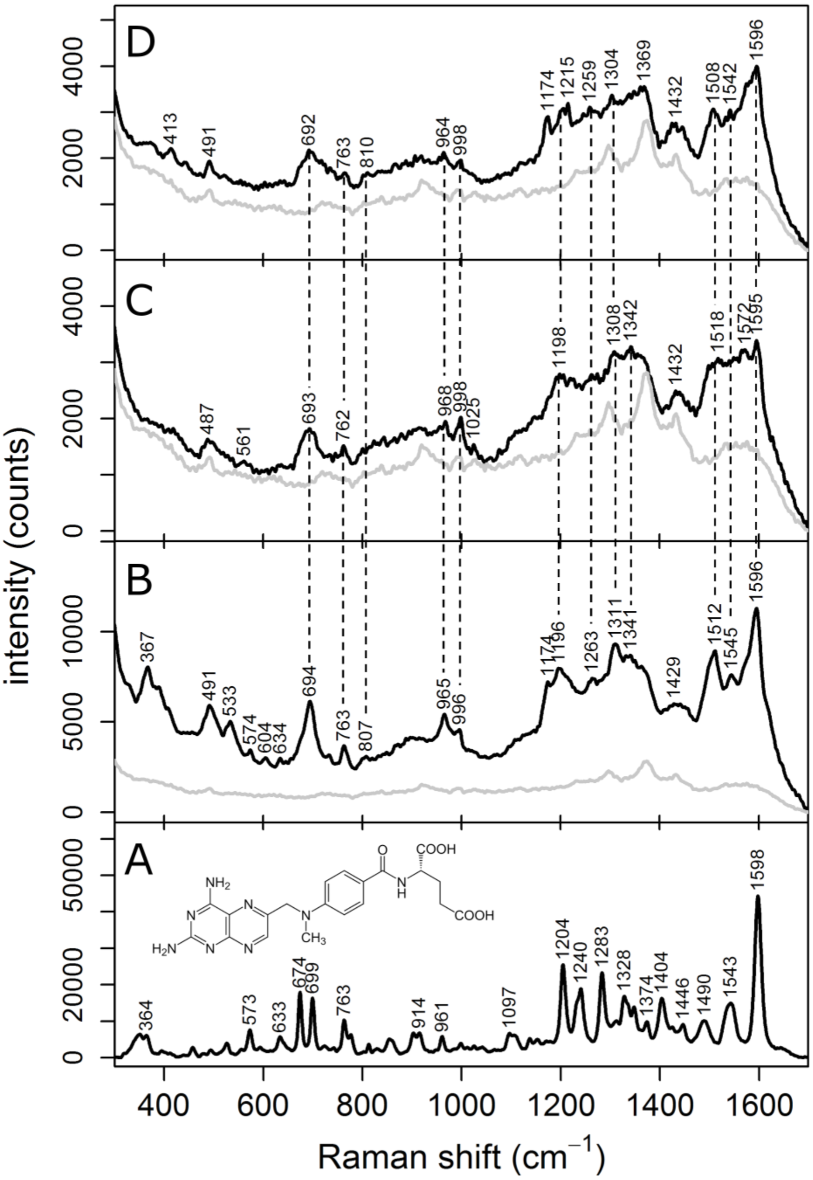

Figure 4.2. (A) Normal Raman spectrum of MTX powder; (B) SERS spectrum of MTX 10 µM in PBS, (C) SERS spectrum of MTX in 4% BSA–PBS, and (D) SERS spectrum of MTX diluted in human serum (1:4, v/v). The background signal of the substrate (grey line) is reported for comparison together with SERS spectra. The chemical structure of MTX is reported for reference in (A). All spectra were collected using an excitation at 785 nm.

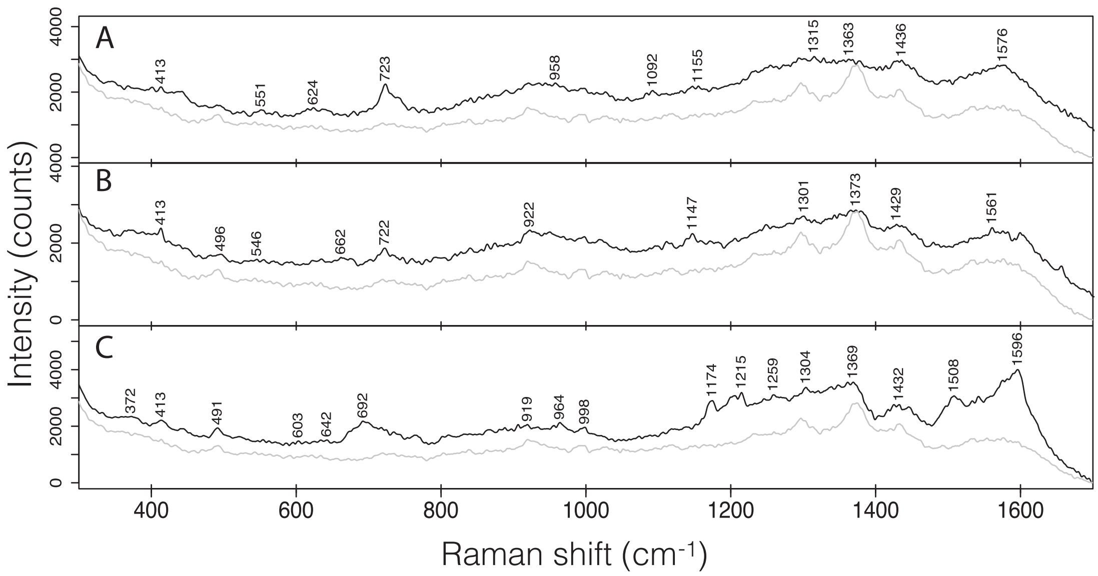

Figure 4.3. (A) SERS spectrum of human serum, (B) SERS spectra of diluted human serum (1:4, v/v, PBS). (C) SERS spectrum of MTX diluted in human serum (1:4, v/v, PBS). The background signal of the substrate (grey line) is reported for comparison together with SERS spectra. All spectra were collected using an excitation at 785 nm.

The characteristic Raman bands of MTX were consistent with those previously reported for this drug[117,131–133]. Compared to the normal Raman, the SERS bands of the MTX solution in PBS had slightly different positions, relative intensities and widths, as is often observed for SERS spectra. Such differences are explained by invoking surface selection rules (for changes in relative intensities) and direct interaction of some molecule moieties with the metal surface (for shifts of band frequencies). Moreover, an underlying background due to traces of amorphous carbon in SERS spectra can be inferred from a generally increased intensity around 1360 and 1560 cm^{-1}, due to two broad bands (also called “cathedral bands”) originating from the stretching modes of sp^2 carbons[134,135]. Such bands are often observed when employing solid SERS substrates, because of a minimal photodegradation as a consequence of laser illumination. However, amorphous carbon has a very high Raman cross-section, so that even small quantities will yield a detectable background. In the measurements, the presence of amorphous carbon is kept to a minimum by ensuring a low laser power density (see

Experimental Section), and thus it is not interfering with MTX detection. Also worth mentioning is the definite background signal given by the SERS substrates themselves, reported in light grey in fig. 4.2 along with the SERS spectra. This background, (see also figure 3.12 of chapter 3) is largely due to the SERS signal of citrate ions[136], originally present as stabilizing adsorbates on the surface of colloidal c-Au NPs and as aggregating agent used to prepare the SERS substrates. Being constant, this substrate background can be assumed not to interfere with MTX detection. Despite some differences, several bands in the SERS spectra were observed at Raman shifts very close to those of the normal Raman spectrum of MTX, so that in some cases a direct correlation between the Raman and SERS modes is straightforward. This is the case for the normal Raman bands at 699, 763, 961, 1204 and 1598 cm^{-1}, whose correspondence to their SERS counterparts is evident for all three SERS spectra reported. A detailed and complete assignment of the SERS bands of MTX to vibrational modes, as well as a detailed description of the MTX–metal interaction, is out of the scope of this work, and it would require carrying out an ab initio computational study at the level of Density Functional Theory (DFT). The reader interested in a tentative assignment of the SERS bands is referred to ref[131–133].

As this paper is concerned with MTX detection in diluted serum, it is noteworthy that the SERS bands appearing at 491, 694, 965, 996, 1512 and 1596 cm^{-1} in the spectrum of MTX in PBS solution (B) can be easily retrieved in both the SERS spectra of MTX in presence of albumin (C) and in diluted serum (D). In other words, MTX can be detected with SERS even in a complex medium such as diluted serum. Moreover, the presence of albumin appears to affect the MTX SERS signal, both in terms of absolute intensity [(C) spectrum is less intense than (B)] as well as in terms of slight band shifts. This is not unexpected, since MTX is known to bind to albumin, so that only about 50% of the drug is found as a "free" molecule in serum, while the other 50% is tightly bound to the protein. Indeed, the absolute intensity of MTX in presence of albumin, as well as that of MTX in serum, is approximately 40% of the absolute intensity counts observed for the drug in PBS, i.e. without the protein. Considering that the enhancement due to SERS dramatically decreases with distance from the metal surface, so that only MTX molecules directly adsorbed onto the SERS substrate will significantly contribute to the signal, this decrease in SERS intensity can be readily explained assuming that albumin-bound MTX are prevented from adsorbing onto the metal, while free MTX must compete for the surface with albumins themselves.

In the case of human serum, the complexity and variability in the matrix composition pose an even harder challenge for calibration and analysis. Serum has several thousands of components, with more than 4000 metabolites[137], some of which have a high affinity for gold surfaces, as proven by the intense SERS signal given by serum when using Au metal colloids[11]. To be observed, MTX must compete with all the serum constituents for adsorption. However, serum MTX concentration can be high, relative to most metabolites, and, while the presence of albumin appears to affect the overall intensity, MTX affinity for Au appears competitive enough to keep its SERS signal well detectable. This affinity can be partially explained by looking at its chemical structure: heterocyclic nitrogens, carboxylate groups as well as primary amine groups present in MTX are capable of a strong interaction with gold[69].

Such a strong MTX–Au interaction is responsible for the intense MTX SERS signal, and it makes the detection of this drug possible even in diluted serum. Indeed, other authors have previously reported the quantification of aqueous solutions of MTX based on SERS spectra. Hidi et al. used the SERS band around 965 cm^{-1} for quantitative detection through univariate analysis by relating the peak area directly to the MTX concentration in KOH solution[117].

However, because of the increased complexity and lower S/N ratio of the SERS spectra obtained in the presence of albumin or in diluted serum, the correlation of any individual band area with the MTX concentration was rather low.

As consequence, a univariate regression approach resulted in a poor prediction of the MTX content, as reported in figure 4.4.

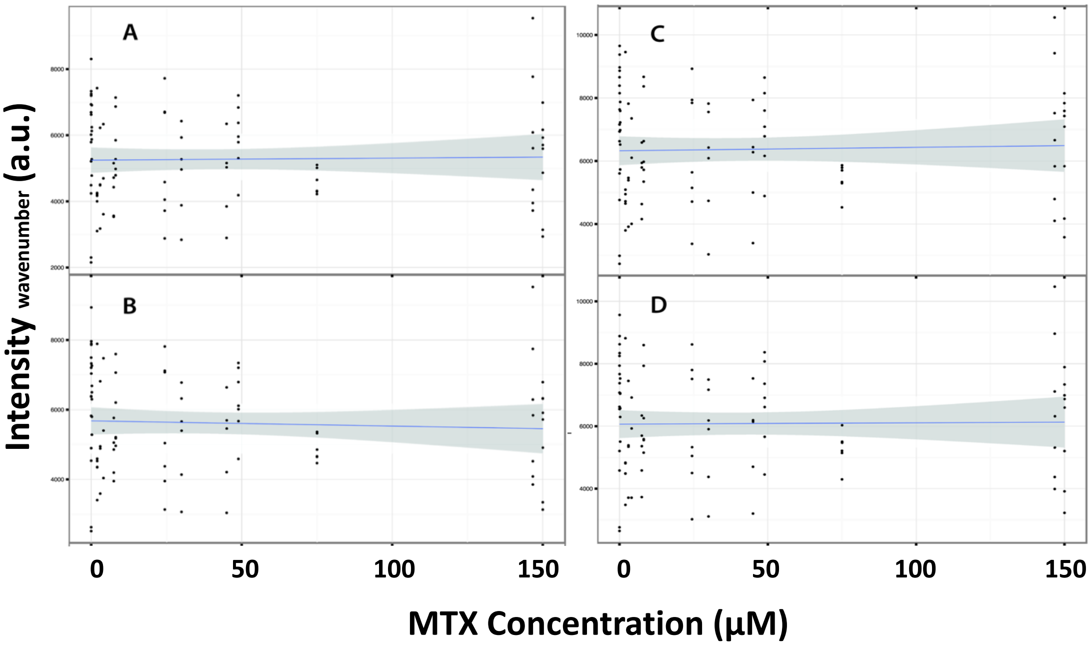

Figure 4.4. Conventional linear univariate evaluation of the spectral response was performed using specific Raman bands [(A) 692 cm^{-1}; (B) 965 cm^{-1}, (C) 1508 cm^{-1} (D) 1596 cm^{-1}] in the SERS spectrum of MTX in human serum. The signal intensities were plotted against the reference concentrations, and a first-order least-squares regression line was calculated.

Nonetheless, the spectral signature of MTX is specific, and many Raman shifts (to be considered as variables for chemometrics purposes) were correlated to the MTX concentration. These features made selective measurements of MTX possible by combining spectral information across a wide range of wavenumbers. As stated, the wide region between 350 and 1700 cm^{-1} was considered to build a multivariate calibration model that incorporates much of the available spectral information. In figure 4.5, the plots of calibration model in prediction for MTX concentration in (A) 4% BSA – PBS and (B) diluted human serum are reported.

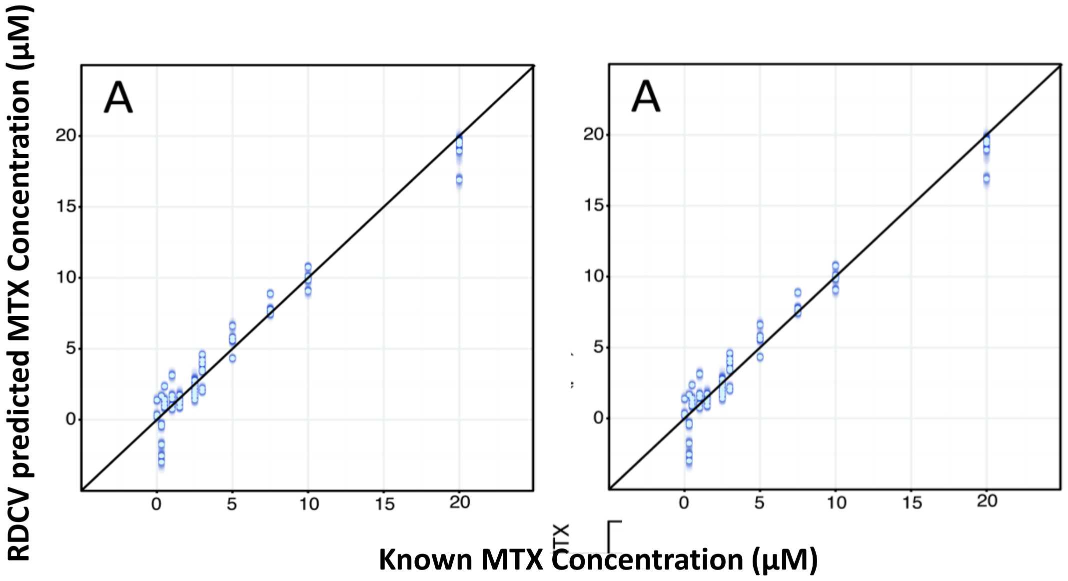

Figure 4.5. Plots from Repeated Double Cross Validation (RDCV) of SERS data collected in (A) 4% BSA–PBS, and (B) diluted human serum. The results from the 100 repetitions in RDCV are reported in blue (for 4% BSA–PBS they are very close together and therefore mostly hidden); the means of 93 predictions are reported in light blue.

The multivariate model calibration provided a MTX concentration prediction in 4% BSA – PBS solution (A) with a RMSEP of 1.08 µM.

The PLSR modelling process was repeated for the calibration of MTX concentration in diluted human serum, using the stability selection and pre-processing steps reported in the experimental section. The multivariate calibration model for this system yields a RMSEP of 31.57 µM. Finally, the LOD and LOQ for MTX detected on c-Au substrates were found to be 17.4 and 38.3 µM, respectively.

Based on these values, it can be concluded that the model produces a poorer prediction than the one built for the surrogate matrix. This is somewhat expected, considering the increased complexity of real serum with comparison to a buffered albumin solution. Considering that in this preliminary study we used serum samples from a single donor, inter-individual variations in serum composition can be ruled-out as a reason for the increased dispersion observed for data obtained from diluted serum with respect to those from buffered albumin solution. As serum itself does not yield intense SERS bands (see fig. 4.3 A and B), usual experimental errors involved in sample preparation and spiking might be indirect sources of variation in the SERS data by modulating the interaction of MTX with the metal surface.

The observed prediction error for MTX is still significantly higher than what is observed for established reference HPLC-MS/MS methods[138], and thus an increase in the precision of the SERS method is still necessary. Considering the difficulty of achieving quantification in a complex matrix using SERS, however, the results reported in this study still represent a significant step forward.

Moreover, it is important to note that the SERS substrate used in this study was not specifically adapted to target MTX. A gold surface might be functionalized to promote a selective adsorption of the analyte of interest while maintaining the integrity and activity of the compound[139], at the same time preventing the competition for the adsorption sites with the other serum components. Various strategies can be suggested to increase the affinity of the substrates for the drugs, including molecular recognition approaches such as MIP (molecularly imprinted polymers)[140] and artificial peptides. Such approaches are currently under investigation by our group, so that in the future the accuracy and precision of MTX quantification can be further improved. Furthermore, a functionalization of the SERS substrates would broaden the applicability of our SERS/PLSR method, paving the way to its use with those chemotherapeutic drugs lacking the strong affinity for Au surfaces shown by MTX.

4.3.2 Imatinib detection and quantification in surrogate matrixes and human serum

c-Ag solid SERS substrates (see chapter 3) were firstly used as nanostructured material for Imatinib detection. A first trial was performed with a milli-Q 1 mM solution of IMT. Contrary to MTX and despite the high drug concentration, it was not possible to acquire any IMT SERS spectra with these substrates. The IMT molecular structure, SERS spectra of IMT 1 mM, the c-Ag substrate background (SERS spectrum of c-Ag substrate without the drug) and the Raman spectrum of the IMT powder are reported in figure 4.6. From a comparison of these spectra, it is clear that no bands of IMT can be observed in any spectrum (apart, as obvious, in the IMT powder). There are no differences with the BK spectrum of c-Ag substrates produced by the citrate adsorbed on the NPs surfaces. This means that the drug adsorption is somehow hindered: the IMT affinity for the Ag surface, perhaps, is not high enough to displace the already adsorbed citrate ions.

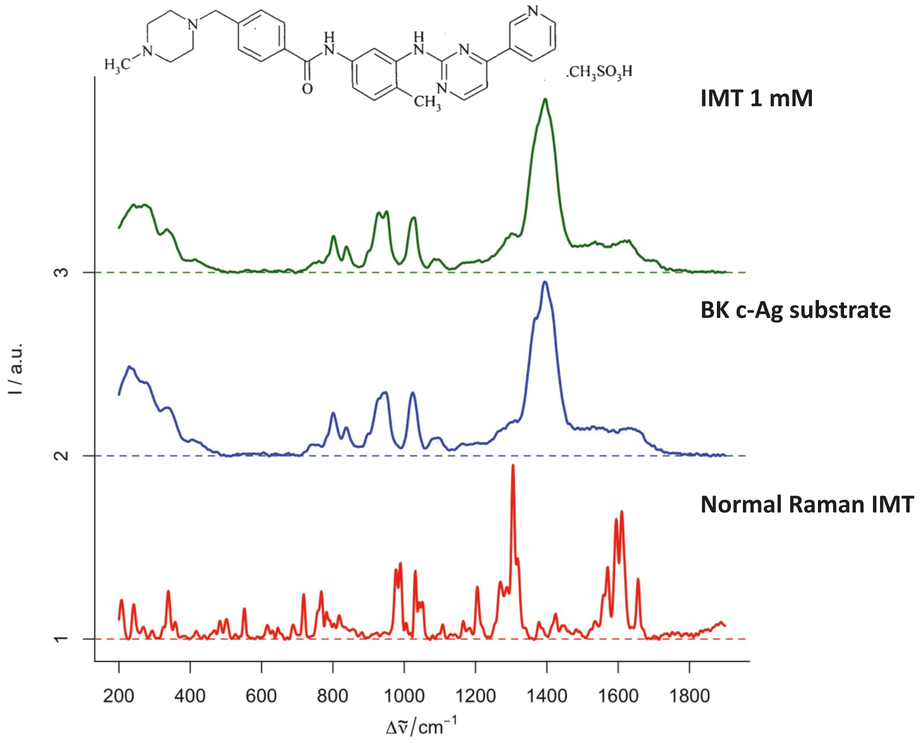

Figure 4.6. Molecular structure of Imatinib; comparison of Raman spectrum (in red) of IMT powder, background of c-Ag solid substrate (in blue) and SERS spectrum of IMT 1 mM (in green). All spectra are baseline subtracted, normalized and have been acquired with 532 nm laser.

For this reason, a second trial was performed with h-Ag substrates. With such kind of substrate, it was finally possible to detect the drug: the normal Raman spectra and the SERS spectra of IMT at different concentrations (0.7 – 30 μM) in PBS solution are reported in figure 4.7A. Moreover, the background of h-Ag substrates does not feature bands overlapping or interfering with those of IMT (see figure 3.19-c in chapter 3).

So far, we do not have an explanation supported by scientific data about how IMT can be detected with h-Ag NPs and not with c-Ag ones. Both substrates are capped by a negatively charge layer. Nevertheless, differently from c-Ag substrates, the h-Ag ones are “citrate-free”, as the capping layer is constituted by chloride ions and the aggregating agent used in the substrates production is KNO_3. Thus, on these bases, it is possible to hypothesize that the citrate covering the NPs surfaces could somehow hinder the adsorption of the IMT onto the NPs.

The univariate calibration of IMT in PBS has been done with h-Ag substrates. The related calibration curve is reported in figure 4.7B.

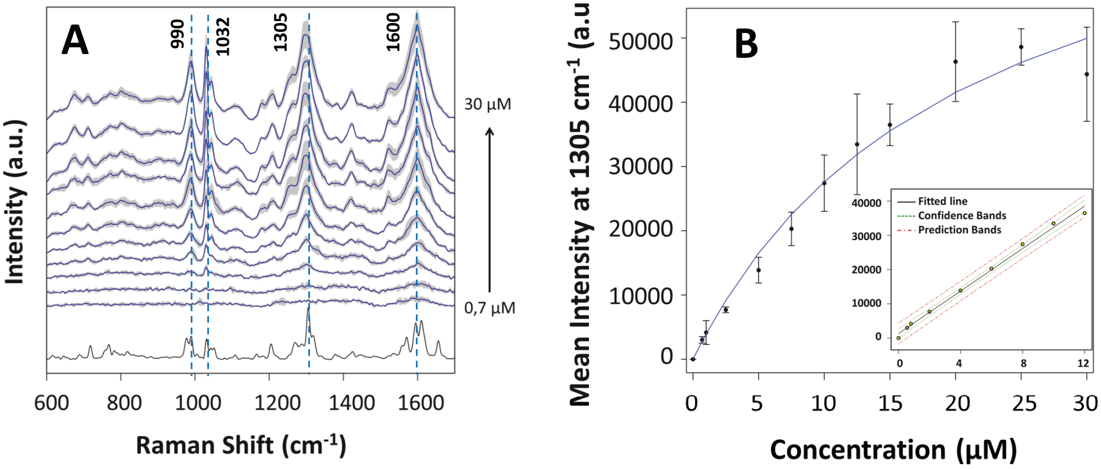

Figure 4.7. A) Normal Raman spectrum of the powder of IMT and SERS spectra of IMT in PBS solution at several concentrations acquired at 532 nm on h-Ag substrates. B) Corresponding Langmuir fits of the peak intensity at 1305 cm^{-1} vs IMT concentration. In the inset the linear response of the intensity with the concentration is reported; the concentration range is 0.7 ~ 12.5 µM. In black is reported the linear fit, in green the confidence bands and in red the prediction bands.

This preliminary study was performed using a 532 nm laser as excitation wavelength and focusing on the region between 600 and 1700 cm^{-1}. Then, to build the calibration curve, the variation of the intensity of a selected peak (1305 cm^{-1}) of the SERS spectra was plotted versus the variation of the concentration.

From the figure 4.7A, it is possible to observe that IMT SERS spectra consist of four bands that match with some of those present in the normal Raman spectra of the drug. Moreover, the peaks observed in the SERS spectra of the IMT solutions, did not present significant shifts when compared with the normal Raman spectrum. This could indicate a weak adsorption (i.e. physisorption) of the molecule on the nanoparticles surfaces, which does not involve a chemical mechanism but only the electromagnetic mechanism of the SERS effect[27]. Therefore, despite the chloride ions layer, IMT can be sufficiently near the surface to “feel” the electromagnetic field generated from the NPs without necessarily being adsorbed directly to the metal surface.

The Raman and SERS bands observed for the IMT were consistent with those reported in literature[119,141]. In particular, according with the ab initio theoretical study performed by A. Srivastava et al.[141], the SERS band observed at 992 cm^{-1} is due to the aminopyrimidine ring out of plane bending and the mesylene salt (S=O) stretching; the band at 1030 cm^{-1} is due to the stretching and deformation of the Pyridine ring; the band at 1305 cm^{-1} is generated by the N-methyl piperazine ring twisting and wagging normal mode and the band at 1600 cm^{-1} is due to another ring deformation.

In model solutions (i.e. PBS, BSA-PBS), IMT SERS spectra feature bands sufficiently narrow, with a relatively good S/N ratio and which do not interfere with the bands generated from the background; this in turn allows a univariate regression approach with a good prediction of IMT concentration. In fact, the univariate calibration curve, obtained among the 11 standard solutions in PBS, is reported in figure 4.6B. The peak at 1305 cm^{-1} was selected to build the calibration and the fitting was made with a Langmuir function. The curve, according with a Langmuir type adsorption[66], features a first linear part where it is possible to quantify the analyte concentration. The linear range was found to be 0.7 ~ 12.5 μM and feature an $R^2 = 0.9931$. Then, at the concentration of 15 μM, the curve reaches a plateau, indicating the saturation of the available binding sites for the adsorption of the analytes on the surface. The LOD for IMT in PBS solution is found to be 1.9 μM and the LOQ is 3.5 μM.

Nevertheless, real-samples such as human serum are constituted of thousands of metabolites and proteins[11]. Therefore, to get closer to a real system, a subsequent analysis was performed with 4% BSA – PBS IMT solutions. These measurements are not clinically relevant because IMT is known to bind preferentially to AGP[120,122]. In particular, in vitro binding studies of IMT incubated in conditions reflecting the clinical situation, reported a free fraction of the drug of 3.1% in AGP and 20% in HSA solutions[122,142]. Nonetheless, measurements in albumin solution can demonstrate that the nanostructured surfaces are not fouled by the protein. Therefore, those substrates can be used with serum without losing their analytical efficiency.

10 calibration standards were analyzed in a concentration range between 2.5 μM and 30 μM. SERS spectra and the related univariate curve, reported in figure 4.7, demonstrate that IMT can be quantified with a univariate regression also in presence of proteins.

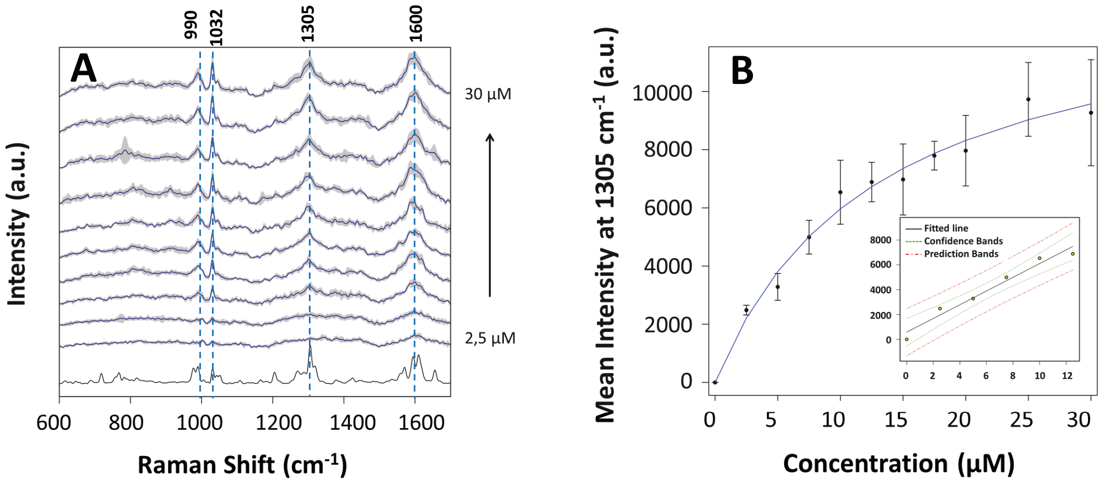

Figure 4.8. A) Normal Raman spectrum of the powder of IMT and SERS spectra of IMT in 4% BSA – PBS solution at several concentrations acquired at 532 nm on h-Ag substrates. B) Corresponding Langmuir fits of the peak intensity at 1305 cm^{-1} vs IMT concentration. In the inset the linear response of the intensity with the concentration is reported; the concentration range is 2.5 ~ 12.5 μM. In black is reported the linear fit, in green the confidence bands and in red the prediction bands.

From the IMT SERS spectra in BSA – PBS solution, it is possible to observe that no other bands generated by fragments of the protein are present in the SERS spectra, indicating that the albumin does not interfere with the SERS measurements of the drug. Nevertheless, as expected, the intensity of SERS spectra of the IMT in BSA – PBS solutions is five times lower compared to the spectra acquired without albumin (figure 4.7). This signal decrease indicates that, for this system, only 20% of the IMT molecules interact with the SERS substrate. This data is in agreement with the binding study performed by Kretz et al., who report a free fraction of 20% in HSA solutions[142]. Beside the signal intensity, also the quantification parameters such as R^2 value, LOD and LOQ were found to be smaller in comparison with the “free-albumin” system. For the IMT in 4% BSA – PBS system the linear range window of concentration was found to be 2.5 ~ 12.5 μM. The linear fitting features an $R^2 = 0.9554$; the LOD is found to be 4.98 μM and the LOQ is 9.39 μM.

Finally, in figure 4.9, normal Raman spectrum, SERS spectrum of human serum and SERS spectra of IMT 20 µM spiked in human serum are reported. As a step toward a POC tool, it was chosen to detect all SERS spectra of IMT in human serum with a portable Raman spectroscopy. Since the instrument is equipped with only NIR laser, data were collected with a 785 nm laser.

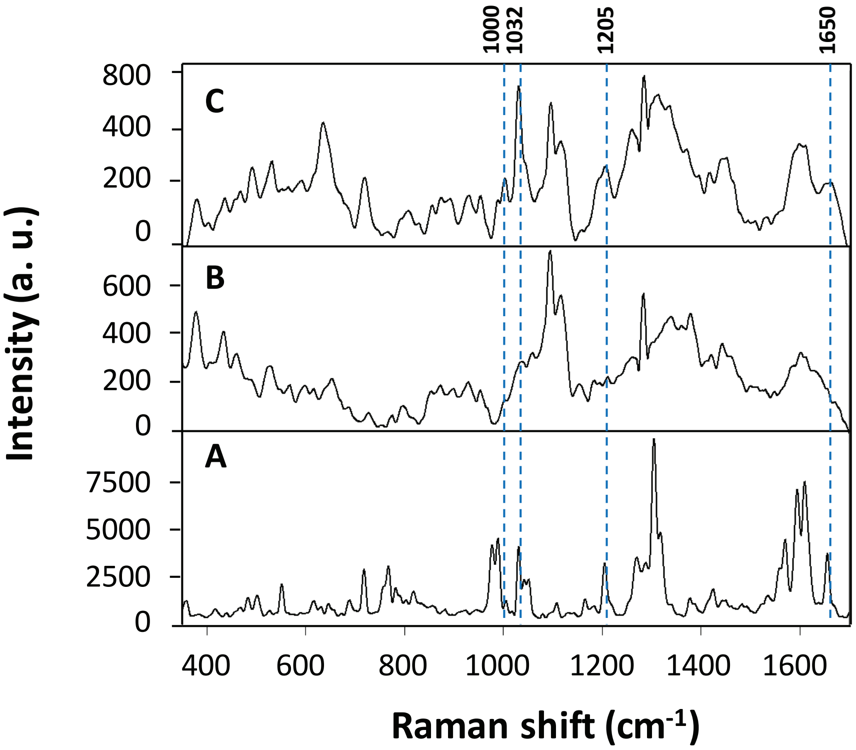

Figure 4.9. (A) Normal Raman spectrum of IMT powder; (B) SERS spectrum of human serum, and (C) SERS spectrum of IMT 20µM in human serum (1:20, v/v). All spectra were collected using an excitation at 785 nm with a portable Raman spectrophotometer.

Comparing the SERS spectrum of IMT in human serum (fig. 4.9A) with the "blank" (the SERS spectrum of human serum, fig. 4.9B), it is possible to recognize four bands belonging to IMT. However, if compared with the IMT spectra in surrogate matrices (fig. 4.7-8), there are some differences in the Raman frequency of the bands. The band which appeared at 990 cm^{-1} with 532 nm laser, with 785 nm is shifted at 1000 cm^{-1}. The bands at 1032 and 1600 cm^{-1} do not appear with 785 nm. Instead, two different bands show up at 1205 and 1650 cm^{-1}, generated by different normal modes of the same rings which generated the bands at 1032 and 1600 cm^{-1}, visible with the 514 nm laser[141].

Different orientations and binding sites of the functional groups on the nanostructural surface, can be excited differently depending on the excitation wavelength[143].

Also in this case, due to the increased complexity of SERS spectra obtained in human serum, a multivariate calibration model was built to predict the IMT concentration. The plot of a calibration model for the prediction for IMT in human serum is reported in figure 4.10, for a concentration range of 0.5 ~ 10 µM. Such concentrations are related with the whole amount of the IMT in the biofluid.

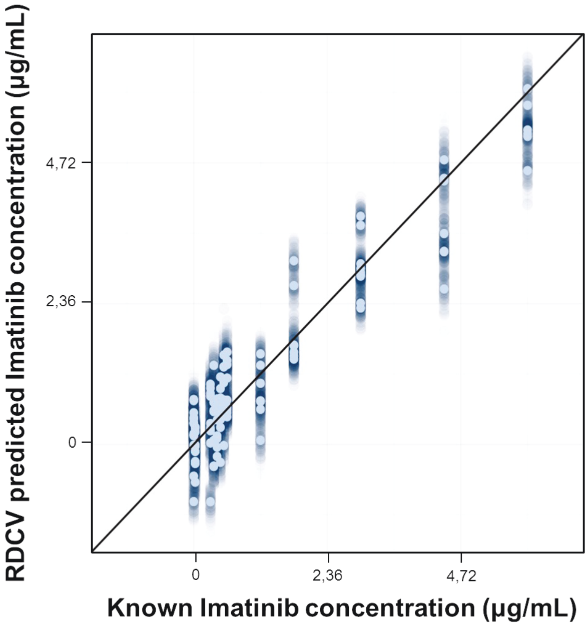

Figure 4.10. Plot with results from Repeated Double Cross Validation (RDCV) of a Partial Least Squares (PLS) regression model obtained from IMT SERS data collected in diluted human serum. The results from the 100 repetitions in RDCV are reported in blue; the means of 93 predictions are reported in light blue.

The multivariate calibration model for this system yields a RMSEP of 1.13 µM (666.38 ng/mL). The LOD and LOQ values are founded to be 2.29 µM (1.35 µg/mL) and 6.0 µM (3.54 µg/mL). The observed prediction error for IMT, despite the relatively low inter- samples repeatability of the h-Ag substrates, is quite lower than the one provided by the model for the system c-Au substrates/MTX in human serum. Also the LOD and LOQ are rather lower for IMT than for MTX. This could be due to the greater affinity of the IMT for the h-Ag NPs, together with the higher EF of the h-Ag substrates compared to those with c-Au NPs (see sections 3.3.1.4 and 3.3.3.1).

It is noteworthy that, considering that the samples were not deproteinized and that most of the drug is bound to serum proteins, the effective concentrations detected by the method presented in this work is quite lower than those reported[122], since they actually correspond to the un-bound drug. Based on the drug-protein affinity constants found in literature, the "real" concentration range detected is 15.5 ~ 310 nM and the "real" LOD and LOQ values are 71 and 186 nM, respectively.

Current protocols for TDM of IMT involve deproteinization of serum samples to release the protein-bound drug before measurements with HPLC-MS[8]. With such validated procedures in fact, the total amount of the drug (i.e. bound + free) is measured.

The results shown in fig. 4.10 are preliminary and are still subject to replication as of the moment when this thesis is being written (December 2016). One of the reasons of the difficult reproducibility could be the relatively low inter-sample repeatability featured by the h-Ag SERS substrates (see section 3.3.3.1 in Chapter 3). Another reason could be related to the extremely low free fraction of IMT in human, and the difficulty in handling the drug. In spite of these repeatability issues, however, this attempt demonstrates in principle the possibility to use SERS as a POC tool for TDM of IMT.

4.4 Conclusions

The work presented in this Chapter clearly shows that, by using paper-made substrates as those described in this thesis, together with an adequate data analysis, the quantification of drugs (in particular MTX and IMT) from biofluids samples with SERS is possible.

In the case of IMT, the importance of the choice of the NPs for the making of the SERS substrates was demonstrated. The molecule/substrate system highlighted the issue of the specificity of the SERS technique. A SERS substrate, in fact, is not "universal", hence each molecule requires a different nanostructured substrate to be detected, which must be tuned in the kind of the metal and the capping agent.

The data reported for MTX provide an interesting estimate of the difference in the quantification performance to be expected for anticancer drugs spiked in human serum with respect to model solutions.

The increasing complexity of the real-life samples related to the presence of proteins and other serum constituents increase the difficulty of the drug detection. However, with a multivariate regression approach it is possible to predict the anticancer drugs concentration in spiked human serum.

For instance, the LOD and LOQ values of IMT in BSA-PBS solutions calculated with univariate analysis were found to be 5 and 9 µM. The same values of the drug in human serum but calculated with multivariate analysis were lower (2 and 6 µM) despite the increase of the system complexity. A comparison of these results demonstrates the improvement brought by a multivariate approach to data analysis of complex matrices. However, the precision (RSMEP) of the model for real samples rather decreases compared to that for surrogate matrices. For instance, the RSMEP of the MTX quantification in serum decreases one order of magnitude with respect to model solutions.

Despite the low precision of the quantification in human serum, the results presented in this study still represent a significant step forward on the development of a new faster and cost-efficient technique in respect with the currently used for the TDM.

Chapter 5

Concluding remarks

In this Ph.D. thesis, the development of repeatable, cost-efficient, durable and sensitive solid SERS substrates for quantitative analysis of antitumoral drugs was reported. Given the commercial availability of extremely compact (pocket-size) and relatively inexpensive (few thousands euros) Raman instrumentation, the aim of this work was to present a methodology based on SERS with solid substrates as a new fast and cost-efficient POC tool for TDM.

The first aspect I would like to point out is the general lack of information in literature, to date, about solid SERS substrates developed with a bottom-up self-assembling approach for quantitative purposes. In particular, no studies are yet available about how the experimental conditions affect the repeatability and reproducibility of this type of SERS substrates. More in general, for SERS substrates there is a lack of standard protocols supported by adequate statistics and, most of the times, the repeatability results are reported only partially. With the systematic study carried out in this work, lasted three-year, it was proposed a first sampling methodology for spectra collection, an approach for the statistical data analysis and a way to present data to reliably assess substrates repeatability.

This work demonstrates that quantification through paper-made SERS substrates, is possible without having to resort to more expensive top-down approaches. However, there are some critical aspects of bottom-up methods which may affect the substrates performance. Timescales (e.g. drying time or incubation time of the substrates) may condition their repeatability and enhancement capacity; moreover, the handling of the substrates is another critical point for their repeatability: sudden movements during the supernatant extraction, for instance, may alter the homogeneity of the NPs layers, leading to a higher intra- and inter- sample variability. However, in view of a scalable production process, an “industrial automation” (a mechanization) of the dip-coating method could eliminate the timescales variability as well as the operator-dependence, leading to more repeatable substrates.

Such kinds of paper-made substrates, along with multivariate analysis, turned out to be apt for quantitative analysis, providing good figures of merit, at least for the specific cases of the drugs examined here. While both the substrates preparation and the precision of the multivariate regression model could be improved, there are some limits which, using not-functionalized substrates, will be difficult to transcend: among these limits we indicate i) the specificity, i) the sensitivity and iii) the concentration range in which a target molecule can be quantified. The analyte detection depends in fact on its affinity for the metal nanostructures. In fact, the substrates worked well for these drugs, but might not work for other drugs, so that the analysis method proposed is not general. Moreover, it is not possible to detect and quantify an analyte under its limit of detection and quantification (of the order of micromolar). Therefore, TDM with such kind of technique and using the substrates presented in this thesis will be feasible provided that some conditions are met: the anticancer drug must have a strong affinity for the NPs and the drug concentration range covering therapeutic plasmatic values must lie between its LOQ and the onset of the plateau in the calibration curve.

Nevertheless, a functionalization of the SERS substrates would broaden the applicability of the method, paving the way to its use with those chemotherapeutic drugs lacking a strong affinity for the NPs surfaces and perhaps lowering the LOD and LOQ of the substrates. Moreover, the inter- samples repeatability problem (i.e. samples produced with different synthesis batches) may be overcome with the use of an internal standard (i.e. a chemical substance added to samples in a constant amount). Thus, normalizing the target analyte signal with that of the internal standard, it is possible to obtain a calibration model whose precision and accuracy will not be affected the inter-sample variability of the substrates.

It is noteworthy that as much as it would be possible to improve the performance of the technique in terms of sensitivity and precision, SERS will not reach results comparable with HPLC/MS. It is a trade-off between gaining in cost and time and losing in sensitivity and precision. Beside the self-evident cost effectiveness of the technique, a faster analysis can provide a better adherence to the plasmatic value of the drug in the patient, allowing an immediate adjustment of the dosage, and hence preventing more successfully the side effects of the chemotherapy.

References

1. Kang, J. S. & Lee, M. H. Overview of therapeutic drug monitoring. *Korean J. Intern. Med.* **24,** 1–10 (2009).
2. Mathers, C. D., Boerma, T. & Ma Fat, D. Global and regional causes of death. *Br. Med. Bull.* **92,** 7–32 (2009).
3. Margaret von Mehren & Nicolas Widmer. Correlations between imatinib pharmacokinetics, pharmacodynamics, adherence, and clinical response in advanced metastatic gastrointestinal stromal tumor (GIST). **37,** 291–299 (2014).
4. Seidel, H. *et al.* Variability in methotrexate serum and cerebrospinal fluid pharmacokinetics in children with acute lymphocytic leukemia: relation to assay methodology and physiological variables. *Leuk. Res.* **24,** 193–199 (2000).
5. Paci, A. *et al.* Review of therapeutic drug monitoring of anticancer drugs part 1 - Cytotoxics. *Eur. J. Cancer* **50,** 2010–2019 (2014).
6. Widmer, N. *et al.* Review of therapeutic drug monitoring of anticancer drugs part two - Targeted therapies. *Eur. J. Cancer* **50,** 2020–2036 (2014).
7. Fornasaro, S., Dalla Marta, S., Rabusin, M., Bonifacio, A. & Sergo, V. Toward SERS-based point-of-care approaches for therapeutic drug monitoring: the case of methotrexate. *Faraday Discuss.* **187,** 485–499 (2016).
8. Haouala, A. *et al.* Therapeutic Drug Monitoring of the new targeted anticancer agents imatinib, nilotinib, dasatinib, sunitinib, sorafenib and lapatinib by LC tandem mass spectrometry. *J. Chromatogr. B Anal. Technol. Biomed. Life Sci.* **877,** 1982–1996 (2009).
9. Bouchet, S. *et al.* Simultaneous determination of nine tyrosine kinase inhibitors by 96-well solid-phase extraction and ultra performance LC/MS-MS. *Clin. Chim. Acta* **412,** 1060–1067 (2011).
10. Widmer, N. *et al.* Determination of imatinib (Gleevec®) in human plasma by solid-phase extraction-liquid chromatography-ultraviolet absorbance detection. *J. Chromatogr. B Anal. Technol. Biomed. Life Sci.* **803,** 285–292 (2004).

11. Bonifacio, A. *et al.* Surface-enhanced Raman spectroscopy of blood plasma and serum using Ag and Au nanoparticles: A systematic study. *Anal. Bioanal. Chem.* **406,** 2355–2365 (2014).
12. Polavarapu, L. & Liz-Marzán, L. M. Towards low-cost flexible substrates for nanoplasmonic sensing. *Phys. Chem. Chem. Phys. Phys. Chem. Chem. Phys* **15,** 5288–5300 (2013).
13. Hasi, W. L. J. *et al.* Chloride ion-assisted self-assembly of silver nanoparticles on filter paper as SERS substrate. *Appl. Phys. A Mater. Sci. Process.* **118,** 799–807 (2014).
14. Ngo, Y. H., Li, D., Simon, G. P. & Garnier, G. Gold nanoparticle-paper as a three-dimensional surface enhanced Raman scattering substrate. *Langmuir* **28,** 8782–90 (2012).
15. Mehn, D. *et al.* Immobilised gold nanostars in a paper-based test system for surface-enhanced Raman spectroscopy. *Vib. Spectrosc.* **68,** 45–50 (2013).
16. Lee, C. H., Hankus, M. E., Tian, L., Pellegrino, P. M. & Singamaneni, S. Highly Sensitive Surface Enhanced Raman Scattering Substrates Based on Filter Paper Loaded with Plasmonic Nanostructures. | *Anal. Chem* **83,** 8953–8958 (2011).
17. Pena-Pereira, F., Duarte, R. M. B. O. & Duarte, A. C. Immobilization strategies and analytical applications for metallic and metal-oxide nanomaterials on surfaces. *TrAC - Trends Anal. Chem.* **40,** 90–105 (2012).
18. Yu, W. W. & White, I. M. Inkjet printed surface enhanced raman spectroscopy array on cellulose paper. *Anal. Chem.* **82,** 9626–9630 (2010).
19. Liu, Q. *et al.* Paper-based plasmonic platform for sensitive, noninvasive, and rapid cancer screening. *Biosens. Bioelectron.* **54,** 128–134 (2014).
20. Lee, C. H., Tian, L. & Singamaneni, S. Paper-based SERS swab for rapid trace detection on real-world surfaces. *ACS Appl. Mater. Interfaces* **2,** 3429–3435 (2010).
21. Webb, J. A., Aufrecht, J., Hungerford, C. & Bardhan, R. Ultrasensitive analyte detection with plasmonic paper dipsticks and swabs integrated with branched nanoantennas. *J. Mater. Chem. C* **2,** 10446–10454 (2014).
22. Desmonda, C., Kar, S. & Tai, Y. Formation of gold nanostructures on copier paper surface for cost effective SERS active substrate - Effect of halide additives.

Appl. Surf. Sci. **367,** 362–369 (2016).

23. Zhu, Y., Zhang, L. & Yang, L. Designing of the functional paper-based surface-enhanced Raman spectroscopy substrates for colorants detection. *Mater. Res. Bull.* **63,** 199–204 (2015).
24. Bartlett, J. W. & Frost, C. Reliability, repeatability and reproducibility: Analysis of measurement errors in continuous variables. *Ultrasound Obstet. Gynecol.* **31,** 466–475 (2008).
25. Smith, E. & Dent, G. *Modern Raman Spectroscopy - A Practical Approach*. *Modern Raman Spectroscopy - A Practical Approach* (2005). doi:10.1002/0470011831
26. Edwards, H. G. M. Raman Microscopy: Developments and Applications. *Meas. Sci. Technol.* **7,** (1996).
27. Aroca, R. *Surface-Enhanced Vibrational Spectroscopy*. (2006). doi:10.1002/9780470035641
28. Fleischmann, M., Hendra, P. J. & McQuillan, A. J. Raman spectra of pyridine adsorbed at a silver electrode. *Chem. Phys. Lett.* **26,** 163–166 (1974).
29. Schlücker, S. *Surface enhanced Raman spectroscopy : analytical, biophysical and life science applications*. (Wiley-VCH Verlag, 2011).
30. Blackie, E. J., Le Ru, E. C. & Etchegoin, P. G. Single-molecule surface-enhanced raman spectroscopy of nonresonant molecules. *J. Am. Chem. Soc.* **131,** 14466–14472 (2009).
31. Etchegoin, P. G. & Le Ru, E. C. A perspective on single molecule SERS: current status and future challenges. *Phys. Chem. Chem. Phys.* **10,** 6079–89 (2008).
32. Unser, S., Bruzas, I., He, J. & Sagle, L. Localized Surface Plasmon Resonance Biosensing: Current Challenges and Approaches. *Sensors (Basel).* **15,** 15684–716 (2015).
33. Ko, H., Singamaneni, S. & Tsukruk, V. V. Nanostructured surfaces and assemblies as SERS media. *Small* **4,** 1576–1599 (2008).
34. Gellner, M., Küstner, B. & Schlücker, S. Optical properties and SERS efficiency of tunable gold/silver nanoshells. *Vib. Spectrosc.* **50,** 43–47 (2009).
35. Garcia-Leis, A., Garcia-Ramos, J. V. & Sanchez-Cortes, S. Silver Nanostars with High SERS Performance. *J. Phys. Chem. C* **117,** 7791–7795 (2013).

36. Vega, M. M. *et al.* Long-term stability of surfactant-free gold nanostars. *J. Nanoparticle Res.* **16,** (2014).
37. Wang, B., Zhang, L. & Zhou, X. Synthesis of silver nanocubes as a SERS substrate for the determination of pesticide paraoxon and thiram. *Spectrochim. Acta Part A Mol. Biomol. Spectrosc.* **121,** 63–69 (2014).
38. Zhang, L., Wang, B., Zhu, G. & Zhou, X. Synthesis of silver nanowires as a SERS substrate for the detection of pesticide thiram. *Spectrochim. Acta Part A Mol. Biomol. Spectrosc.* **133,** 411–416 (2014).
39. Zhang, Y. *et al.* A facile and general route to synthesize silica-coated SERS tags with the enhanced signal intensity. *Sci. Rep.* **5,** 14934 (2015).
40. Feldheim, D. *Metal nanoparticles : synthesis, characterization, and applications*. (Marcel Dekker, 2002).
41. Ros, I. *et al.* SERS Properties of Gold Nanorods at Resonance with Molecular, Transverse, and Longitudinal Plasmon Excitations. *Plasmonics* 1–13 (2014). doi:10.1007/s11468-014-9669-4
42. Kneipp, K., Kneipp, H. & Kneipp, J. Probing plasmonic nanostructures by photons and electrons. *Chem. Sci.* **6,** 2721–2726 (2015).
43. Koh, A. L. *et al.* Electron Energy-Loss Spectroscopy Silver Nanoparticles and Dimers : Influence of Beam Damage and Mapping of Dark Modes. **3,** 3015–3022 (2009).
44. McFarland, A. D. & Van Duyne, R. P. Single Silver Nanoparticles as Real-Time Optical Sensors with Zeptomole Sensitivity. *Nano Lett.* **3,** 1057–1062 (2003).
45. De Jong, W. H. & Borm, P. J. a. Drug delivery and nanoparticles:applications and hazards. *Int. J. Nanomedicine* **3,** 133–149 (2008).
46. Schauermann, S., Nilius, N., Shaikhutdinov, S. & Freund, H.-J. Nanoparticles for heterogeneous catalysis: new mechanistic insights. *Acc. Chem. Res.* **46,** 1673–81 (2013).
47. Bonifacio, A., Cervo, S. & Sergo, V. Label-free surface-enhanced Raman spectroscopy of biofluids: fundamental aspects and diagnostic applications. *Anal. Bioanal. Chem.* 8265–8277 (2015). doi:10.1007/s00216-015-8697-z
48. Sharma, B. *et al.* High-performance SERS substrates: Advances and challenges. *MRS Bull.* **38,** 615–624 (2013).

49. Etchegoin, E. C. L. R. e P. G. *Principles of surface enhanced Raman spectroscopy and related plasmonic effects*. *Oxford: Elsevier* (2009). doi:10.1007/s13398-014-0173-7.2
50. Betz, J. F., Yu, W. W., Cheng, Y., White, I. M. & Rubloff, G. W. Simple SERS substrates: powerful, portable, and full of potential. *Phys. Chem. Chem. Phys.* **16,** 2224–39 (2014).
51. Daniel, M. C. & Astruc, D. Gold Nanoparticles: Assembly, Supramolecular Chemistry, Quantum-Size-Related Properties, and Applications Toward Biology, Catalysis, and Nanotechnology. *Chem. Rev.* **104,** 293–346 (2004).
52. Schmid, G. E. *Nanoparticles: From Theory to Application*. *Nanotechnology* (Wiley-VCH, Darmstadt, 2004).
53. Fan, M., Andrade, G. F. S. & Brolo, A. G. A review on the fabrication of substrates for surface enhanced Raman spectroscopy and their applications in analytical chemistry. *Anal. Chim. Acta* **693,** 7–25 (2011).
54. McQuillan, J. The discovery of surface-enhanced Raman scattering. *Notes Rec. R. Soc.* **63,** 105–109 (2009).
55. Jeanmaire, D. L. & Van Duyne, R. P. Surface raman spectroelectrochemistry. *J. Electroanal. Chem. Interfacial Electrochem.* **84,** 1–20 (1977).
56. Chen, H. Y., Lin, M. H., Wang, C. Y., Chang, Y. M. & Gwo, S. Large-Scale Hot Spot Engineering for Quantitative SERS at the Single-Molecule Scale. *J. Am. Chem. Soc.* **137,** 13698–13705 (2015).
57. Asiala, S. M. & Schultz, Z. D. Characterization of hotspots in a highly enhancing SERS substrate. *Analyst* **136,** 4472–9 (2011).
58. Kleinman, S. L., Frontiera, R. R., Henry, A.-I., Dieringer, J. A. & Van Duyne, R. P. Creating, characterizing, and controlling chemistry with SERS hot spots. *Phys. Chem. Chem. Phys.* **15,** 21–36 (2013).
59. Cheng, M. L., Tsai, B. C. & Yang, J. Silver nanoparticle-treated filter paper as a highly sensitive surface-enhanced Raman scattering (SERS) substrate for detection of tyrosine in aqueous solution. *Anal. Chim. Acta* **708,** 89–96 (2011).
60. Lahr, R. H., Wallace, G. C. & Vikesland, P. J. Raman characterization of nanoparticle transport in microfluidic paper-based analytical devices (uPADs). *ACS Appl. Mater. Interfaces* **7,** 9139–9146 (2015).

61. Vella, S. J. *et al.* Measuring markers of liver function using a micropatterned paper device designed for blood from a fingerstick. *Anal. Chem.* **84,** 2883–2891 (2012).
62. Hu, J. *et al.* Advances in paper-based point-of-care diagnostics. *Biosens. Bioelectron.* **54,** 585–597 (2014).
63. J. Turkevich; P.C. Stevenson; J. Hiller. Synthesis of Gold Nanoparticles Turkevich method. *Discuss. Faraday Soc.* **11,** 55–75 (1951).
64. Lee, P. C. & Meisel, D. Adsorption and surface-enhanced Raman of dyes on silver and gold sols. *J.Phys.Chem.* **86,** 3391–3395 (1982).
65. Leopold, N. & Lendl, B. A New Method for Fast Preparation of Highly Surface-Enhanced Raman Scattering (SERS) Active Silver Colloids at Room Temperature by Reduction of Silver Nitrate with Hydroxylamine Hydrochloride. *J. Phys. Chem. B* **107,** 5723–5727 (2003).
66. Hans-Jürgen Butt, Karlheinz Graf, M. K. *Physics and cemistry of interfaces. Katalog BPS* **XXXIII,** (2014).
67. Langmuir, I. The constitution and fundamental properties of solids and liquids. Part II: Liquids. *J. Am. Chem. Soc.* **39,** 1848–1906 (1917).
68. Brunauer, S., Emmett, P. H. & Teller, E. Adsorption of Gases in Multimolecular Layers. *J. Am. Chem. Soc.* **60,** 309–319 (1938).
69. Guerrini, L. *et al.* Importance of metal-adsorbate interactions for the surface-enhanced raman scattering of molecules adsorbed on plasmonic nanoparticles. *Plasmonics* **2,** 147–156 (2007).
70. Novara, C. *et al.* SERS-active Ag nanoparticles on porous silicon and PDMS substrates: A comparative study of uniformity and Raman efficiency. *J. Phys. Chem. C* **120,** 16946–16953 (2016).
71. Rajapandiyan, P. & Yang, J. Photochemical method for decoration of silver nanoparticles on filter paper substrate for SERS application. *J. Raman Spectrosc.* **45,** 574–580 (2014).
72. Hoppmann, E. P., Yu, W. W. & White, I. M. Highly sensitive and flexible inkjet printed SERS sensors on paper. *Methods* **63,** 219–224 (2013).
73. Joshi, P. & Santhanam, V. Paper-based SERS Active Substrates on Demand. *RSC Adv.* **6,** 68545–68552 (2016).

74. J. Kimling, M. Maier, B. Okenve, V. Kotaidis, H. Ballot, and A. P. Turkevich Method for Gold Nanoparticle Synthesis Revisited. 15700–15707 (2006). doi:10.1021/jp061667w
75. Kim, W. S., Shin, J. H., Park, H. K. & Choi, S. A low-cost, monometallic, surface-enhanced Raman scattering-functionalized paper platform for spot-on bioassays. *Sensors Actuators, B Chem.* **222,** 1112–1118 (2015).
76. Villa, J. E. L., Santos, D. P. Dos & Poppi, R. J. Fabrication of gold nanoparticle-coated paper and its use as a sensitive substrate for quantitative SERS analysis. *Microchim. Acta* 2745–2752 (2016). doi:10.1007/s00604-016-1918-0
77. Polavarapu, L. & Liz-Marzán, L. M. Towards low-cost flexible substrates for nanoplasmonic sensing. *Phys. Chem. Chem. Phys.* **15,** 5288–300 (2013).
78. Zhang, R. *et al.* Highly efficient SERS test strips. *Chem. Commun.* **48,** 5913 (2012).
79. Novara, C. *et al.* SERS-Active Ag Nanoparticles on Porous Silicon and PDMS Substrates: A Comparative Study of Uniformity and Raman Efficiency. *J. Phys. Chem. C* **120,** 16946–16953 (2016).
80. Yamada, K., Henares, T. G., Suzuki, K. & Citterio, D. Paper-based inkjet-printed microfluidic analytical devices. *Angew. Chemie - Int. Ed.* **54,** 5294–5310 (2015).
81. Li, X., Ballerini, D. R. & Shen, W. A perspective on paper-based microfluidics: Current status and future trends. *Biomicrofluidics* **6,** (2012).
82. I. M. White, W. W. Y. A simple filter-based approach to surface enhanced Raman spectroscopy for trace chemical detection. *Analyst* **137,** 1168–1173 (2012).
83. Ross, M. B. *et al.* Structure–Function Relationships for Surface-Enhanced Raman Spectroscopy-Active Plasmonic Paper. *J. Phys. Chem. C* acs.jpcc.6b02019 (2016). doi:10.1021/acs.jpcc.6b02019
84. Lee, C. H., Hankus, M. E., Tian, L., Pellegrino, P. M. & Singamaneni, S. Highly Sensitive Surface Enhanced Raman Scattering Substrates. *Anal. Chem.* **83,** 8953–8958 (2011).
85. Hasi, W.-L.-J. *et al.* Rapid fabrication of self-assembled interfacial film decorated filter paper as an excellent surface-enhanced Raman scattering substrate. *Anal. Methods* **6,** 9547–9553 (2014).

86. Wang, C., Liu, B. & Dou, X. Silver nanotriangles-loaded filter paper for ultrasensitive SERS detection application benefited by interspacing of sharp edges. *Sensors Actuators, B Chem.* **231,** 357–364 (2016).
87. Ave, D. OCEAN OPTICS SERS User Manual.
88. Larmour, I. A., Faulds, K. & Graham, D. SERS activity and stability of the most frequently used silver colloids. *J. Raman Spectrosc.* **43,** 202–206 (2012).
89. Cañamares, M. V., Garcia-Ramos, J. V., Sanchez-Cortes, S., Castillejo, M. & Oujja, M. Comparative SERS effectiveness of silver nanoparticles prepared by different methods: A study of the enhancement factor and the interfacial properties. *J. Colloid Interface Sci.* **326,** 103–109 (2008).
90. Michota, A. & Bukowska, J. Surface-enhanced Raman scattering (SERS) of 4-mercaptobenzoic acid on silver and gold substrates. *J. Raman Spectrosc.* **34,** 21–25 (2003).
91. Giese, B. & Mcnaughton, D. Surface-Enhanced Raman Spectroscopic and Density Functional Theory Study of Adenine Adsorption to Silver Surfaces Surface-Enhanced Raman Spectroscopic and Density Functional Theory Study of Adenine Adsorption to Silver Surfaces. *J. Phys. Chem. B* **106,** 101–112 (2002).
92. Pagliai, M., Caporali, S., Muniz-Miranda, M., Pratesi, G. & Schettino, V. SERS, XPS, and DFT study of adenine adsorption on silver and gold surfaces. *J. Phys. Chem. Lett.* **3,** 242–245 (2012).
93. Ash, A. I., Units, S. H. & Total, A. Product Specification Adenine. **44,** 6–11
94. Zhu, H., Chen, H., Wang, J. & Li, Q. Fabrication of Au nanotube arrays and their plasmonic properties. *Nanoscale* **5,** 3742–3746 (2013).
95. Cai, W. *et al.* Thermal transport in suspended and supported monolayer graphene grown by chemical vapor deposition. *Nano Lett.* **10,** 1645–1651 (2010).
96. Core Team R (2013) R: a language and environment for statistical computing. R Foundation for Statistical Computing, Vienna, Austria.
97. Package, T. & Beleites, A. C. Package ‘ hyperSpec ’. (2015).
98. Kristian Hovde Liland and BjA, rn-H. M. Baseline: Baseline Correction of Spectra. (2014). at <http://cran.r-project.org/package=baseline>
99. Ranke, J. chemCal: Calibration Functions for Analytical Chemistry. (2015).
100. Haiss, W., Thanh, N. T. K., Aveyard, J. & Fernig, D. G. Determination of size

and concentration of gold nanoparticles from UV-Vis spectra. *Anal. Chem.* **79,** 4215–4221 (2007).

101. Wan, Y. *et al.* Quasi-spherical silver nanoparticles: Aqueous synthesis and size control by the seed-mediated Lee-Meisel method. *J. Colloid Interface Sci.* **394,** 263–268 (2013).

102. Barrow, S. J., Rossouw, D., Funston, A. M., Botton, G. A. & Mulvaney, P. Mapping bright and dark modes in gold nanoparticle chains using electron energy loss spectroscopy. *Nano Lett.* **14,** 3799–3808 (2014).

103. Shiohara, A. *et al.* Plasmon Modes and Hot Spots in Gold Nanostar − Satellite Clusters. *J. Phys. Chem. C* **119,** 10836–10843 (2015).

104. Sánchez-Cortés, S. & García-Ramos, J. V. Influence of coverage in the surface-enhanced Raman scattering of cytosine and its methyl derivatives on metal colloids: Chloride and pH effects. *Surf. Sci.* **473,** 133–142 (2001).

105. Fernández Elena Llorente *et al.* State of the art in therapeutic drug monitoring. *Clinical Chemistry and Laboratory Medicine* **48,** 437 (2010).

106. G., S. D. & H., A. K. Imatinib Mesylate — A New Oral Targeted Therapy. *N. Engl. J. Med.* **346,** 683–693 (2002).

107. Barnhart, K., Coutifaris, C. & Esposito, M. The pharmacology of methotrexate. *Expert Opin. Pharmacother.* **2,** 409–417 (2001).

108. Patil Smita, J., Doijad Rajendra, C. & Dhumal Priya, P. Development of UV-spectrophotometric method for the determination of Imatinib Mesylate (ITM) in bulk and formulation. *Asian J. Pharm. Clin. Res.* **6,** 54–57 (2013).

109. Ciekot, J., Goszczyński, T. & Boratyński, J. Methods for methotrexate determination in macromolecular conjugates drug carrier. *Acta Pol. Pharm. - Drug Res.* **69,** 1342–1346 (2012).

110. Li-Wan-Po, A., Farndon, P., Craddock, C. & Griffiths, M. Integrating pharmacogenetics and therapeutic drug monitoring: Optimal dosing of imatinib as a case-example. *Eur. J. Clin. Pharmacol.* **66,** 369–374 (2010).

111. Ishikawa, Y. *et al.* Trough plasma concentration of imatinib reflects BCR-ABL kinase inhibitory activity and clinical response in chronic-phase chronic myeloid leukemia: A report from the BINGO study. *Cancer Sci.* **101,** 2186–2192 (2010).

112. Picard, S. *et al.* Trough imatinib plasma levels are associated with both

cytogenetic and molecular responses to standard-dose imatinib in chronic myeloid leukemia Brief report Trough imatinib plasma levels are associated with both cytogenetic and molecular responses to sta. *Blood* **109,** 3496–3499 (2007).

113. Awidi, A. *et al.* Relationship of serum imatinib trough level and response in CML patients: Long term follow-up. *Leuk. Res.* **34,** 1573–1575 (2010).
114. Molimard, M. *et al.* Definition of an imatinib trough concentration threshold in the treatment of advanced gastrointestinal stromal tumors (GIST). in *ASCO Annual Meeting Proceedings* **29,** 10013 (2011).
115. Graf, N., Winkler, K., Betlemovic, M., Fuchs, N. & Bode, U. Methotrexate pharmacokinetics and prognosis in osteosarcoma. *J. Clin. Oncol.* **12,** 1443–1451 (1994).
116. Rahiem Ahmed, Y. A. A., and Y. H. Prevention and management of high dose methotrexate toxicity. *J . Cancer Sci. Ther.* **5,** 106–112 (2013).
117. Hidi, I. J. *et al.* LOC-SERS: towards point-of-care diagnostic of methotrexate. *Anal. Methods* **6,** 3943–3947 (2014).
118. Yang, J., Tan, X., Shih, W. C. & Cheng, M. M. C. A sandwich substrate for ultrasensitive and label-free SERS spectroscopic detection of folic acid / methotrexate. *Biomed. Microdevices* **16,** 673–679 (2014).
119. Rath, S. *et al.* Raman spectroscopy for detection of imatinib in plasma: A proof of concept. *J. Innov. Opt. Health Sci.* **8,** (2015).
120. Widmer, N. *et al.* Population pharmacokinetics of imatinib and the role of α1-acid glycoprotein. *Br. J. Clin. Pharmacol.* **62,** 97–112 (2006).
121. Petain, A. *et al.* Population pharmacokinetics and pharmacogenetics of imatinib in children and adults. *Clin. Cancer Res.* **14,** 7102–7109 (2008).
122. Haouala, A. *et al.* Prediction of free imatinib concentrations based on total plasma concentrations in patients with gastrointestinal stromal tumours. *Br. J. Clin. Pharmacol.* **75,** 1007–18 (2013).
123. Di Muzio, E. *et al.* Imatinib binding to human serum albumin modulates heme association and reactivity. *Arch. Biochem. Biophys.* **560,** 100–112 (2014).
124. B.H. Mevik, r. W. No Title. *J. Stat. Softw.* **18,** 1–24 (2007).
125. J. Friedman and T. Hastie. glmnet: Lasso and elastic-net regularized generalized linear models, , R package. (2009).

126. Strimmer, S. G. and K. No Title. *Bioinformatics* **28,** 2270–2271 (2012).
127. Gschwandtner, P. F. and M. mvoutlier: Multivariate outlier detection based on robust methods. *R Packag. version 2.0.6* (2015). at <http://www.statistik.tuwien.ac.at/public/filz/>
128. Filzmoser, K. V. and P. Introduction to multivariate statistical analysis in chemometrics. (2009).
129. Peter, F., Bettina, L. & Kurt, V. Repeated double cross validation for classification models. *J. Chemom.* **23,** 160–171 (2009).
130. Xu, Q. A. & Madden, T. L. *Analytical methods for therapeutic drug monitoring and toxicology*. (Wiley, 2011).
131. Ozaki, Y., King, R. W. & Carey, P. R. Methotrexate and folate binding to dihydrofolate reductase. Separate characterization of the pteridine and p-aminobenzoyl binding sites by resonance Raman spectroscopy. *Biochemistry* **20,** 3219–25 (1981).
132. Seng, G., Bolard, J., Chinsky, L. & Turpin, P. Y. Resonance Raman spectra of methotrexate. *J. Raman Spectrosc.* **13,** 100–102 (1982).
133. Saperstein, D. D., Rein, A. J., Poe, M. & Leahy, M. F. Binding of methotrexate to Escherichia coli dihydrofolate reductase as measured by visible and ultraviolet resonance Raman spectroscopy. *J. Am. Chem. Soc.* **100,** 4296–4300 (1978).
134. Álvarez-Puebla, R. A. Effects of the excitation Wavelength on the SERS spectrum. *J. Phys. Chem. Lett.* **3,** 857–866 (2012).
135. Sánchez Cortés, S. & García Ramos, J. V. Anomalous Raman bands appearing in surface-enhanced Raman spectra. *J. Raman Spectrosc.* **29,** 365–371 (1998).
136. Munro, C. H., Smith, W. E., Garner, M., Clarkson, J. & White, P. C. Characterization of the Surface of a Citrate-Reduced Colloid Optimized for Use as a Substrate for Surface-Enhanced Resonance Raman Scattering. *Langmuir* **11,** 3712–3720 (1995).
137. Psychogios, N. *et al.* The human serum metabolome. *PLoS One* **6,** (2011).
138. Sonemoto, E. *et al.* Practical determination of methotrexate in serum of rheumatic patients by LC-MS/MS. *Biomed. Chromatogr.* **26,** 1297–1300 (2012).
139. Sperling, R. a & Parak, W. J. Surface modification, functionalization and bioconjugation of colloidal inorganic nanoparticles. *Philos. Trans. A. Math. Phys.*

Eng. Sci. **368,** 1333–1383 (2010).

140. Kamra, T., Zhou, T., Montelius, L., Schnadt, J. & Ye, L. Implementation of molecularly imprinted polymer beads for surface enhanced raman detection. *Anal. Chem.* **87,** 5056–5061 (2015).

141. Srivastava, A. *et al.* Study of polymorphism in imatinib mesylate: A quantum chemical approach using electronic and vibrational spectra. *Spectrochim. Acta Part A Mol. Biomol. Spectrosc.* **103,** 325–332 (2013).

142. Kretz, O., Weiss, H. M., Schumacher, M. M. & Gross, G. In vitro blood distribution and plasma protein binding of the tyrosine kinase inhibitor imatinib and its active metabolite, CGP74588, in rat, mouse, dog, monkey, healthy humans and patients with acute lymphatic leukaemia. *Br. J. Clin. Pharmacol.* **58,** 212–216 (2004).

143. Ye, J. *et al.* Excitation wavelength dependent surface enhanced Raman scattering of 4-aminothiophenol on gold nanorings. *Nanoscale* **4,** 1606–1611 (2012).

Acknowledgments

This Ph.D. work has been carried out in a scientific collaboration with the National Cancer Institute (CRO) in Aviano, partially funded by AIRC (Associazione Italiana per la Ricerca sul Cancro) project 5 x 1000 n. 12214. It has been also partly supported by IRCCS Burlo Garofolo.

Support from COST Action BM1401 Raman-based applications for clinical diagnostics (Raman4Clinics) is also kindly acknowledged.

I would like to acknowledge prof. Fabrizio Giorgis and Dr. Chiara Novara (Politecnico of Torino, IT) for our pleasant and, for sure, instructive collaboration.

I am really grateful to prof. Santiago Sánchez Cortés (Instituto de Estructura de la Materia, IEM – CSIC, Madrid, SP) for all the support and the knowledge he gave me during my period in Spain.

Finally, last but not least, I am really thankful to the research group of which I was part: prof. Valter Sergo, prof. Alis Bonifacio, Dr. Stefano Fornasaro, Elisa Gurian, prof. Vanni Lughi. Thank you all for making me feel like family.